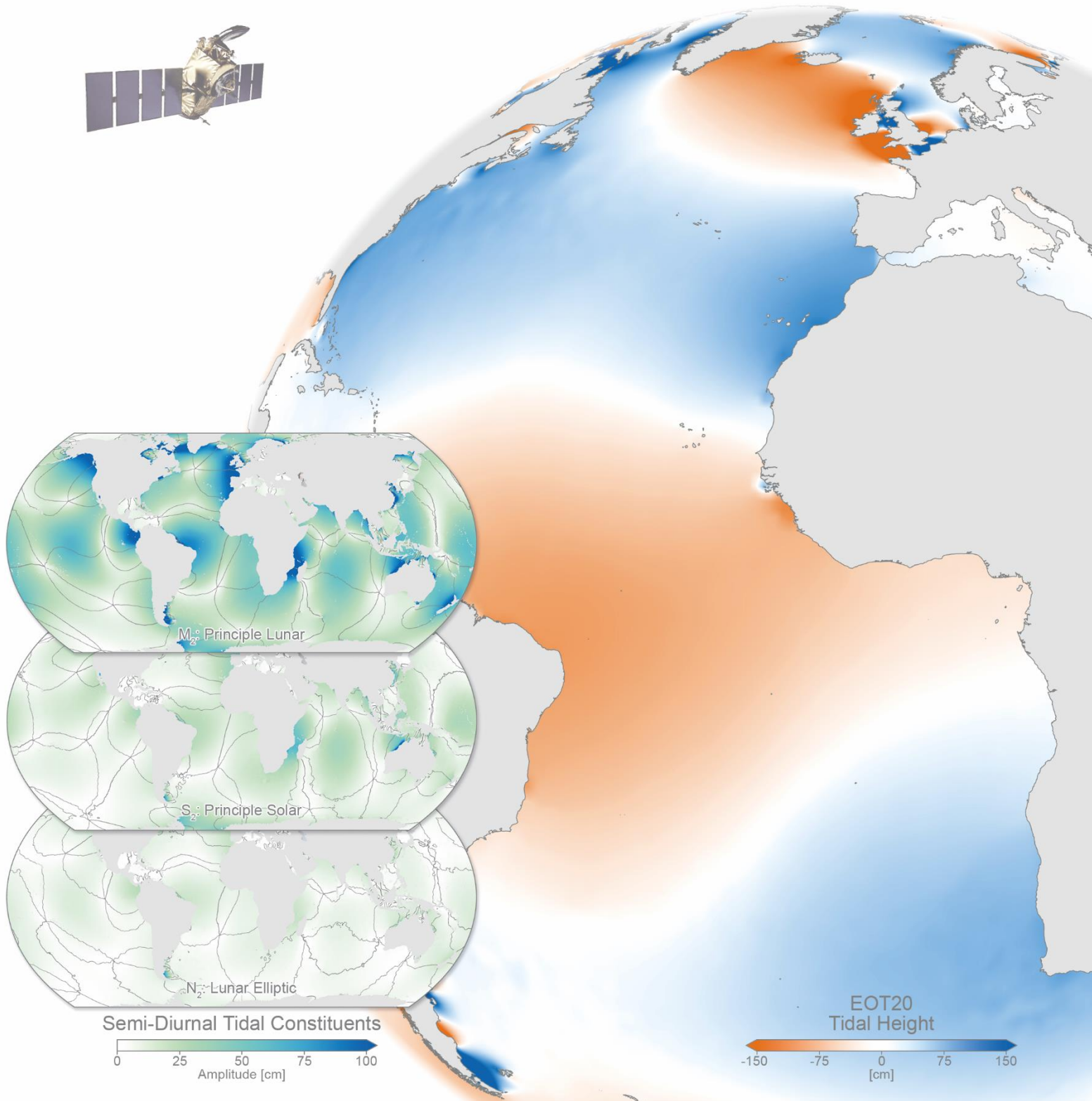


# Annual Report 2021

Deutsches Geodätisches Forschungsinstitut  
der Technischen Universität München  
(DGFI-TUM)



## **Front cover:** EOT20: DGFI-TUM's new global model of ocean tides

Accurate knowledge of ocean tides is required for numerous practical applications, including maritime navigation and coastal protection. Tides are also important for the analysis of geodetic data, for example, in the observation of sea surface processes by satellite altimetry, in the realization of reference systems as well as in the determination of high-resolution gravity fields using dedicated satellite missions such as the Gravity Recovery and Climate Experiment (GRACE).

With EOT20, DGFI-TUM has released the latest model in a series of empirical ocean tide (EOT) models in 2021. Although tidal models have made significant progress in recent years, the coastal region remains a challenge due to the complexity of coastlines, poorly resolved bathymetry, and contamination of altimetry radar echoes by land. Building on recent advances in coastal altimetry, EOT20 represents a step forward in tidal estimation and shows improved results compared to its predecessor and other global tidal models, especially in the coastal region.

The image on the title page shows on the left three of the major tidal components of the EOT20 model (semi-diurnal components M2, S2, and N2). In total, the model comprises 17 components that allow the determination of tidal heights anywhere in the ocean at any point in time. On the globe, the tidal height for 13:00 h CET on December 5, 2021 is shown as an example. The large-scale and uniform tidal heights in the open ocean are clearly visible, whereas very complex tidal regimes exist in marginal seas and near the coast, for example in the North Sea or the Patagonian Shelf. For more information on EOT20, see Section 2.2 of this report.

Technische Universität München  
TUM School of Engineering and Design  
Department Aerospace and Geodesy  
Deutsches Geodätisches Forschungsinstitut (DGFI-TUM)

Arcisstr. 21  
D - 80333 München

[www.dgfi.tum.de](http://www.dgfi.tum.de)

# Contents

<b>Preface</b>	<b>1</b>
<b>1 Research Area Reference Systems</b>	<b>7</b>
1.1 Analysis of Space-Based Microwave Observations . . . . .	9
1.2 Analysis of Satellite Laser Ranging Observations . . . . .	12
1.3 Computation of Satellite Orbits . . . . .	14
1.4 Determination of Reference Frames . . . . .	17
<b>2 Research Area Satellite Altimetry</b>	<b>30</b>
2.1 Multi-Mission Analysis . . . . .	30
2.2 Sea Surface . . . . .	32
2.3 Inland Altimetry . . . . .	45
<b>3 Cross-Cutting Research Topics</b>	<b>50</b>
3.1 Atmosphere . . . . .	51
3.2 Regional Gravity Field . . . . .	64
3.3 Standards and Conventions . . . . .	69
<b>4 Scientific Transfer</b>	<b>74</b>
4.1 Functions in Scientific Bodies . . . . .	74
4.2 Publications . . . . .	79
4.3 Presentations . . . . .	83
4.4 Participation in Meetings, Symposia, Conferences . . . . .	90
4.5 Guests . . . . .	94
4.6 Internet Portals . . . . .	95
<b>5 Projects</b>	<b>99</b>
<b>6 Personnel</b>	<b>101</b>
6.1 Lectures and Courses at Universities . . . . .	101
6.2 Lectures at Seminars, Schools, and Public Relations . . . . .	102
6.3 Thesis Supervision . . . . .	102
6.4 Conferral of Doctorates . . . . .	103
6.5 International Research Stays . . . . .	103



# Preface

## The Institute

The Deutsches Geodätisches Forschungsinstitut (DGFI-TUM) is a research institute of the Technical University of Munich (TUM). It is part of the Chair of Geodetic Geodynamics within the Department of Aerospace and Geodesy of the TUM School of Engineering and Design.

The scientific focus of DGFI-TUM is basic research in the field of Space Geodesy. The research work pursues the goal of precisely measuring and investigating the geometric and physical properties of the Earth system and their changes over time. To this end, DGFI-TUM processes, analyzes and combines observation data from all relevant space geodetic observing systems and complementary data sources in close international and interdisciplinary cooperation. A central aspect of the institute's research has always been the precise determination of the geometric figure of the Earth and its temporal changes. For the solid Earth, this involves in particular the realization of terrestrial reference and height systems on a global and regional scale as well as of the celestial reference system. With respect to water surfaces, a key focus of DGFI-TUM is on the precise determination of the changing sea level, the surface dynamics of the oceans and the water levels of inland waters using satellite altimetry.

The strategic orientation of DGFI-TUM is reflected in its division into the two research areas *Reference Systems* and *Satellite Altimetry* (Fig. 1). The research areas are complemented by three overarching research topics, which include the study of the state and dynamics of the atmosphere (with a focus on ionospheric disturbances and space weather impacts), the determination of high-resolution regional gravity fields, and the enhancement of consistency in the analysis of geodetic data by establishing uniform standards and conventions in an international context.

Within the framework of the Research Group Satellite Geodesy (Forschungsgruppe Satellitengeodäsie, FGS), the institute contributes to the scientific data processing of the Geodetic Observatories Wettzell (Germany) and AGGO (Argentina). In addition, it operates several GNSS stations distributed worldwide.

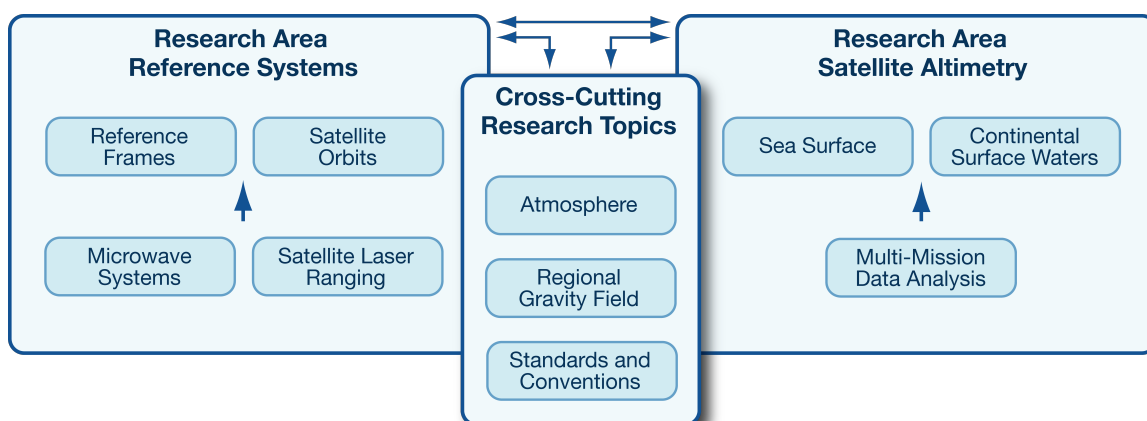


**Figure 1:** Research Areas of DGFI-TUM

## National and international involvement

The institute was established in 1952 by the German Geodetic Commission (Deutsche Geodätische Kommission, DGK) as an independent research facility at the Bavarian Academy of Sciences and Humanities (BAW) in Munich. Since 2015, it has been part of the TUM. For almost seven decades, DGFI has been continuously involved in a large variety of nationally and internationally coordinated geodetic research activities and is intensively networked with renowned research institutions around the world. The research direction of DGFI that has shaped the Institute was and is the advancement of mathematical and physical geodesy. In the course of the institute's history, this included geometric methods of astronomical geodesy, land surveying and satellite triangulation as well as dynamic methods of gravimetry and satellite geodesy.

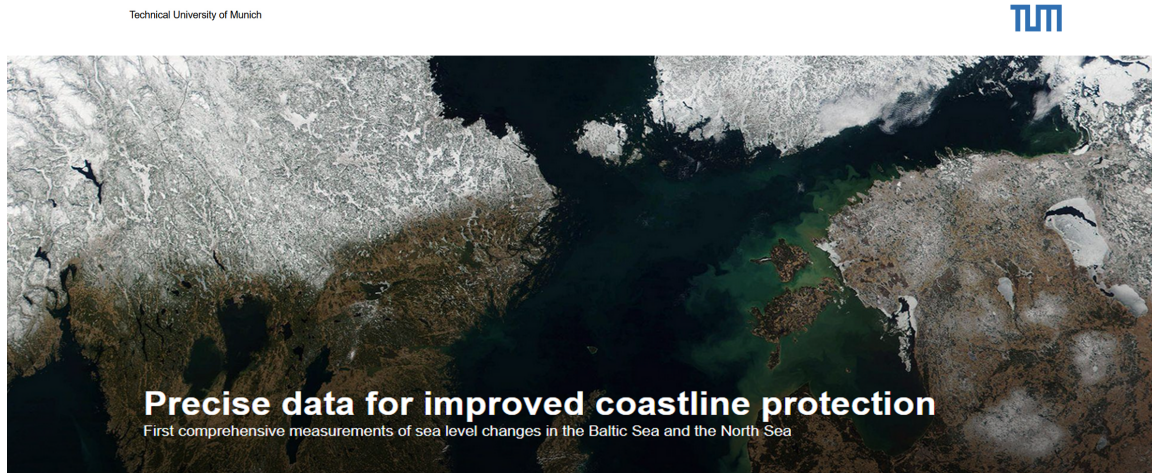
Many of the research projects carried out at DGFI were of great importance for the scientific progress of geodesy. In the first decades after its foundation, the essential work included geodetic-astronomical observations, triangulation and height measurements, among others as part of the IAG project for the readjustment of the European triangulation and for the adjustment of the European levelling network. Later, the focus shifted to the geodetic use of artificial Earth satellites. DGFI was involved in the first worldwide network of satellite triangulation and played a leading role in the development of dynamic methods of satellite geodesy for the precise determination of satellite orbits, the Earth's gravity field and point positions. With the further development of modern space geodetic techniques and the expansion of the worldwide geodetic infrastructure in the 1980s and 1990s, the enhancement of the Geodetic Observatory in Wettzell and in the course of DGFI's participation in the DFG Collaborative Research Center *Satellite Geodesy* (SFB 78), the further development of theories and methods for the definition and realization of terrestrial reference systems became a key focus of the Institute. Since satellite altimetry became operational as a geodetic observation technique towards the mid-1990s, the observation and scientific analysis of water surfaces has complemented the research program.

DGFI-TUM is involved in central positions in international scientific organizations, especially within the framework of the International Union of Geodesy and Geophysics (IUGG), the International Astronomical Union (IAU) and the International Association of Geodesy (IAG) (see Section 4.2). Since many years, the Institute has been an important pillar of IAG's Global Geodetic Observing System (GGOS). GGOS advocates for the implementation of geodetic infrastructure and analysis capabilities necessary for Earth system monitoring and global change research, and coordinates the generation of high quality science data products under pre-defined standards and conventions. DGFI-TUM provides the current GGOS Vice President, chairs one of the two GGOS Bureaus (Bureau of Products and Standards) and leads two of the three GGOS Focus Areas (FA Unified Height System; FA Geodetic Space Weather Research). In addition, the Institute recognizes the outstanding importance of IAG's Scientific Services, which form the backbone of the national and international spatial data infrastructure. Within this framework, DGFI-TUM operates data centers, analysis centers and research centers. It performs leading roles and supporting functions in IAG's commissions, projects, working and study groups and thus contributes to shape the future direction of international geodetic research.

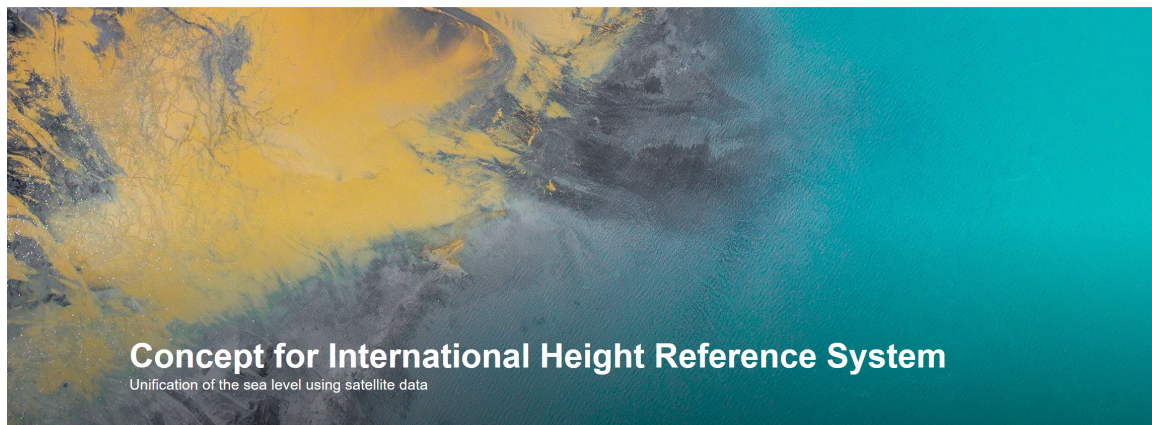
The institute participates in research programs of the European Union (EU) and the European Space Agency (ESA) and cooperates in activities of the United Nations (UN). In this regard, DGFI-TUM is involved in the implementation of a UN Resolution for a Global Geodetic Reference Frame (GGRF) and provides an IAG representative to the UN Committee of Experts on Global Geospatial Information Management (UN-GGIM) Working Group for the GGRF.

## Research highlights of particular scientific and public interest

During the year 2021, several scientific results gained broad attention in the scientific community and in the public. The following activities and publications can be highlighted:



- **Sea level changes in the North Sea and Baltic Sea:** Led by DGFI-TUM, an international team of researchers has created the first comprehensive data sets of regional sea level changes in the North Sea and Baltic Sea, including coastal areas and regions covered by sea ice. The data sets provide new insights into long-term and seasonal sea level changes over the past quarter century. This information is of vital importance for planning protective measures and for understanding dynamic processes in the oceans and the climate system. The underlying algorithms, which make it possible to track sea level changes also in coastal areas and beneath sea ice, were developed within the framework of the ESA Baltic Sea Level project (Baltic SEAL). The data sets created (Baltic SEAL and North SEAL) are publicly available. Methods and results are described in the publications *Absolute Baltic Sea Level Trends in the Satellite Altimetry Era: A Revisit* (Frontiers in Marine Science, 2021, doi:[10.3389/fmars.2021.647607](https://doi.org/10.3389/fmars.2021.647607)) and *North SEAL: A new Dataset of Sea Level Changes in the North Sea from Satellite Altimetry* (Earth System Science Data, 2021, doi:[10.5194/essd-13-3733-2021](https://doi.org/10.5194/essd-13-3733-2021)); for more information see Section 2.2 of this report. TUM and ESA reported about these studies in press releases.
- **New global ocean tide model EOT20 (Title page):** Ocean tides play a vital role in various practical applications, especially in the coastal environment. In addition, tides are of importance in geodetic data analysis, for example in improving the observation of sea surface processes from satellite altimetry and in determining high-resolution gravity fields from missions such as GRACE-FO. In 2021, DGFI-TUM published a new empirical ocean tide model (EOT), continuing a long line of successful predecessors. The new model, named EOT20, shows improved results compared to other global tide models, especially in the coastal region. The model's accuracy was evaluated using in-situ tide gauge data. Error reduction was found for the eight major tidal constituents in EOT20 compared to other global ocean tide models in the coastal region, with an error reduction of 0.2 cm compared to the next best model (FES2014b). The ocean tide and load tide datasets of EOT20 are freely available via SEANOE (doi:[10.17882/79489](https://doi.org/10.17882/79489)). Methodology and results are described in the publication *EOT20: a global ocean tide model from multi-mission satellite altimetry*, Earth System Science Data, 2021, doi:[10.5194/essd-13-3869-2021](https://doi.org/10.5194/essd-13-3869-2021). Details can be found in Section 2.2.



- **Implementation of the International Height Reference System (IHRIS):** The IHRIS was defined in 2015 by the International Association of Geodesy (IAG) as the conventional global height system. It makes it possible for the first time to relate all height measurements worldwide to a uniform height system. The IHRIS is of great importance for all applications in which geodetic measurements and Earth observations are related over long distances, between different countries or even worldwide. For example, the IHRIS forms the geodetic basis for the survey to redefine the height of Mount Everest in 2020 or for cross-border structures such as tunnels or bridges. Under the leadership of DGFI-TUM and supported by strong international cooperation within the IAG, the theoretical concept of the IHRIS as well as the roadmap for its implementation were developed. This is reported in the article *Strategy for the realisation of the International Height Reference System (IHRIS)*, Journal of Geodesy, 2021, doi:[10.1007/s00190-021-01481-0](https://doi.org/10.1007/s00190-021-01481-0). The focus is on strategies for determining consistent physical heights at globally distributed reference points and on the usability and long-term sustainability of the IHRIS; see Section 1.4 for more details. This work was also subject of a TUM press release in 2021.
- **Global coastal attenuation of wind-waves:** Knowledge of ocean wave heights at the coast is essential for several operational applications, ranging from coastal protection to energy exploitation. Led by DGFI-TUM, an international team has analyzed reprocessed sea surface height data from radar altimetry, specifically tailored to improve the quality and quantity of coastal measurements. The results, published in the article *Global coastal attenuation of wind-waves observed with radar altimetry* (Nature Communications, 2021, doi:[10.1038/s41467-021-23982-4](https://doi.org/10.1038/s41467-021-23982-4)), provide a global picture of the average wave climate when going from offshore to the coast. The typical attenuation of the waves when approaching the coast is quantified to be about 20% of the wave height reached offshore. As a consequence, the energy flux transported by the waves is calculated to decline by about 40% on a global average. More information is provided in Section 2.2.
- **Successful implementation of an operational system for space weather monitoring for the German Space Situational Awareness Center:** Over a period of 7.5 years, DGFI-TUM developed an operational system for space weather monitoring for the German Space Situational Awareness Center (Weltraumlagezentrum, WRLageZ) in the OPTIMAP project. Space weather affects the electron content (VTEC) and electron density of the ionosphere and can lead to serious damage and failures of the electrotechnical infrastructure (such as power supply, navigation and communication systems). A key component of OPTIMAP was the development of a software application that provides real-time ionospheric information and forecasts for up to five days ahead based on GNSS data streams and other satellite



data (*Real-time monitoring of ionosphere VTEC using Multi-GNSS carrier-phase observations and B-splines*, *Space Weather*, 2021, doi:[10.1029/2021sw002858](https://doi.org/10.1029/2021sw002858)). The model has a latency of about 30 seconds and its quality is superior to other real-time data products currently available. Details on OPTIMAP can be found in Section 3.1.

- **Improved modeling of atmospheric drag in precise orbit determination:** A major problem in the precise orbit determination (POD) of low-Earth-orbiting satellites is the modeling of atmospheric drag, which depends mainly on thermospheric density. Normally, thermospheric densities at satellite positions are determined by empirical models, which have limited accuracy. But conversely, satellites orbiting the Earth within the thermosphere can be used to derive thermospheric density information because of their sensitivity to perturbing accelerations. DGFI-TUM, together with the Institute of Geodesy and Geoinformation at the University of Bonn, derived thermospheric density corrections for the NRLMSISE-00 model from in-situ acceleration measurements on board CHAMP and GRACE and from Satellite Laser Ranging (SLR). While the model tends to overestimate the thermospheric density at low solar activity and needs to be scaled down, the model underestimates the density values at high solar activity and needs to be scaled up. Results of the study are published in the article *Scale Factors of the Thermospheric Density: A Comparison of Satellite Laser Ranging and Accelerometer Solutions* (*Journal of Geophysical Research: Space Physics*, 2021, doi:[10.1029/2021JA029708](https://doi.org/10.1029/2021JA029708)); for details see Section 3.1.
- **Mission Earth: Geodynamics and Climate Change Observed Through Satellite Geodesy:** Led by DGFI-TUM, this popular science book was published in 2021 by four TUM authors. It deals with the measurement of the Earth through the ages and is aimed at readers interested in Earth science. The book highlights the socially particularly relevant questions of how modern geodesy contributes to a better understanding of geodynamic processes in the Earth system with highly accurate satellite data, and it shows what fundamental contributions geodesy can make to determine the effects of progressive climate change. Answers are given as to how these changes can be precisely measured from space in order to obtain reliable statements about, for example, the melting of the ice sheets or the threat to coastal regions from continuously rising sea level. Illustrative examples show how deeply global positioning and navigation with satellites have already penetrated our everyday lives. The book also contains three interview contributions with the publicly known scientists Günter Hein, Harald Lesch and Stefan Rahmstorf. The book is published by the Springer Verlag in German (doi:[10.1007/978-3-662-62338-1](https://doi.org/10.1007/978-3-662-62338-1)) and English (doi:[10.1007/978-3-662-64106-4](https://doi.org/10.1007/978-3-662-64106-4)).





# 1 Research Area Reference Systems

*Reference systems on Earth and in space form the fundamental framework for referencing geodetic and astronomical observations. Highly accurate realizations of these systems, the so-called reference frames, are of utmost importance for positioning and navigation on Earth and in the solar system as well as for the measurement of time. Theoretical and practical aspects of reference systems and their realization have been a central topic of the DGFI-TUM for decades.*

*Research in this field relies on the space geodetic observation techniques Very Long Baseline Interferometry (VLBI), Satellite Laser Ranging (SLR), Global Navigation Satellite Systems (GNSS), and Doppler Orbitography and Radiopositioning Integrated by Satellite (DORIS). The Institute's core products include global and regional realizations of three-dimensional geodetic reference systems determined from the combination of the above-mentioned observation techniques. The focus of the research is on the development of refined analysis strategies and models of these observation techniques as well as on the development of advanced methods to combine them. Research activities also include the consistent realization of terrestrial and celestial reference systems including Earth Orientation Parameters (EOP) and their application for Earth system studies. Further focal points are the realization of vertical reference systems and the determination of precise satellite orbits.*

*As a basis for research in this field, DGFI-TUM is developing its own analysis and combination software DOGS (DGFI Orbit and Geodetic parameter estimation Software). Research on reference systems benefits from the institute's long-standing involvement in international scientific organizations, especially within the International Association of Geodesy (IAG) and the International Astronomical Union (IAU). DGFI-TUM operates, mostly by virtue of long-term commitments, Data Centers, Analysis Centers and Combination Centers (Table 1.1).*

**Table 1.1:** Long-term commitments of DGFI-TUM in international organizations related to the Research Area Reference Systems.

Organization	DGFI-TUM Commitments
International Earth Rotation and Reference Systems Service (IERS)	International Terrestrial Reference System (ITRS) ITRS Combination Center
International GNSS Service (IGS)	Regional Network Associate Analysis Center for SIRGAS (RNAAC-SIR)
International Laser Ranging Service (ILRS)	Global Data and Operation Center (EDC), Analysis Center (AC)
International VLBI Service for Geodesy and Astrometry (IVS)	Analysis Center (AC), Combination Center (jointly with BKG)
International DORIS Service (IDS)	Associate Analysis Center (AAC)

## Enhancement of the DOGS software

in 2021, the three libraries DOGS-OC (Orbit Computation), DOGS-RI (Radio Interferometry) and DOGS-CS (Combination and Solution) of the DGFI Orbit and Geodetic parameter estimation Software (DOGS) were further developed. The following sections give an overview of the improvements and new functions.

**DOGS-Orbit Computation (OC):** This library is used for precise orbit determination (POD) of spherical and non-spherical geodetic satellites in different altitude regimes (satellites in low to high Earth orbit) and for the analysis of SLR and DORIS observations. The analysis results can be transferred to DOGS-CS via normal equations (NEQs) with orbit parameters, station coordinates and selected EOP. The library is also used to perform simulations of the SLR and DORIS ground infrastructure or space segment (new satellite missions, satellite visibility tests, etc.). DOGS-OC is also able to re-scale (geo-)physical models, such as models of the high atmosphere (Zeitler et al., 2021, see Section 3.1).

The updates, improvements and new models implemented in DOGS-OC:

- new/modified checks of the input data,
- updated import and processing of DORIS observations (see Section 1.1, DORIS data analysis),
- refined treatment of wavelength-specific range biases (see Section 1.2, SLR data analysis),
- new station-dependent SLR measurement model for the TOPEX/Poseidon satellite (see Section 1.3, Orbit modeling for altimetry satellites),
- update of existing and implementation of the new thermosphere model NRLMSISE 2.0,
- refined and coherent handling of the internal tapes (local binaries used by DOGS-OC),
- refined handling of leap seconds.

**DOGS-Radio Interferometry (RI):** This library sets up and solves the NEQ systems for the analysis of VLBI observations. With VLBI, the distances between each two antennas observing the same quasi-stellar radio source (quasar) at the same time can be estimated. In addition, the positions of these quasars and the entire set of EOP can be derived, providing the orientation of the terrestrial reference system (TRS) in the celestial reference system (CRS).

The updates, improvements and new models implemented in DOGS-RI:

- new format for non-tidal loading (NTL) data,
- sub-daily parameterization of EOP,
- calculation of matrix ranks in different processing stages,
- new naming convention for handling different radio frequencies,
- second approach for galactic aberration: correction of the theoretical delay,
- export of datum-free normal equations after outlier removal and clock correction.

**DOGS-Combination and Solution (CS):** In 2021, the CS library of DOGS was prepared to compute the DTRF2020, DGFI-TUM's new realization of the International Terrestrial Reference Frame (ITRF) (see Section 1.4). A major update of the CS library in 2020 and numerous changes required a completely new internal handling of the parameter metadata. This task also includes updated interfaces from and to the SINEX format (Solution INdependent EXchange).

For validation purposes, a new routine was added to DOGS-CS. This routine enables Helmert transformations (infinitesimal similarity) based on different transformation setups. In addition to estimating up to 14 Helmert parameters, the routine also provides information about the transformation residuals for each individual observing station as well as statistical information about the transformation itself. The routine is able to handle different types of input data and offers the possibility to iteratively eliminate outliers within the transformation.

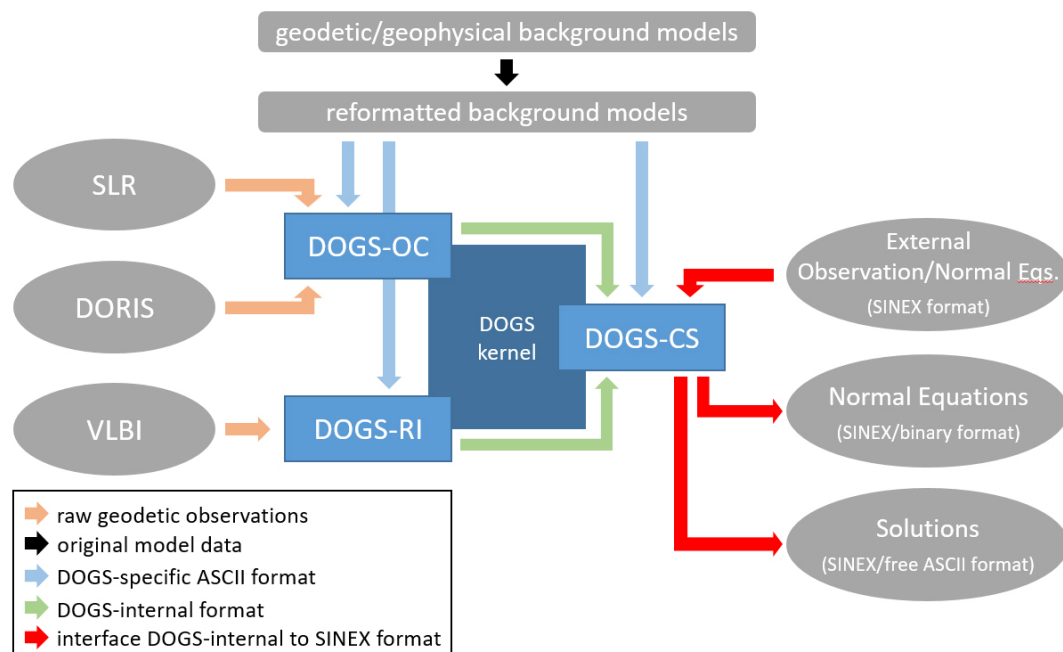


**Figure 1.1:** Flow chart of DGFI-TUM's orbit and geodetic parameter estimation software DOGS

DOGS-CS is used for research and development within the framework of the ITRS Combination Center (CC) operated by DGFI-TUM and the CC of the International VLBI Service for Geodesy and Astrometry (IVS) operated jointly by DGFI-TUM and the Federal Agency for Cartography and Geodesy (Bundesamt für Kartographie und Geodäsie, BKG). The development of DOGS-CS is largely determined by the requirements of these international projects.

## 1.1 Analysis of Space-Based Microwave Observations

### VLBI data analysis

Since 2008, DGFI-TUM has acted as an operational Analysis Center (AC) of the IVS, which organizes the world-wide collaboration in VLBI observations and analysis. In this role, DGFI-TUM provides solutions (in the form of datum-free normal equations) for the twice-weekly rapid turnaround VLBI sessions, processed using DGFI-TUM's VLBI analysis software DOGS-RI. New developments regarding this software are described in the previous chapter of this report.

In 2021, a key focus was on the preparation and reprocessing of the VLBI data over the entire observation time span from 1979 until 2021 as input for the computation of the 2020 realization of the International Terrestrial Reference System (see Section 1.4, computation of DTRF2020). VLBI is one of the four space geodetic techniques contributing to the ITRS realization, and DGFI-TUM has participated in the preparation of the corresponding data in two ways. On the one hand, DGFI-TUM has provided its own VLBI solution ("dgf2020a"), and on the other hand, since DGFI-TUM operates the IVS Combination Center together with BKG, it has been involved in combining all individual AC solutions into a common IVS contribution to the ITRS 2020 realization. The combined solution is superior to the individual solutions in terms of accuracy and stability (see Hellmers et al. 2021).

DGFI-TUM's individual VLBI contribution to the ITRS 2020 realization, 'dgf2020a', also includes radio source positions, giving the opportunity to continue research on the consistent realization of the terrestrial (TRS) and celestial reference systems (CRS), together with the corresponding

Earth Orientation Parameters. A preliminary TRS/CRS solution was presented at the European VLBI meeting 2021 (see Fig. 1.2, and Glomsda et al. 2021a), but analyses are still ongoing. In particular, the strategies for combining the legacy and the new VGOS (VLBI Global Observing System) observations still need to be refined: The corresponding station networks are basically separated, and the estimated source positions may differ due to the different radio frequencies observed with legacy and VGOS antennas.

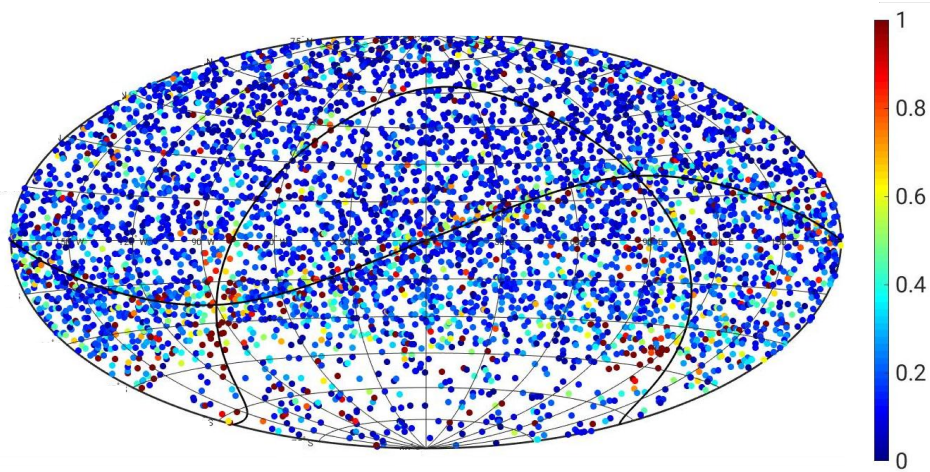


**Figure 1.2:** Formal errors (in [mas]) of the estimated radio source positions (in the equatorial coordinate system of the celestial sphere) in the consistent realization of TRS and CRS with 'dgt2020a'.

Studies of the impact of non-tidal loading (NTL) also continued, both generally in relation to DTRF2020 (see Section 1.4) and specifically for the VLBI analysis. The studies on the impact of NTL on the session-wise VLBI solutions were completed (see Glomsda et al. 2021b), and work started on investigating their impact on the long-term TRF solutions.

### DORIS data analysis

DGFI-TUM has been participating in the International Doppler Orbitography and Radiopositioning Integrated by Satellite (DORIS) Service (IDS) as an Associated Analysis Center since 2019 (Rudenko et al. 2021). In 2021, the DORIS data analysis focused on updating and validating calculations. For this purpose, some new background models for the precise orbit determination of altimetry satellites were implemented (see Section 1.3) and the algorithm for modeling the satellite attitude in DOGS-OC was optimized. For the validation of orbit solutions, the analysis program was extended, which calculates the differences of satellite coordinates provided in SP3 format and allows the comparison of different internal and external orbit solutions.

### GNSS data analysis

DGFI-TUM supports different international initiatives such as the International GNSS Service (IGS) Multi-GNSS Experiment (MGEX), the IGS Tide Gauge Benchmark Monitoring (TIGA), modeling of surface deformations, determination of dense velocity fields, and the ITRF densification in Latin America by SIRGAS (Sistema de Referencia Geocéntrico para Las Américas). This support is realized by installing and providing data of GNSS continuously operating stations, by computing loosely constrained daily and weekly normal equations for GNSS networks, and by determining GNSS station constant velocities based on cumulative solutions. Recent efforts are devoted to the reprocessing of the SIRGAS GNSS historical data from January 2000 to December 2020 based on the ITRF2014 (IGS14/IGb14) with two main purposes:

- to compute an improved solution for the SIRGAS reference frame to ensure its long-term reliability and stability (see SIRGAS, Section 1.4),
- to investigate the realization of GNSS-based regional geocentric reference systems directly and epoch-wise, without the usual transformation onto a global reference frame, but by combining GNSS with SLR and VLBI normal equations using a minimum network configuration on a weekly basis (see Section 1.4). For this reason, reprocessing includes not only SIRGAS regional stations, but also globally distributed IGS stations co-located with VLBI and SLR (see Fig. 1.3).

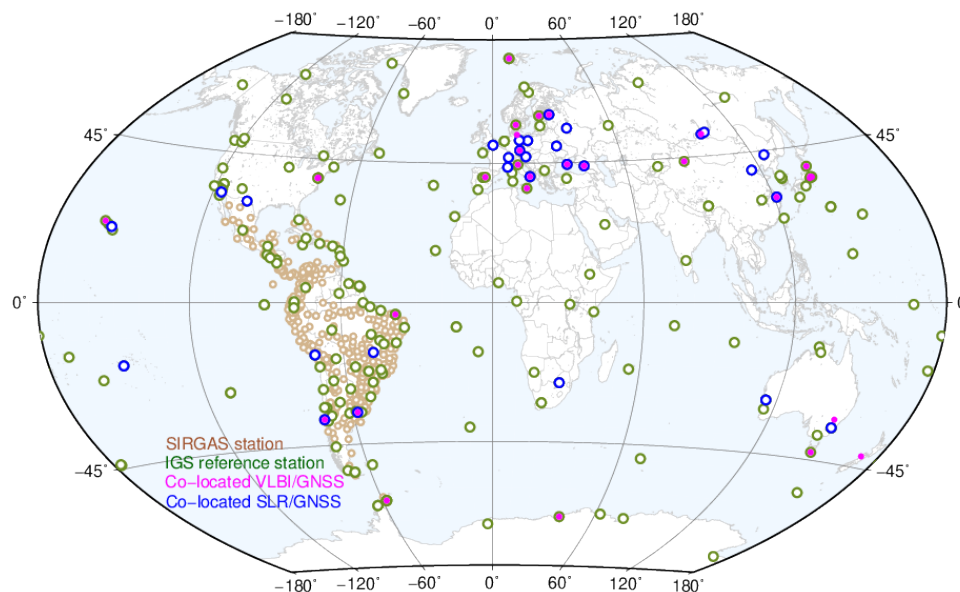


**Figure 1.3:** GNSS network processed to investigate the realization of regional geocentric reference systems directly and epoch-wise by combining GNSS, SLR and VLBI normal equations (adapted from Sánchez and Kehm, 2021).

In this data analysis, different network configurations were evaluated. In the first one, only the GNSS stations co-located with SLR and VLBI techniques were considered (blue circles and magenta dots in Fig. 1.3). This station distribution proved to be unsuitable as most of these stations are located in the northern hemisphere and the computation of GNSS satellite orbits and GNSS-based EOPs is significantly degraded. To overcome this drawback, additional GNSS stations were included to ensure the most homogeneous global distribution of the network. After many empirical experiments, it was concluded to process the core stations of the IGS reference frame together with the SIRGAS regional stations. However, when computing GNSS satellite orbits, satellite clock offsets, EOPs and station positions simultaneously, low reliability of EOPs and GNSS orbits was found due to the dense station distribution in one particular region (see Fig. 1.3). Therefore, the strategy for analyzing GNSS data is based on a two-step procedure: (a) determination of orbits and EOPs based on a global network and (b) processing of the GNSS data fixing the previously determined orbits and EOPs. Since this procedure is currently used in the computation of regional reference frames, it was concluded that regional GNSS data, even if they have a global station distribution, can still be based on the final IGS products. It is important that the datum parameters given to the GNSS normal equations by fixing the GNSS orbits and the EOPs are removed before combining them with the SLR and VLBI normal equations. Further details on the reprocessing of the SIRGAS data and the geocentric realization of regional epoch reference frames are given in Section 1.4 (Regional terrestrial reference frame in Latin America / Geocentric realization of regional epoch reference frames).

## 1.2 Analysis of Satellite Laser Ranging Observations

### SLR data analysis

DGFI-TUM serves as an Analysis Centre (AC) of the International Laser Ranging Service Analysis Standing Committee (ILRS-ASC). In 2021, the main task of the DGFI-TUM AC was the reprocessing of SLR observations to LAGEOS-1/-2 (LA-1/-2) and Etalon-1/-2 (ET-1/-2) in the framework of the ILRS contribution to the ITRS 2020 realization (see Section 1.4, Computation of DTRF2020). The reprocessing is based on a catalogue of settings previously defined by the ILRS-ASC, including an up-to-date conventional gravity field model of the Earth, an updated conventional secular pole model, and a refined model for LAGEOS-1/-2 and Etalon-1/-2 center-of-mass offset from the optical phase center of the retroreflectors (i.e. satellite-specific target signature). In addition, the reprocessing is based on long-term mean range biases (RBs) calculated by the ILRS CC in Italy from input data of the DGFI-TUM AC and other ILRS ACs within the ILRS Station-Systematic Error Monitoring Pilot Project (SSEM PP); see previous DGFI-TUM Annual Reports. As an example, Fig. 1.4 shows the mean RBs for the station Herstmonceaux (UK) compared to the weekly estimated RBs of the DGFI-TUM AC. The long-term mean RBs were compiled into a refined version of the official ILRS Data Handling File (DHF) used for the ITRS 2020 realization.

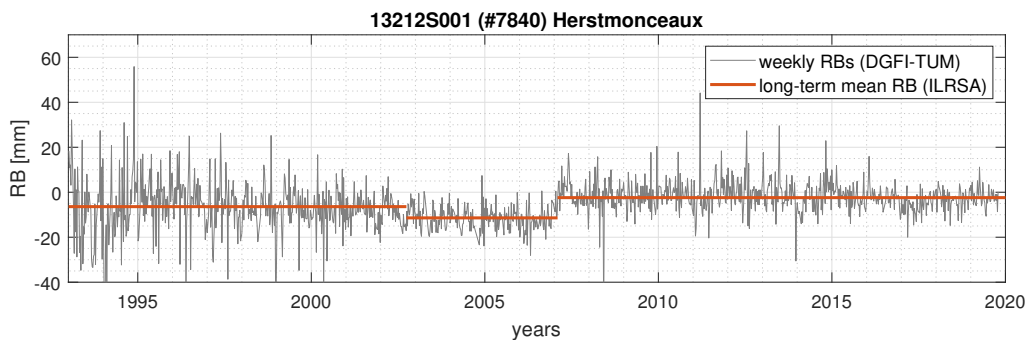


**Figure 1.4:** Weekly range biases estimated at the DGFI-TUM ILRS AC (input time series to ILRS SSEM PP) and long-term mean range biases estimated from the combined ILRSA SSEM PP solutions. The orange mean values are compiled by ILRSA into the refined ILRS Data Handling File used for the ITRS 2020 realization.

Based on the new ILRS DHF, DGFI-TUM computed a time series of 15-day and weekly solutions between 1982 and 2021 (ILRS solution v400; cf. Tab. 1.2). Until 1993.0, only SLR observations up to LAGEOS-1 were used for the reprocessing. This solution was provided to the ILRS CC in Italy (ILRSA), which calculated 15-day and weekly combined solutions of all available (up to seven) ILRS ACs. Fig. 1.5 shows the estimated time series of the translation and scale parameters of the DGFI-TUM AC v400 solutions and the two ILRSA solutions for the ITRS 2014 and 2020 realizations. Fig. 1.6 shows the respective spectra of all time series.

**Table 1.2:** Routine and project-specific solutions computed by the DGFI-TUM ILRS AC during 2021. (\*) Ajisai, LARES, Stella, Starlette

ILRS code	description
v170	Daily LA-1/-2 and ET-1/-2 TRF and EOP solutions
v70	Weekly LA-1/-2 and ET-1/-2 TRF and EOP solutions
v70-sp3c	Weekly LA-1/-2 and ET-1/-2 orbit solutions
—	Daily orbit predictions for LA-1/-2 and ET-1/-2 and others (*)
v400	ITRS 2020 realization



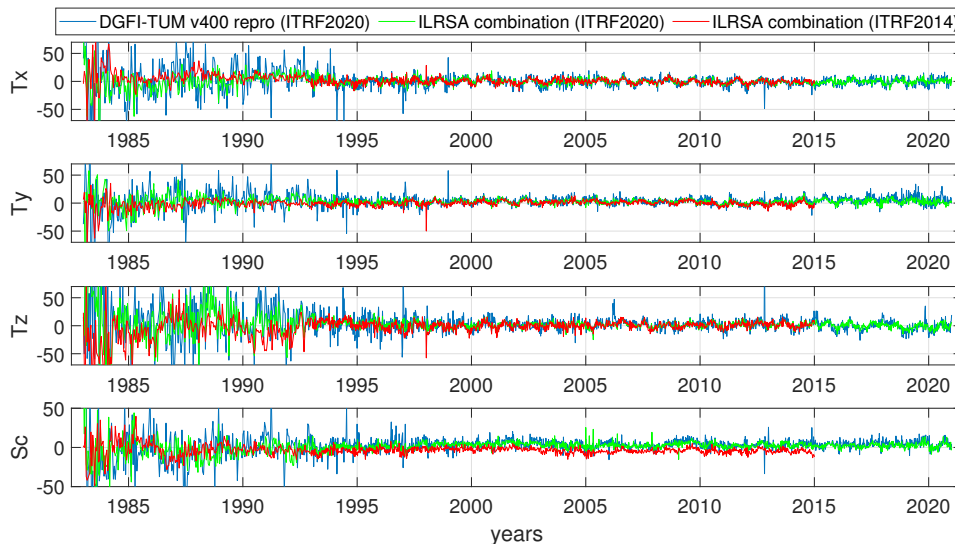


**Figure 1.5:** Estimated time series of translation and scale parameters [mm] of the DGFI-TUM ILRS AC v400 solutions and the two ILRSA solutions for the ITRS 2014 and 2020 realizations.

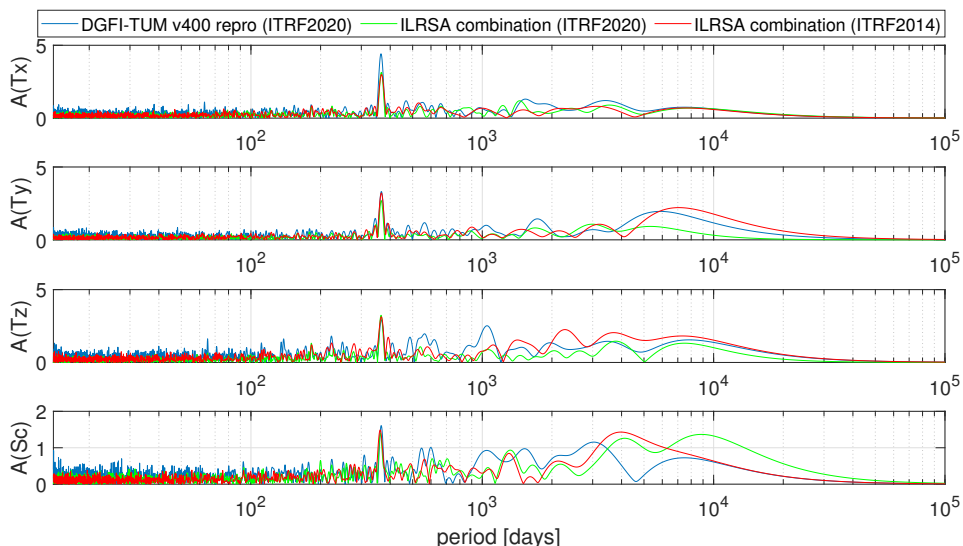


**Figure 1.6:** Amplitude spectra of the estimated time series of translation and scale parameter [mm] of the DGFI-TUM ILRS AC v400 solutions and the two ILRSA solutions for the ITRS 2014 and 2020 realizations.

Especially in the early years (until 1993), the new long-term mean RBs have a considerable influence on the combined LA-1 only solutions (red vs. green lines). After 1993, all translation time series agree very well with each other. In contrast, the scale time series of the ILRS contribution to the ITRS 2020 realization (green) shows an offset of several millimeters compared to the contribution to the ITRS 2014 realization (red). This results from the newly computed satellite target signatures and the new long-term mean RBs of the ILRS DHF. The amplitude spectra of the time series match very well, except for the very long periods in the spectra of the scale time series due to the previously mentioned offset.

In addition to the reprocessing for the ITRS 2020 realization, DGFI-TUM regularly (daily and weekly; cf. Table 1.2) computes solutions for station coordinates and EOP based on SLR observations to LA-1/-2 and ET-1/-2. In addition, daily 7-day predictions for all spherical satellites currently in orbit are computed and delivered to the EUROLAS Data Center (EDC) operated by DGFI-TUM (see below).

## SLR data management

DGFI-TUM has operated the EUROLAS Data Center (EDC) since the founding of the ILRS in 1998. The EDC is one of two ILRS Data Centers worldwide (the second one is the Crustal Dynamics Data Information System, CDDIS, operated by NASA). The EDC, as an ILRS Operation Center (OC) and as an ILRS Data Center (DC), has the task of ensuring the quality of the submitted data. There is a daily and hourly data exchange with the NASA OC and CDDIS. All data and products are publicly available to the ILRS community via ftp (<ftp://edc.dgfi.tum.de>) and the dedicated website <https://edc.dgfi.tum.de>; see Section 4.6.

The EDC maintains various mailing lists for the exchange of information, data and results. In 2021, 69115 Consolidated Prediction Format (CPF) files of 104 satellites were made available to SLR stations. In addition, the EDC distributed SLR-Mails (43 messages in 2021), SLR-Reports (705 in 2021), SLR-Urgent (61 in 2021) and Rapid-Service-Mails (3 in 2021).

In 2021, 231429 pass segments of normal points (NPT) were submitted by 43 SLR stations observing 116 different satellites. There were four new satellite missions tracked by SLR stations, namely HY-2D, ELSA-d (Chaser), TUBIN and QZS-1R. ILRS stations, prediction providers and Analysis Centers worked on the implementation of the new Consolidated Laser Ranging Data (CRD) format 2.0 and the Consolidated Prediction Format (CPF). From 1 January 2022, CPF version 2 will be the official format for predictions in the ILRS. The CRD version 2 format will follow on 1 March 2022 as the official format for NPT and FRD data in the ILRS.

## 1.3 Computation of Satellite Orbits

### Orbit modeling for altimetry satellites

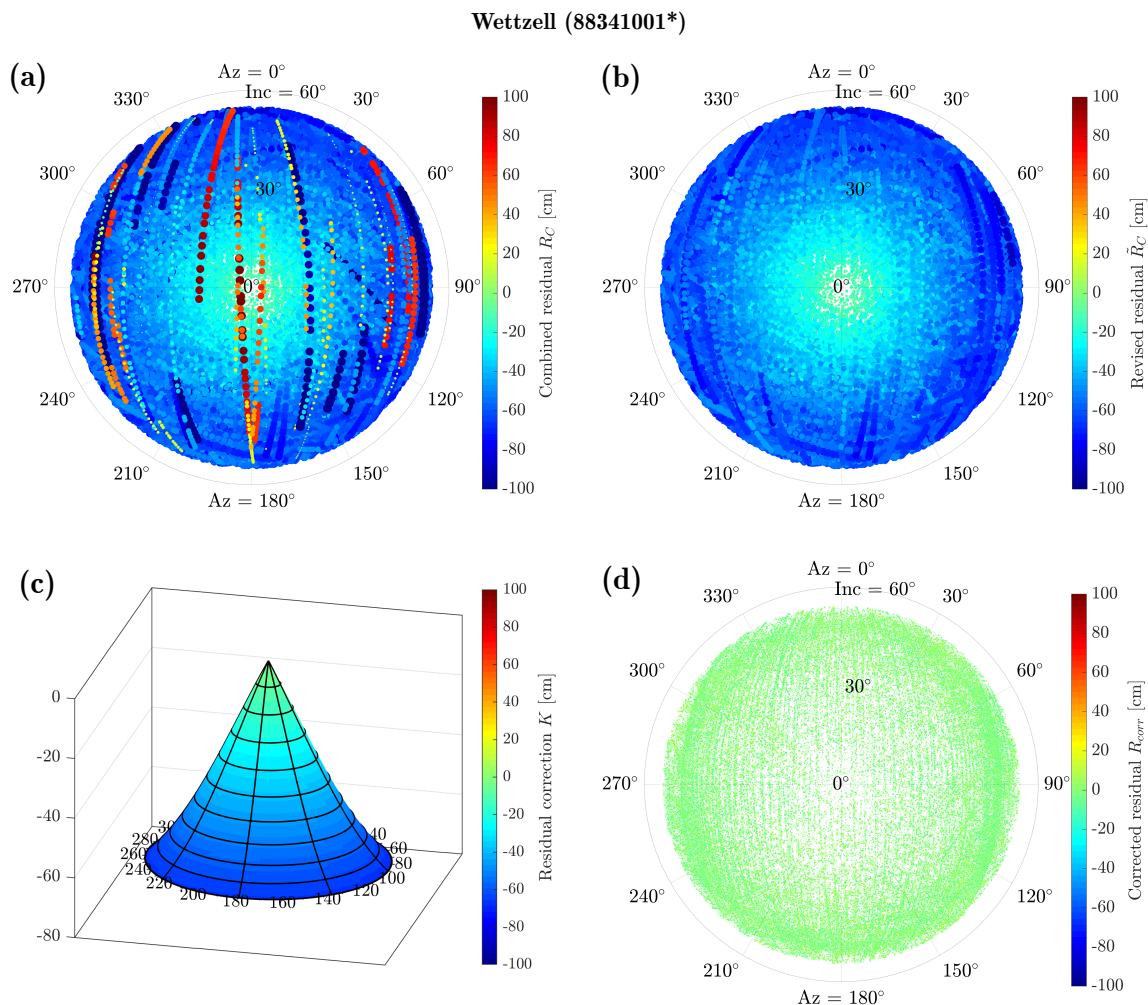
Precise knowledge of the orbits of altimetry satellites is crucial for accurately determining the position of a reference point located on the satellite from which the distance to the water surface is measured. In order to determine this position to centimeter and subcentimeter level, precise knowledge of the gravitational and non-gravitational forces acting on the altimetry satellites as well as the positions of the ground stations in a well-defined reference frame are required. In recent years, significant progress has been made in the precise orbit determination of altimetry satellites (International Altimetry Team, 2021). However, the development and further elaboration of the models for current and past altimetry missions is still required and ongoing.

#### *Determination of station-dependent SLR measurement corrections for TOPEX/Poseidon*

The TOPEX/Poseidon altimetry mission was operational between 1992 and 2005 and had the main objective of monitoring variations in global and regional sea level and ocean circulation. It is one of the first major altimetry missions and the predecessor of the Jason satellites and Sentinel-6A. For precise orbit determination, the spacecraft was equipped with a DORIS and a GPS receiver, as well as a laser retroreflector array (LRA) that served as a target for satellite laser ranging measurements from ground stations. The enormous size of the laser retroreflector array (LRA), with a diameter of over 1.6 m, resulted in optical phase center variations of up to several decimeters. These fluctuations are a major limiting factor in deriving centimeter-level orbit solutions and therefore must be addressed by applying a range correction to each laser ranging measurement.

DGFI-TUM has developed an analytical correction function based on an empirical analysis of normal point observation data to the TOPEX/Poseidon spacecraft. The function uses the angle of view of the observation as seen from the LRA in combination with parameters that were

derived in an iterative estimation procedure. The obtained range correction is added to the modeled distance. Station-dependent correction parameters were estimated to account for the observation technology and data processing at each site.



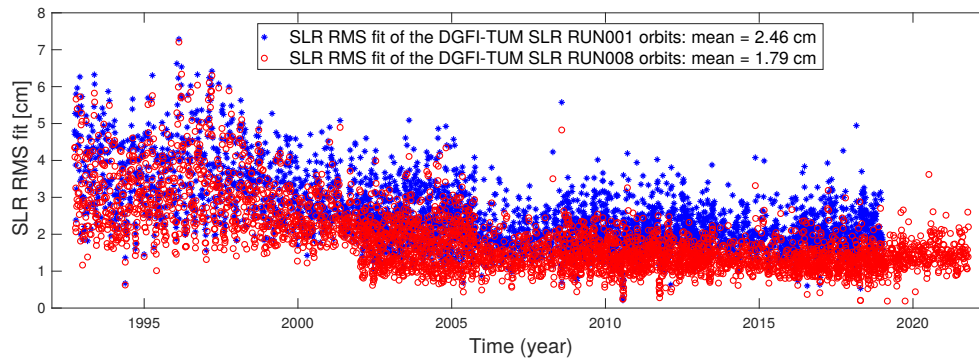
**Figure 1.7:** Range correction for SLR measurements of the Geodetic Observatory Wettzell to TOPEX/Poseidon: (a) Normal point residuals in the retroreflector frame; (b) Polar plot of revised residuals; (c) Range correction function based on the azimuth and incidence angle; (d) Enhanced range residuals obtained by applying the range correction.

Figure 1.7 shows the colour-coded SLR normal point residuals of the Geodetic Observatory Wettzell in the upper left polar plot. After the rejection of outliers (coloured dark blue, orange and red), revised residuals are obtained (panel b). A clear dependence on the angle of incidence in the retroreflector frame can be seen. This dependence is compensated for by the correction function, which forms the cone that can be seen in the lower left visualization (panel c). By applying the correction to each range measurement, the incidence dependence is removed and improved residuals are obtained (panel d). Similar correction functions are applied to the measurements of each SLR station that tracked the TOPEX/Poseidon satellite. Applying these correction functions reduces the root mean square (RMS) fit of the SLR observations over the entire duration of the mission from 33.78 to 1.97 cm. For more information about the parameter estimation and the correction function see <sup>(1)</sup>.

<sup>1</sup>Zeithöfler J., et al.: *Station-dependent satellite laser ranging measurement corrections for TOPEX/Poseidon*. Advances in Space Research, submitted

### Improvements in the accuracy of altimetry satellite orbits

In 2021, the orbit modeling for altimetry satellites was further elaborated in the DGFI-TUM software DOGS-OC. A new EIGEN-GRGS.RL04.MEAN-FIELD time-variable gravity field model<sup>2</sup> was implemented. In addition, numerous tests were performed on the optimal set of estimated parameters. The orbit of Jason-3 was extended by another 2.8 years from 9 January 2019 to 24 October 2021. Using these improvements in the background models and parameterization, new DGFI-TUM SLR RUN008 orbits were determined for the altimetry satellites TOPEX/Poseidon (27 September 1992 - 9 October 2005), Jason-1 (13 January 2002 - 30 June 2013), Jason-2 (20 July 2008 - 2 October 2019) and Jason-3 (17 February 2016 - 24 October 2021).



**Figure 1.8:** RMS differences of SLR observations of TOPEX/Poseidon, Jason-1, Jason-2, and Jason-3 of DGFI-TUM SLR RUN001 and RUN008 orbits.

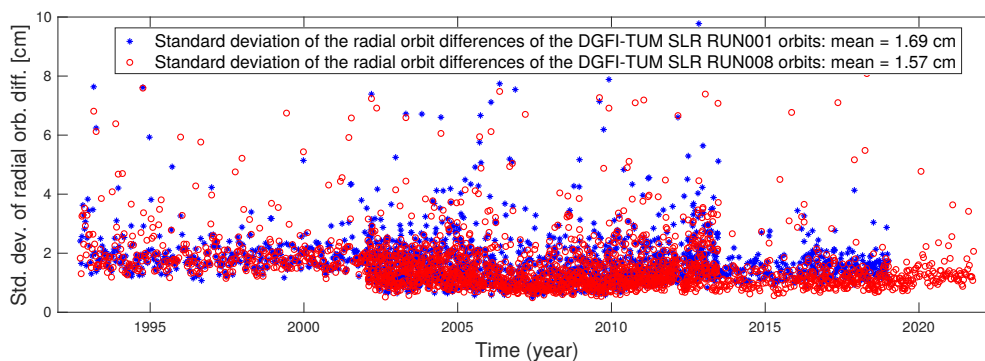


**Figure 1.9:** Standard deviation of the orbit differences in the radial directions of DGFI-TUM SLR RUN001 and RUN008 orbits with respect to GFZ VER13 orbits of TOPEX/Poseidon and Jason-1 and CNES POE-F orbits of Jason-2 and Jason-3. A few outliers larger than 10 cm were excluded when computing the mean values.

The orbits of the Jason satellites were derived using observation-based attitude realization<sup>3</sup>. The RMS fits of the SLR observations of these new orbits show a reduction (improvement) of 27% from 2.46 cm to 1.79 cm over the entire period from 27 September 1992 to 24 October 2021, compared to the DGFI-TUM SLR RUN001 orbits derived in 2019 using older background models and less dense parameterization (Fig. 1.8). The mean values of the RMS fits of the SLR observations are 1.37 cm for Jason-1, 1.35 cm for Jason-2, and 1.38 cm for Jason-3 for the DGFI-TUM SLR RUN008 orbits. The new orbits also show a reduction in the standard deviation of the orbit differences in the radial direction with respect to the GFZ

<sup>2</sup>Lemoine, J.M., et al.: *EIGEN-GRGS.RL04.MEAN-FIELD - Mean Earth gravity field model with a time-variable part from CNES/GRGS RL04*. IDS Workshop, 24-29 September 2018, Ponta Delgada, Portugal

<sup>3</sup>Bloßfeld M., et al.: *Observation-based attitude realization for accurate Jason satellite orbits and its impact on geodetic and altimetry results*. Remote Sensing, doi:10.3390/rs12040682, 2020

VER13 orbits of TOPEX/Poseidon and Jason-1<sup>4</sup> and CNES POE-F orbits of Jason-2 and Jason-3 (<https://cddis.nasa.gov/archive/doris/products/orbits/ssa/>), compared to the DGFI-TUM SLR RUN001 orbits. The improvement is 1.69 cm to 1.57 cm over the same time span (Fig. 1.9).

## 1.4 Determination of Reference Frames

### ITRS Combination Center of DGFI-TUM: DTRF2020

The International Earth Rotation and Reference Systems Service (IERS) has the task to release the new 2020 realization of the International Terrestrial Reference System (ITRS). Many institutions worldwide are engaged in the preprocessing, analysis and combination of the observations. As one of worldwide three ITRS Combination Centers of the IERS, DGFI-TUM is in charge of providing an independent ITRS realization, the DTRF2020.

The main tasks of the ITRS CC at DGFI-TUM in 2021 were (i) the analysis of the input data of the space geodetic techniques and the computation of one TRF solution per method, (ii) the approximation of the post-seismic deformation for stations affected by earthquakes, (iii) the analysis of the correction data for non-tidal loading provided by two institutions to decide which to use for the DTRF2020, and (iv) the analysis of the time series of datum parameters with respect to the realization of the DTRF2020 datum. The DTRF2020, the successor to the DTRF2014 (Seitz et al. 2021), is scheduled for publication in the first half of 2022.

#### *Analysis of space geodetic techniques*

The technique-specific input data were provided by IVS, ILRS, IGS and IDS between March and August 2021 and analyzed by the ITRS CC at DGFI-TUM. The analysis started with the reconstruction of normal equations from the input data series provided in the form of SINEX files. Brief feedback on the data was provided directly to the IAG Scientific Services. Figures 1.10 and 1.11 give an overview of the input data and their parameterization.

	VLBI (IVS)	SLR (ILRS)	GNSS (IGS)	DORIS (IDS)
# SINEX files	6210	1704	9851	1456
Solution type	session-wise NEQs	weekly and 15-day solutions	daily solutions	weekly solutions
Time-span/ years	1979-2021.0 41	1983-2021.0 38	1994-2021.0 27	1993-2021.0 28
# stations: all	156	151	1906	202
# included	<b>119</b>	<b>100</b>	<b>1425</b>	<b>161</b>
# DTRF2014	113	99	1409	153

**Figure 1.10:** Input data for the DTRF2020 provided by the IAG Scientific Services.

	Pole offsets	Pole rates	UT1- UTC	LOD	Nutation offsets
VLBI	x	x	x	x	x
SLR	x			x	
GNSS	x	x		x	
DORIS	x				

**Figure 1.11:** Parameters included in the input data.

<sup>4</sup>Rudenko S., et al.: *Impact of terrestrial reference frame realizations on altimetry satellite orbit quality and global and regional sea level trends: switch from ITRF2008 to ITRF2014*. Solid Earth, doi:10.5194/se-10-293-2019, 2019

Solution time series were then calculated for each technique as well as a first TRF solution per technique. Residual time series were analyzed with regard to discontinuities and outliers. Figure 1.12 shows the global DTRF2020 station network, the number of stations and the number of discontinuities. The time series were mainly evaluated visually, as this provides much better results than automated methods. Especially for GNSS, this was a very complex and labour-intensive task. Existing lists from the IAG Scientific Services, the discontinuities used in DTRF2014 and, for GNSS, the Nevada Geodetic Laboratory database (<http://geodesy.unr.edu/NGLStationPages/GlobalStationList>) were used as supporting information. Nevertheless, a re-analysis of the years already covered by the DTRF2014 was necessary. The time series of GNSS station positions are most affected by discontinuities due to many instrumental changes. An example time series of the station Marseille (France) is given in Figure 1.13.

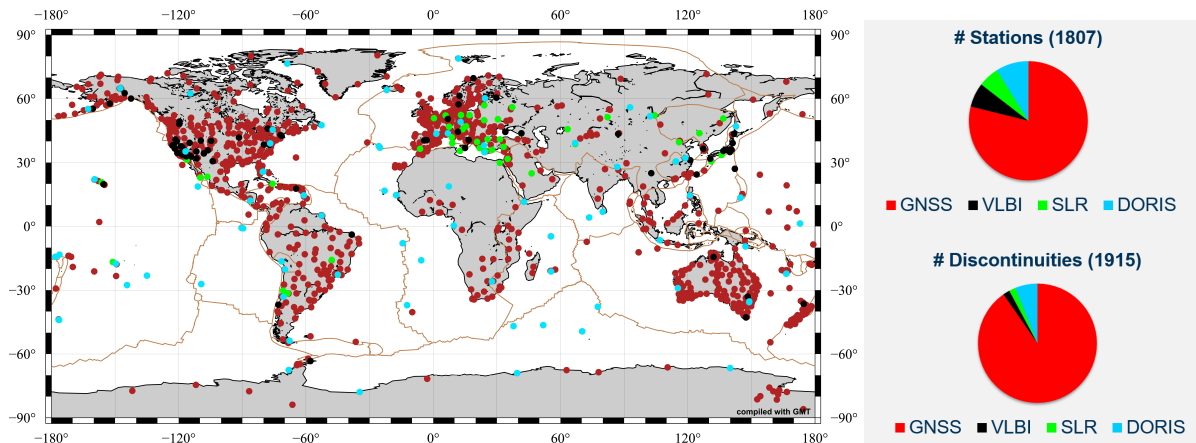


**Figure 1.12:** DTRF2020 station network (left) and the number of stations and the number of discontinuities for each contributing technique (right).

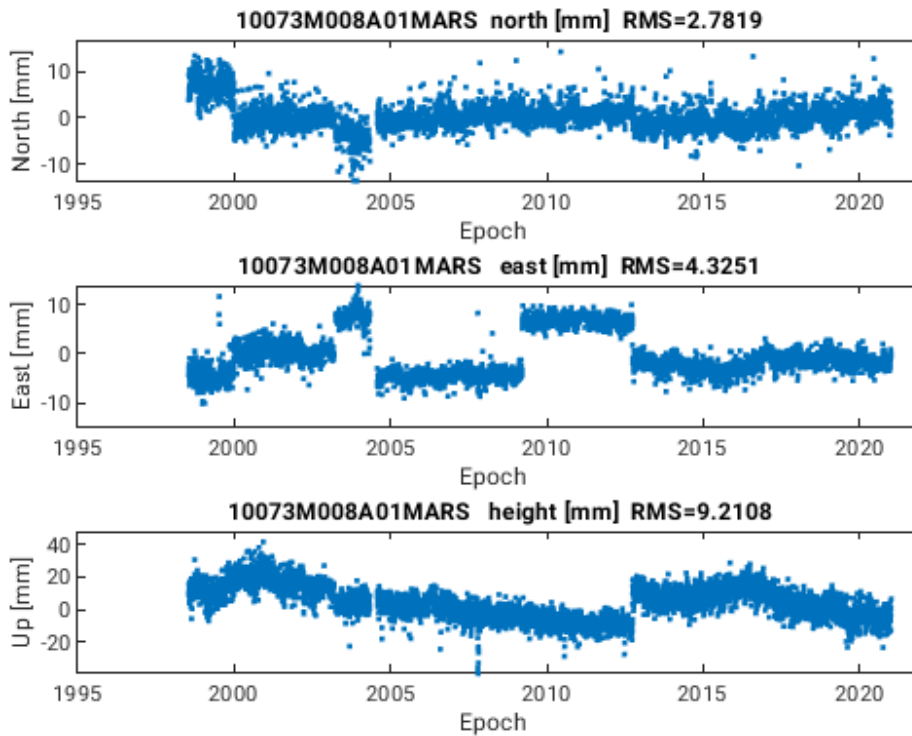


**Figure 1.13:** Station position time series of the GNSS station Marseille (France) with respect to the GNSS TRF solution.

### Approximation of post-seismic deformation

In DTRF2020, for the first time, the post-seismic deformation in the station motions is approximated by a combination of logarithmic and exponential functions. The approximations are then used to reduce the post-seismic deformation from the input normal equations (NEQ) before the station velocities are parameterized. In the approximation, in addition to the amplitudes of the two approximation functions, the respective decay times are also considered as unknown parameters, making the approximation a non-linear problem. It is solved by applying three different search algorithms, which yield very homogeneous results. The approximation is done for each component (North, East, up) separately. Figure 1.14 shows the approximation for the post-seismic motion of GNSS station Kashima after the Tohoku earthquake on 11 March 2011.

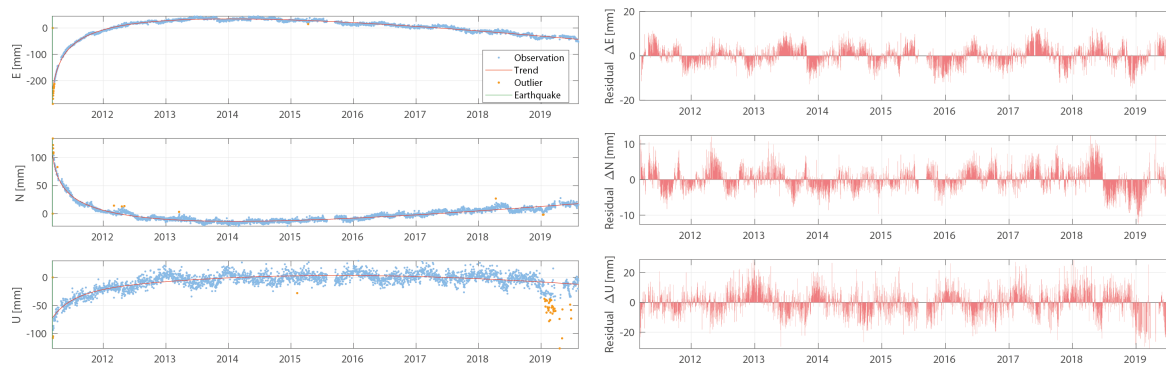


**Figure 1.14:** Approximation of the post-seismic motion at the GNSS station Kashima (Japan) after the Tohoku earthquake 2011 (left) and remaining residuals (right). The approximation is done by a combination of logarithmic and exponential functions.

### Analysis of non-tidal loading corrections derived from geophysical models

For the DTRF2020, the instantaneous station positions are corrected for non-tidal loading signals. Respective site displacements are generated from a geophysical model for non-tidal loading at NEQ level (Glomsda et al. 2021b). Two potential sources for such displacements were identified: the dedicated non-tidal loading data for the ITRS 2020 realization of the Global Geophysical Fluid Center (GGFC) and the operational non-tidal loading data of the Earth System Modeling Group of the Deutsches GeoForschungsZentrum Potsdam (ESMGFZ). The latter have the great advantage that they are updated daily and thus allow a timely extrapolation of the DTRF2020. The suitability of both data sets for application in a secular reference frame (like the DTRF2020) was investigated in detail: The raw time series of site displacements were compared and the contribution of both data sets to the geocenter motion was analyzed. The displacements were validated using the residuals of the daily GNSS positions. Figure 1.15 shows as an example the up-component of the time series of the station position of the GNSS station Sao Luis (Brazil) together with the non-tidal loading signals provided by GGFC and ESGFZ. Ultimately, the dedicated GGFC data were selected because, in contrast to the ESGFZ data, they do not contain intermediate changes in the linear trends of the displacement and geocenter motion time series. Such trend changes are difficult to handle in the realization of secular reference frames, even if they were a genuine geophysical phenomenon. In the case of ESGFZ, however, they are a result of the operational nature of the data, which favors the timely adaption of model updates over a complete reprocessing of the previous displacement series. Apart from this, the two data sets in our study were of similar quality. The GGFC displacements will be extended every few months so that, as with the ESGFZ data, non-tidal loading can be applied to extrapolate the DTRF2020<sup>5</sup>.

<sup>5</sup>Glomsda M., et al.: *Comparison of non-tidal loading data for application in a secular terrestrial reference frame*. Earth, Planets and Space, submitted

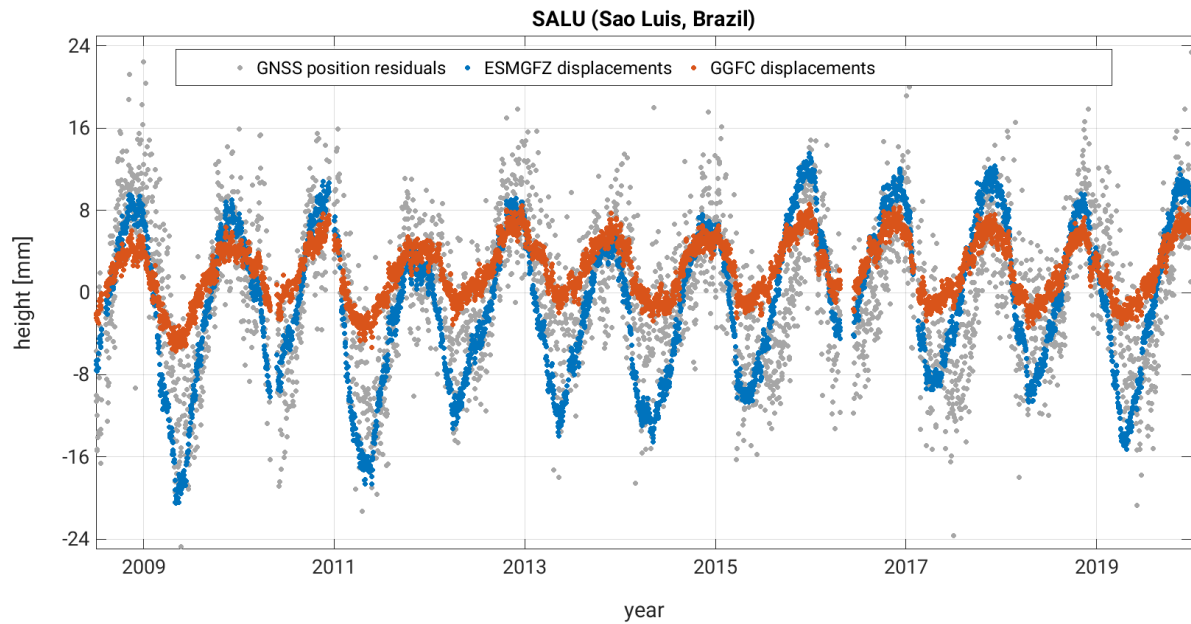


**Figure 1.15:** Time series of the up-component of the station Sao Luis (Brazil) with respect to the GNSS TRF solution and non-tidal loading corrections including atmosphere, hydrology and ocean provided by GGFC and ESMGFZ.

#### Analysis of datum parameter time series

The transformation of the weekly or session-wise solutions with the technique-specific TRF solutions provides time series for the datum parameters. The analysis of the intrinsic datum information used for the realization of the DTRF2020 datum is of great importance with regard to the long-term stability of the DTRF2020. Figure 1.16 shows the SLR translation time series as well as the SLR, VLBI and GNSS scale time series. It should be noted that GNSS provides for the first time an independent scale based on disclosed Galileo z-PCOs (phase center corrections in z-direction at the Galileo satellites). All time series show no signatures that have a significant impact on the individual linear fit, so that the entire time series will be further investigated for the realization of the DTRF2020 datum.

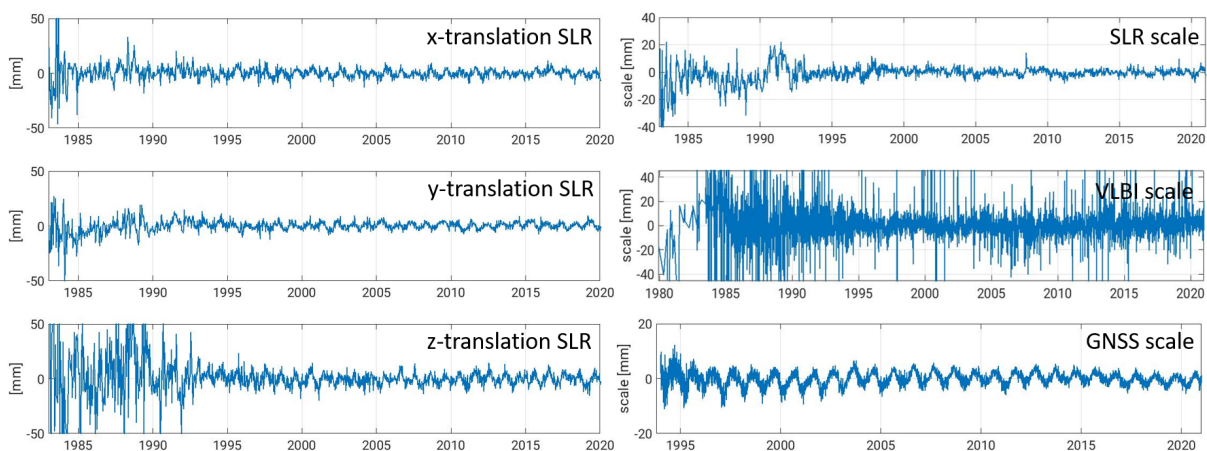


**Figure 1.16:** SLR translation time series (left) and SLR, VLBI and GNSS scale time series (right).



## International Height Reference Frame (IHRF)

The IAG introduced in 2015 the International Height Reference System (IHRF) as the conventional standard for the precise determination of physical heights worldwide. The IHRF is a gravity potential-based reference system: the vertical coordinates are geopotential numbers ( $C_P = W_0 - W_P$ ) referring to an equipotential surface of Earth's gravity field realized by the IAG conventional value  $W_0 = 62\,636\,853.4 \text{ m}^2\text{s}^{-2}$ . The spatial reference of the position P for the potential  $W_P = W(\mathbf{X})$  is given by the ITRF coordinates  $\mathbf{X}$ . The realization of the IHRF is the International Height Reference Frame (IHRF): a global reference network with precise geopotential numbers referring to the IHRF.

As the reference value  $W_0$  is constant and conventionally adopted, the main challenge in the establishment of the IHRF is the reliable determination of the potential values  $W_P$ . Accordingly, recent efforts concentrate on the computation and accuracy assessment of potential values  $W_P$  as IHRF coordinates based on the existing resources, namely, global gravity models of high resolution (GGM-HR), regional gravity field modeling (based on the outcomes of the Colorado Experiment, see below), and existing physical height systems (vertical datum unification into the IHRF/IHRF). As an example, Fig. 1.17 shows the geopotential number differences obtained after determining potential values using different approaches to solve the Geodetic Boundary Value Problem (GBVP). Based on this analysis and supported by a strong international collaboration in the frame of the IAG, DGFI-TUM has implemented a detailed roadmap for the realization of the IHRF (Sánchez et al. 2021), including:

- Strategy for the determination and evaluation of IHRF coordinates depending on the data availability (especially surface gravity data and topography models),
- Strategy for the appropriate handling of permanent tide effects in the determination of IHRF coordinates in the mean-tide system,
- Strategy to improve the input data required for the determination of IHRF coordinates,
- Strategy for the IHRF station selection in regional and national densifications,
- Strategy to ensure the usability and long-term sustainability of the IHRF.

A cornerstone of all this work is the successful completion of the so-called Colorado Experiment under the coordination of DGFI-TUM. Within this experiment, fourteen groups from different countries computed geoid undulations, height anomalies, and potential values in Colorado (USA) using the same gravity and topography input data provided by US National Geodetic Survey (NGS), but different modeling strategies. The fourteen solutions represent the state-of-the-art in precise gravity field modeling of high resolution and the results of this experiment provide a benchmark in the calibration of regional gravity field modeling methods (more details in Wang et al. 2021).

The central role of DGFI-TUM is not only related to the coordination of the Colorado Experiment, but also to the analysis of gravity data by computing height anomalies and potential values using spherical radial basis functions (see Section 3.2). The DGFI-TUM solution (No. 9 in Fig. 1.17, bottom left) is the only one based on this methodology and presents the best agreement in terms of standard deviation ( $0.09 \text{ m}^2\text{s}^{-2}$ , equivalent to 0.009 m) with respect to the mean value obtained from all solutions. The high performance of DGFI-TUM's quasi-geoid solution compared to the other ones is also discussed in Wang et al. (2021).

To continue advancing the methodologies needed for a reliable implementation of the IHRF, DGFI-TUM together with TUM's Chair of Astronomical and Physical Geodesy (APG) started the **DFG Project Geo-H** (Enhanced Geopotential Field Modeling as Basis for the Establishment of Precise Height Systems) in September 2021.

Main objectives of Geo-H are:

- To quantify with high reliability the error budget of the physical height determination,
- To develop new concepts and methods towards improved geopotential solutions and their accuracy assessment,
- To provide scientific guidelines for the realization of globally consistent geopotential-based height systems.

This project is also set up as the perfect platform to continue developing DGFI-TUM's radial basis functions' method for the precise regional gravity field modeling (see Section 3.2). DGFI-TUM's research on the IHRS/IHRF has a widely international acceptance and has been the subject of numerous publications, not only in specialized fields, but also in magazines and media for non-specialists; see e.g., Sánchez (2021).

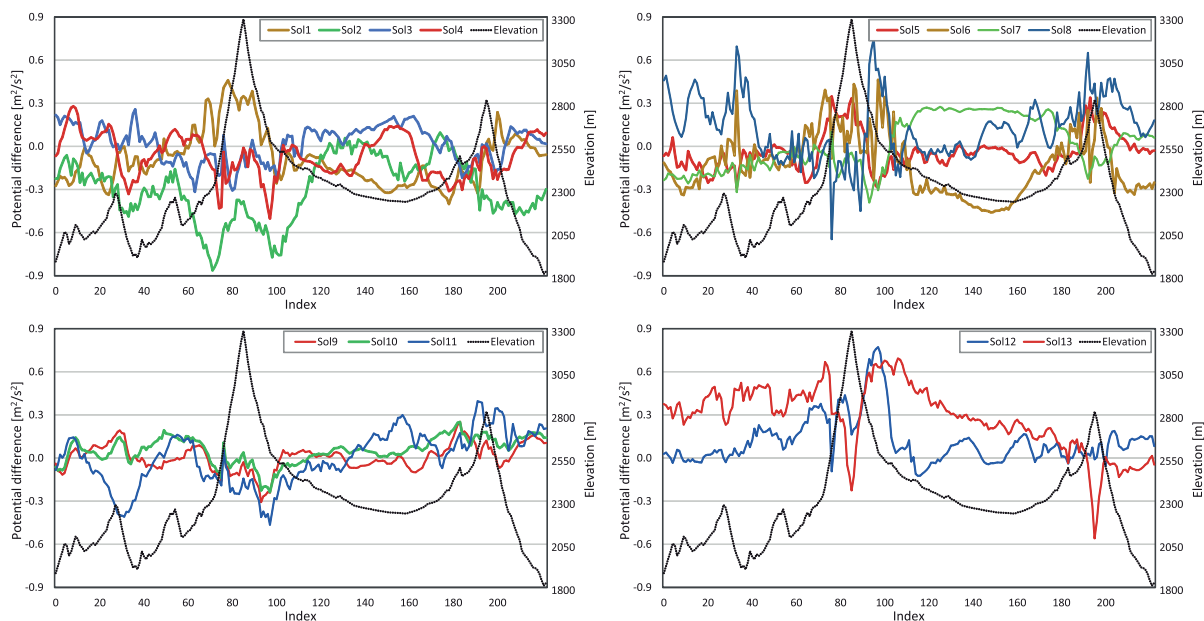


**Figure 1.17:** Geopotential number differences with respect to the mean value of thirteen solutions. Solutions are grouped according to the main data processing approach, adapted from Sánchez et al. (2021): (a) Solutions based on the scalar-free GBVP after Molodeny's Theory using FFT integration and a Wong-Gore (or similar) modification of the integral kernel (top left); (b) Solutions based on the scalar-free GBVP after Molodeny's Theory with a least-squares modification of Stokes' formula with additive corrections (top right); (c) Solutions based on least-squares collocation (10 and 11) and spherical radial basis functions (9) (bottom left); (d) Solutions based on the scalar-free GBVP after Stokes' Theory and converted to the quasi-geoid using the Bouguer Anomaly-based term (bottom right).

### GGOS Focus Area Unified Height System (GGOS-FA-UHS)

DGFI-TUM coordinates the GGOS Focus Area "Unified Height System" (GGOS-FA-UHS) since July 2015. GGOS-FA-UHS (formerly Theme 1) was established at the GGOS Planning Meeting (February 1 - 3, 2010, Miami, Florida, USA) to lead and coordinate the efforts required for the establishment of a global unified height system that serves as a basis for the standardization of height systems worldwide. Starting point were the results delivered by the IAG Inter-Commission Project 1.2 Vertical Reference Frames (IAG-ICP1.2-VRF), which was operative from 2003 to 2011. During the 2011-2015 term, different discussions focused on the best possible definition of a global unified vertical reference system resulted in the IAG resolution for the definition and realization of an International Height Reference System (IHRS) that was approved during the 2015 General Assembly of the International Union of Geodesy and

Geophysics (IUGG) in Prague, Czech Republic. In the term 2015-2019, actions dedicated to investigate the best strategy for the realization of the IHRF (i.e., the establishment of the IHRF) were undertaken. In particular, a preliminary station selection for the IHRF reference network was achieved (Fig.1.18) and different computation procedures for the determination of potential values as IHRF coordinates were evaluated (see previous Section).

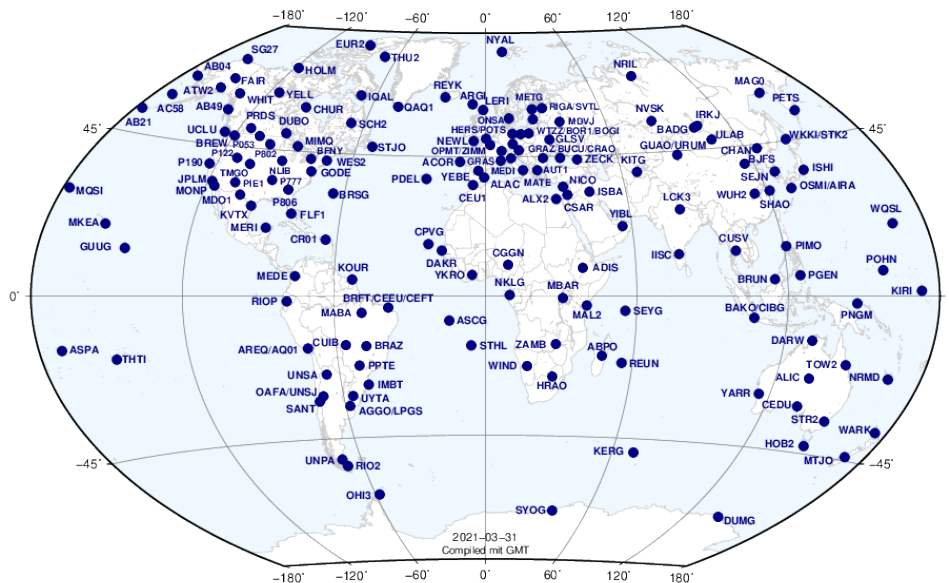


Figure 1.18: IHRF reference network as of 31 March 2021.

At present, a special issue on Reference Systems in Physical Geodesy hosted by the *Journal of Geodesy* is almost completed. This special issue includes the scientific description of the best available strategies for the (quasi-)geoid modeling as well as key contributions for the establishment of the IHRF/IHRF and the IGRS/IGRF (International Gravity Reference System and Frame). DGFI-TUM contributed to this special issue with three first-authored and one second-authored publications, among them Sánchez et al. (2021) and Wang et al. (2021).

The ongoing activities of the GGOS-FA-UHS are:

- Based on the procedures described by Sánchez et al. (2021), to coordinate with regional/national experts in gravity field modeling the determination of potential values at the IHRF reference stations (Fig. 1.18),
- To refine standards, conventions, and guidelines to support a consistent determination of the IHRF at regional and national levels,
- With the support of the IAG Commission 2 (Gravity Field), the International Gravity Field Service (IGFS) and the Inter-Commission Committee on Theory (ICCT) to promote the study of quality assessment in the determination of potential values and determination of potential changes with time.
- In agreement with the IGFS and the IAG Commission 2, to design a strategy to install an operational infrastructure within the IGFS to ensure the maintenance and availability of the IHRF in a long-term basis. Aspects to be considered are: (i) Updates of the IHRF definition and realization according to future improvements in geodetic theory and observations; (ii) Regular updates of the IHRF according to new stations, coordinate changes with time, improvements in the estimation of reference coordinates and modeling of the Earth's gravity field, etc.; (iii) Support in the realization and utilization of the IHRF at regional and national level; and (IV) To guarantee an organizational and operational infrastructure to ensure the sustainability of the IHRF.

## Regional terrestrial reference frame in Latin America (SIRGAS)

DGFI-TUM acts as the IGS Regional Network Associate Analysis Center for SIRGAS (IGS RNAAC SIRGAS) since June 1996. The main objective of the IGS RNAAC SIRGAS is the development of analysis strategies to ensure the long-term reliability and stability of the regional reference frame. SIRGAS (Sistema de Referencia Geocéntrico para las Américas) is the regional densification of the ITRF in Latin America. Currently, it is composed of about 450 continuously operating GNSS (GPS + GLONASS + GALILEO + BEIDOU) stations, which are processed by 10 analysis centers on a weekly basis. DGFI-TUM's research in the context of SIRGAS is focused on (a) defining the best strategy for the datum realization and observation combination within the regional reference frame processing; (b) improving modeling and representation of the reference frame kinematics to ensure a suitable transformation of station positions between pre- and post-seismic frame realizations; and (c) to assess non-linear station movements within the reference frame computation to improve the estimation of epoch coordinates.

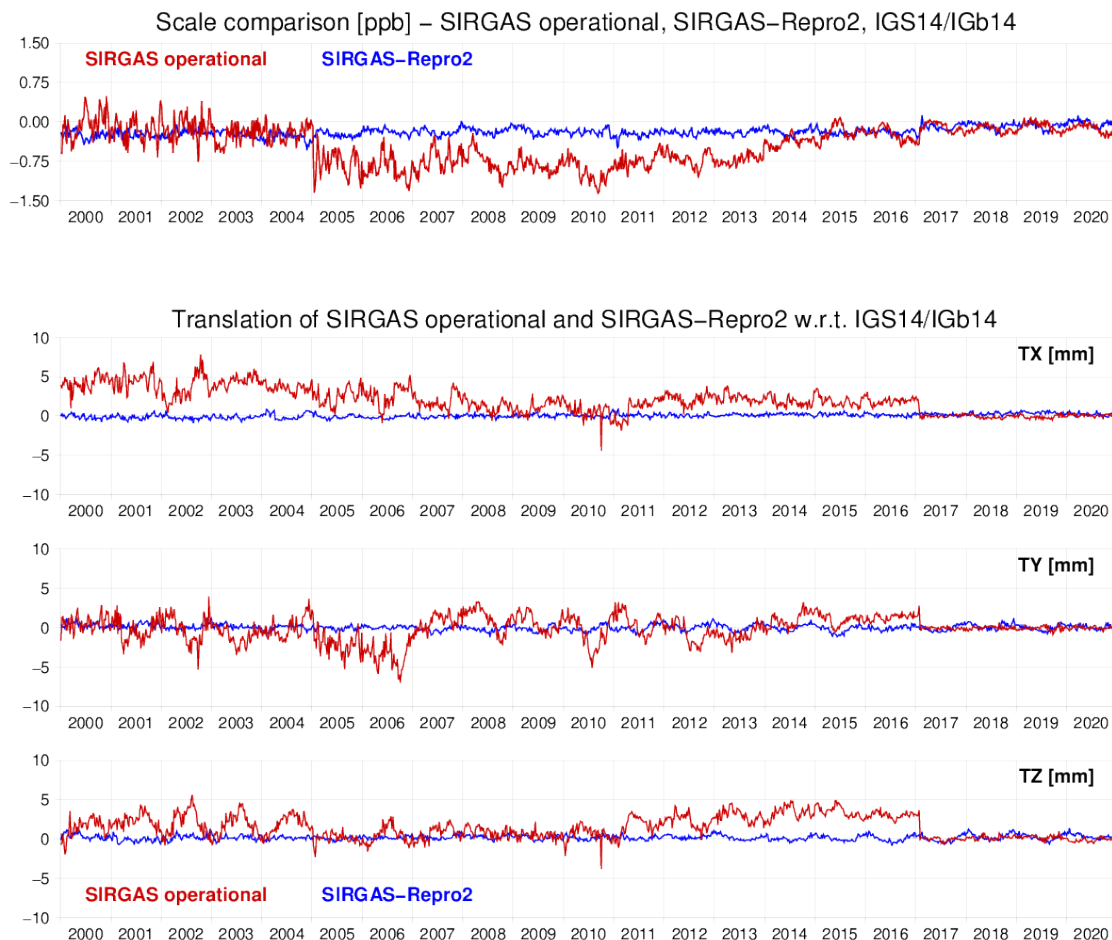


**Figure 1.19:** Transformation parameters (scale and translations) between the operational weekly SIRGAS solutions (transformed to IGS14/IGb14) and SIRGAS-Repro2 weekly coordinates.

The operational SIRGAS products refer to the IGS reference frame valid at the time when the GNSS data are routinely processed. DGFI-TUM performed in 2010 a first reprocessing campaign of the SIRGAS reference network in order to determine SIRGAS coordinates based on absolute corrections for the GPS antenna phase center variations and referring to the IGS05 reference frame. A reprocessing referring to the IGS08/IGb08 frame was not un-

dertaken. In this way, the SIRGAS weekly normal equations presently refer to different reference frames: IGS05 (from January 2000 to April 2011), IGS08/IGb08 (from April 2011 to January 2017), IGS14/IGb14 (since January 2017). To ensure the long-term stability of the SIRGAS reference frame, DGFI-TUM performed a second reprocessing (hereinafter referred to as SIRGAS-Repro2) of the SIRGAS GNSS historical data since January 2000 using the ITRF2014 (IGS14/IGb14) as reference frame. Figure 1.19 shows the transformation parameters between the operational weekly SIRGAS solutions (transformed to IGS14/IGb14) and SIRGAS-Repro2 weekly coordinates referring to the IGS14/IGb14. Figure 1.20 depicts the RMS differences between the operational weekly SIRGAS solutions (transformed to IGS14/IGb14) and SIRGAS-Repro2 weekly coordinates with respect to the weekly coordinates of the IGS stations in IGS14/IGb14. The large values before April 2017, when the ITRF2014 was adopted for the generation of the IGS products, makes it evident that there is a need to reprocess the historical data of any reference frame whenever a new ITRF solution is released.

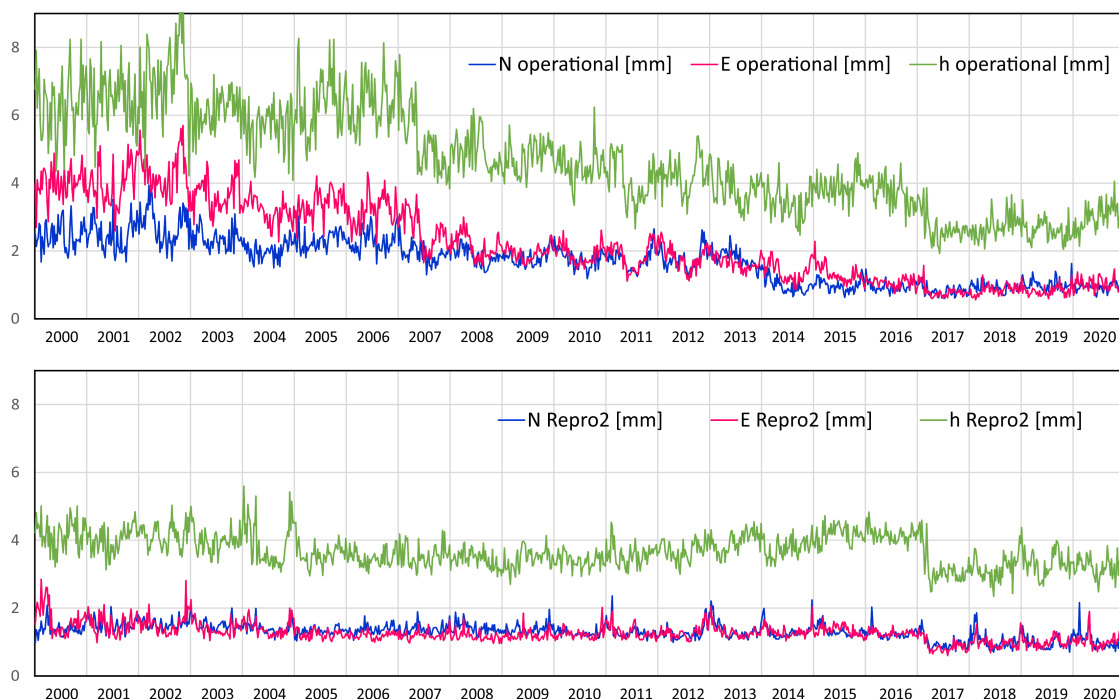


**Figure 1.20:** RMS values of the differences between the operational weekly SIRGAS solutions (transformed to IGS14/IGb14, upper panel) and SIRGAS-Repro2 weekly coordinates (lower panel) with respect to the weekly coordinates of the IGS stations in IGS14/IGb14. The discontinuity observed in April 2017 is a consequence of changing the antenna phase center variation model after adopting the ITRF2014 for the generation of the IGS products.

Current efforts concentrate on modeling post-seismic deformation for SIRGAS stations affected by strong earthquakes as a complement to a 21-year cumulative solution of the SIRGAS reference frame. Figure 1.21 shows the horizontal velocities obtained in the usual computation of reference frames by segmentation of the time series to fit station linear motions. Post-seismic modeling should be performed for about 40 stations (Fig. 1.22).

Analysis strategies, research results, and scientific data sets generated by DGFI-TUM in its functions as SIRGAS Analysis Centre and IGS RNAAC SIRGAS are provided at [www.sirgas.org](http://www.sirgas.org) and [ftp.sirgas.org](ftp://ftp.sirgas.org).

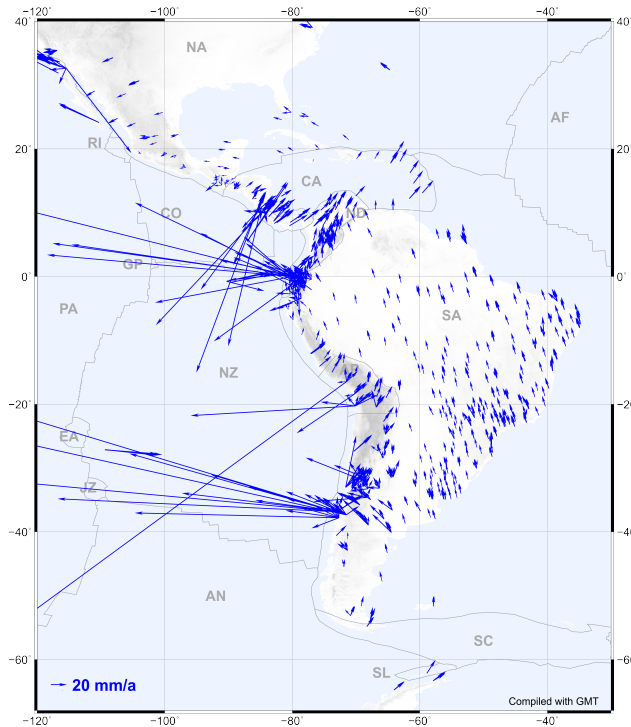


**Figure 1.21:** SIRGAS horizontal velocities obtained in the usual computation of reference frames by segmentation of the time series to fit linear motions.

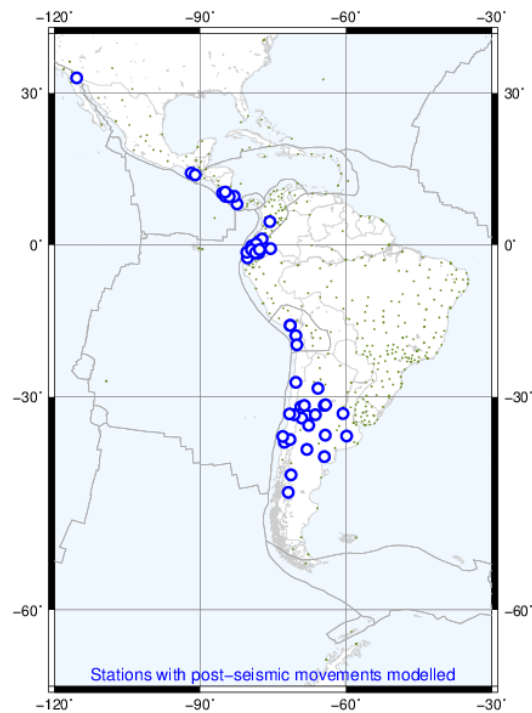


**Figure 1.22:** SIRGAS stations with post-seismic effects to be modeled as a complement to a 21-year cumulative solution of the SIRGAS frame.

## Geocentric realization of regional Epoch Reference Frames

Today, there is a vital interest in global geodetic applications, such as the use of precise positioning and navigation systems, or the accurate detection and monitoring of Earth system processes at different spatial scales. It is essential that the observations provided by different observing systems are related to a unique global reference frame so that they can be correlated and evaluated together.

The ITRF is the global reference frame used in geodesy. However, in order to provide users with local access to the reference frame, the ITRF is densified by (usually GNSS-based) regional reference frames. These regional reference frames are aligned to the ITRF datum via No-Net-Rotation (NNR) and No-Net-Translation (NNT) constraints. While the linear parameterization of the ITRF results in its origin reflecting the Earth's center of mass (CM) only in a mean sense (i.e. on secular time scales), station displacements on seasonal and short time scales in geodetic networks aligned to the ITRF datum rather relate to the geometric center of the Earth, often referred to as the center of figure (CF)<sup>6</sup>. Consequently, displacements represented in reference frames aligned with the ITRF datum do not show the full geophysical signal and require a correction for the variation of the ITRF origin with respect to the instantaneous geocenter.

At the example of the Latin American SIRGAS network, the feasibility of a stable datum realization for a weekly Epoch Reference Frame (ERF) was investigated, where the datum is realized using global networks. The physically defined datum parameters origin and scale were realized from SLR and VLBI observations, while the orientation was realized by an NNR constraint over a global GNSS network (Fig. 1.23). The combination was performed at the NEQ level, introducing measured local ties at co-location sites as constraints. A filtering procedure for SLR and VLBI data was applied to improve the long-term stability of the realized datum.

<sup>6</sup>Dong, D., et al.: *Origin of the International Terrestrial Reference Frame*. Journal of Geophysical Research: Solid Earth, doi:76210.1029/2002JB002035, 2003

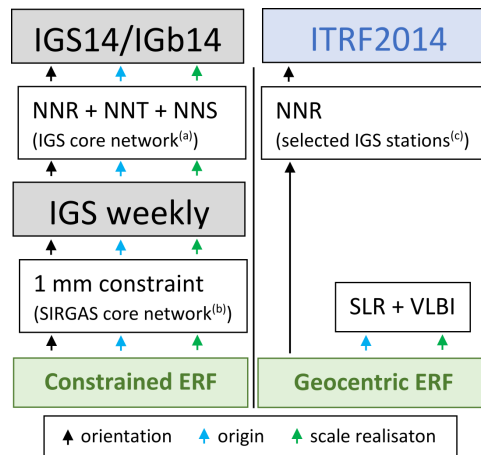


**Figure 1.23:** Concepts of datum realization for the SIRGAS regional ERFs aligned to the ITRF datum (left) and a direct geocentric realization of the SIRGAS regional ERFs as realized in this study (right). The datum of the IGS14/IGb14 and the ITRF2014 reference frames is considered identical. Figure taken from <sup>(7)</sup>.

The input data used was a reprocessed five-satellite SLR constellation including Etalon-1/2, LAGEOS-1/2 and LARES, as well as VLBI session data from DGFI-TUM reprocessing for the ITRS 2020 realization and a reprocessed SIRGAS network extended with global IGS sites (see Section 1.1, Fig. 1.3). The technique-specific input data were provided in the form of weekly (SLR, GNSS) or session-wise (VLBI) normal equations (NEQs) in SINEX format. Comparing the results with geophysical non-tidal loading (NTL) models of the Earth System Modeling Group of Deutsches GeoForschungsZentrum Potsdam (ESMGFZ), it could be shown that the geocentric displacement time series realized with the new approach directly reflect seasonal geophysical processes in a CM-related system (Fig. 1.24).

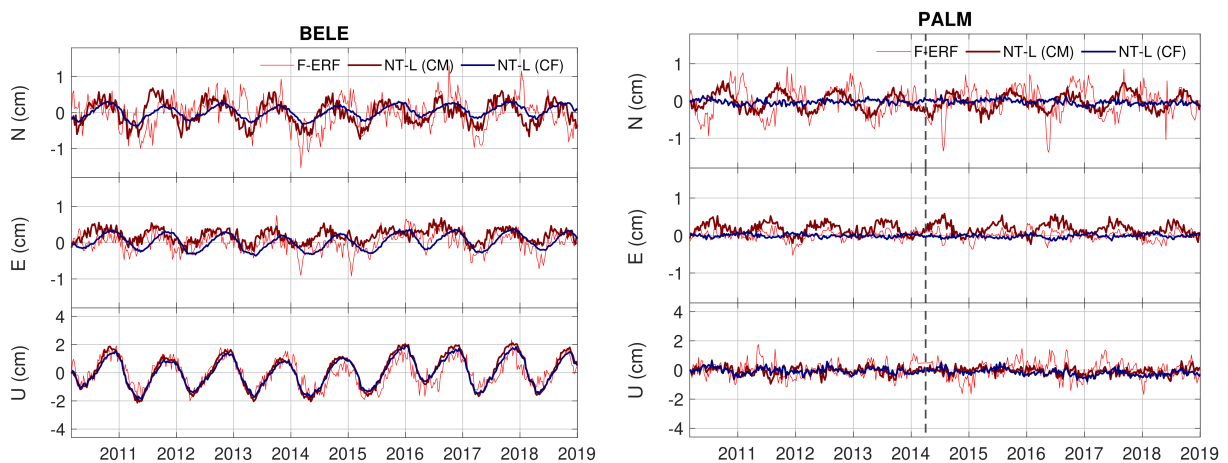


**Figure 1.24:** Coordinate time series of stations BELE (Belém, Brazil, left) and PALM (Palmer, Antarctica, right) from the geocentric filtered ERF solution (F-ERF) compared with the ESMGFZ NTL time series in CM- and CF-frames. Figure adapted from <sup>(7)</sup>.

The fundamental advantage of the developed approach is that the resulting geodetic displacement time series are geocentric at all epochs and can be used directly to investigate underlying geophysical processes. Since the approach incorporates global networks and does not have to rely on co-location sites in the region of interest, it is conceptually transferable to any other - potentially seismically active - region. Details of the developed combination and filter strategy are described in <sup>(7)</sup>.

<sup>7</sup>Kehm A., et al.: *Combination strategy for geocentric realisation of regional epoch reference frames*. Journal of Geophysical Research, submitted

## Mass transports in the cryosphere and their impact on Earth rotation

The DFG project CIEROT aims to determine the long-term shift of the Earth's rotation pole caused by climate-related mass changes in the Antarctic and Greenland ice sheets (AIS/GIS). These mass changes are estimated based on gravity field changes observed with the Gravity Recovery and Climate Experiment (GRACE) mission and ice sheet height changes measured by satellite altimetry (Göttl et al, 2021). To investigate the effects of ice loss on polar motion, both types of data are converted into effective angular momentum functions, also called polar motion excitation functions ( $\chi_1$ ,  $\chi_2$ ). On seasonal time scales, the effect of ice mass loss is relatively small compared to atmospheric, oceanic and hydrological excitations, but it still is an important factor for the closure of the angular momentum budget.

Investigations of the mass changes showed that in particular the component  $\chi_1$  is influenced by the superposed effect of AIS and GIS, whereas in component  $\chi_2$  both contributions almost compensate each other (Fig. 1.25). Ice loss in Greenland causes a pole drift toward  $39.0^\circ$  West with an amplitude of 3.1 mas/year. Ice mass change in Antarctica causes a pole drift toward  $55.7^\circ$  East with an amplitude of 2.3 mas/year. With regard to seasonal polar motion, the ice mass changes of the two ice sheets only play a subordinate role and contribute a few percent to the overall effect. Again, the contribution of GIS is larger than that of AIS, and due to the different seasons the signals from GIS and AIS behave out of phase.

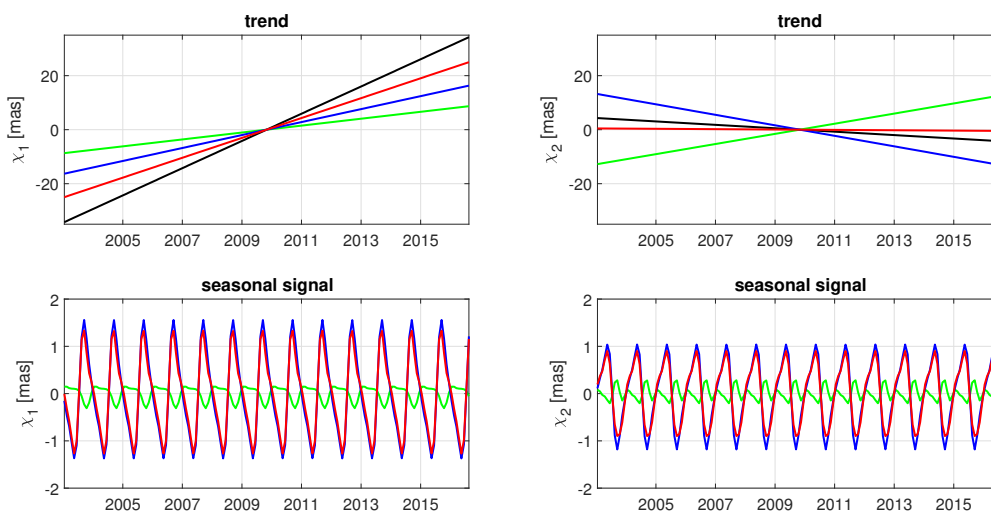


**Figure 1.25:** Trends and seasonal signals of the polar motion excitation functions  $\chi_1$  and  $\chi_2$  for AIS (green), GIS (blue), AIS+GIS (red) and the overall effect including atmosphere, oceans, hydrology and solid Earth (black).

## Related publications

Glomsda M., Seitz, M., Bloßfeld M., Kehm A., Gerstl M., Angermann D.: *First VLBI-only TRF/CRF solution based on DGFI-TUM data for ITRF2020*. Proceedings of the 25th EVGA Working Meeting, 2021a

Glomsda M., Bloßfeld M., Seitz M., Seitz F.: *Correcting for site displacements at different levels of the Gauss-Markov model - A case study for geodetic VLBI*. Advances in Space Research, doi:10.1016/j.asr.2021.04.006, 2021b



- Göttl F., Groh A., Schmidt M., Schröder L., Seitz F.: *The influence of Antarctic ice loss on polar motion: an assessment based on GRACE and multi-mission satellite altimetry*. Earth, Planets and Space, doi:[10.1186/s40623-021-01403-6](https://doi.org/10.1186/s40623-021-01403-6), 2021
- Hellmers H., Modiri S., Bachmann S., Thaller D., Bloßfeld M., Seitz M. Gipson J.: *Combined IVS contribution to the ITRF2020*. Proceedings of the 25th EVGA Working Meeting, 2021
- International Altimetry Team: Abdalla S., Abdeh Kolahchi A., ... Dettmering D., ... Passaro M., ... Rudenko S., ... Schwatke C., ... et al.: *Altimetry for the future: Building on 25 years of progress*. Advances in Space Research, doi:[10.1016/j.asr.2021.01.022](https://doi.org/10.1016/j.asr.2021.01.022), 2021
- Rudenko S., Bloßfeld M., Zeitlhöfler J.: *DGFI-TUM Associate Analysis Center*. In: Soudarin L. and Ferrage P. (Eds.), International DORIS Service Activity Report 2019-2020, 2021
- Sánchez L.: *Das neue Internationale Höhenreferenzsystem (IHR)*. FORUM: Zeitschrift des Bundes der Öffentlich bestellten Vermessungsingenieure e.V., 3/2021, 4-13, 2021
- Sánchez L., Kehm A.: *SIRGAS Regional Network Associate Analysis Centre (IGS RNAAC SIRGAS) Technical Report 2020*. International GNSS Service Technical Report 2020, 135-146, doi:[10.48350/156425](https://doi.org/10.48350/156425), 2021
- Sánchez L., Ågren J., Huang J., Wang Y.M., Mäkinen J., Pail R., Barzaghi R., Vergos G.S., Ahlgren K., Liu Q.: *Strategy for the realization of the International Height Reference System (IHR)*. Journal of Geodesy, doi:[10.1007/s00190-021-01481-0](https://doi.org/10.1007/s00190-021-01481-0), 2021
- Seitz M., Bloßfeld M., Angermann D., Seitz F.: *DTRF2014: DGFI-TUM's ITRS realization 2014*. Advances in Space Research, doi:[10.1016/j.asr.2021.12.037](https://doi.org/10.1016/j.asr.2021.12.037), 2021
- Wang Y.M., Sánchez L., Ågren J., Huang J., Forsberg R., Abd-Elmotaal H.A., Ahlgren K., Barzaghi R., Bašić T., Carrion D., Claessens S., Erol B., Erol S., Filmer M., Grigoriadis V.N., Isik M.S., Jiang T., Koç Ö., Krcmaric J., Li X., Liu Q., Matsuo K., Natsiopoulou D.A., Novák P., Pail R., Pitoňák M., Schmidt M., Varga M., Vergos G.S., Véronneau M., Willberg M., Zingerle P.: *Colorado geoid computation experiment: overview and summary*. Journal of Geodesy, doi:[10.1007/s00190-021-01567-9](https://doi.org/10.1007/s00190-021-01567-9), 2021

## 2 Research Area Satellite Altimetry

*Accurate knowledge and continuous monitoring of the world's water resources are essential for human life and development - especially in the face of climate change. Since 1992, satellite altimetry has enabled precise observation of the water surface and its changes over time - continuously and worldwide, even in remote areas without ground infrastructure. Originally designed to observe the water level of the open ocean, today satellite altimetry is used to determine different parameters of the water surface and their changes over time, in the open ocean as well as in coastal and polar seas and also in inland waters. These parameters include the so-called Essential Climate Variables (ECV) defined by the Global Climate Observing System (GCOS): sea level, sea state, surface currents and level changes of lakes and rivers.*

*DGFI-TUM is working on advanced methods to further improve the quality and applicability of satellite altimetry observations for various phenomena of the oceanic and continental hydrosphere. Accurately determining the geometric shape of the water surface in space and time and investigating its temporal changes in terms of underlying dynamic processes in both components of the Earth's global water cycle is one of the primary research goals of DGFI-TUM.*

*The satellite altimetry data used at DGFI-TUM now cover a period of almost 30 years and thus enable the recording of long-term climate changes. While only a few missions provided data in the early years, ten satellites are now operating simultaneously. This necessitates careful harmonization and calibration of the data, but also enables unprecedented spatial resolution (Section 2.1). In addition, the altimetry instruments on board the satellites are also constantly being improved, so that the data are becoming more accurate and have a higher along-track resolution. Particularly worth mentioning here is the launch of the Sentinel-6 mission in November 2020, whose data has become available for the first time in 2021.*

*In order to achieve optimal data use for various applications in the ocean and inland, the Institute operates its own database in which the measurements of all missions since 1992 are kept. The data are combined into a multi-mission data set that is used in ocean research (section 2.2) and continental hydrology (section 2.3). In addition to studying the ECVs mentioned above, DGFI-TUM also investigates derived quantities such as river discharge, surface water storage and vertical land motion.*

### 2.1 Multi-Mission Analysis

#### **Altimeter database updates**

DGFI-TUM maintains its own altimeter database, which is continuously updated with the latest measurements and correction models. The consistently preprocessed high-resolution multi-mission data provide the basis for targeted investigations. In 2021, the first data from the new Sentinel-6A Michael Freilich mission were integrated. This mission continues the successful NASA/CNES missions TOPEX/Poseidon and Jason-1 to -3 and flew in tandem with Jason-3 in 2021.

Thanks to its interleaved mode, Sentinel-6 can measure in parallel in low resolution (LR) and high resolution (HR) mode, the latter also called SAR mode. This allows for the first time ever a detailed comparison of both measurement modes under exactly the same conditions.

A first cross calibration applying DGFI-TUM's multi-mission crossover analysis MMXO<sup>1</sup> shows a mean range bias of 9.5 mm for Sentinel-6 LR data and of 3.5 mm for HR data with respect to Jason-3 in the period March to December 2021 (Fig. 2.1). During these first months of observation, no significant drift could be detected for either the LR or HR data.

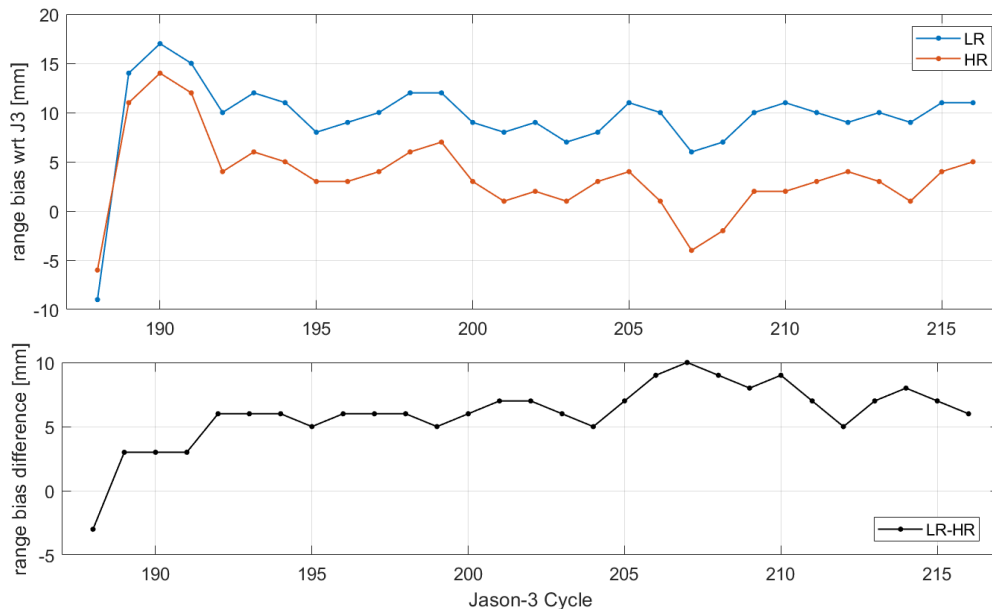


**Figure 2.1:** Sentinel-6 range bias with respect to Jason-3 for LR data (blue) and HR data (red) and their difference (bottom; black) for the period March to December 2021.

## Long-term behavior of ionospheric correction

For a highly accurate determination of water levels from altimetry measurements, numerous range corrections must be applied to account for environmental conditions. One of these is the ionospheric correction, which compensates for the influence of free electrons in the Earth's high atmosphere. An important aspect here is high long-term stability, so that no artificial jumps or drifts affect the derived parameters, such as the change in global mean sea level (GMSL).

In the case of dual-frequency altimeters, the ionospheric range correction can be estimated directly from the altimetry measurements. However, in the case of single carrier frequency missions (such as Cryosat-2 or Saral), data from external models are often used. One possible source are Global Ionosphere Maps (GIM), which are calculated based on GNSS measurements and represent the vertical total electron content (VTEC). These corrections are also part of the altimetry data sets, the so-called geophysical data records (GDR).

A recent study of DGFI-TUM (Dettmering and Schwatke, 2022) has now shown that applying the GIM corrections underestimates the GMSL rise by up to 1 mm/year, depending on the period studied. The reason for this is that the GIM corrections currently included in the GDR do not take into account the plasmasphere bordering the ionosphere above. Neglecting the influence of the plasmasphere leads to systematic errors with an 11-year cycle that have a significant impact on the estimate of global mean sea level change. The impact for the period 1999-2021 is estimated to be about 0.3 mm/year. It is recommended that additional scaling of the available corrections is applied to reduce the trend error to below 0.05 mm/year.

<sup>1</sup>Bosch W., Dettmering D., Schwatke C.: *Multi-mission cross-calibration of satellite altimeters: constructing a long-term data record for global and regional sea level change studies*. Remote Sensing, doi:10.3390/rs6032255, 2014

## 2.2 Sea Surface

### Global coastal sea level

In the framework of the **ESA Climate Change Initiative (CCI) Sea Level project**, a novel altimetry-based coastal sea level data record has been created. Many coastal regions are exposed to sea level rise and thus increasingly threatened by flooding risks during extreme events. In this context, DGFI-TUM has a project task of particular relevance by developing and testing improved radar signal processing techniques to exploit the radar signal in the coastal zone and to correct the measurements.

During 2021, a study illustrated the benefit of the X-TRACK/ALES processing used in this project (Birol et al., 2021). This processing matches three main elements that differ from the classic open ocean processing chain: firstly, the reprocessing of altimetric waveforms with a specific fitting algorithm aimed at improving the quality and quantity of the range measurements in the coastal zone; secondly, the application of a high-rate sea state bias, i.e. the correction of the range measurements for errors related to the interaction of the radar signal with ocean waves; thirdly, a selection of corrections and geophysical adjustments to the radar signal specifically selected and filtered to enhance the validity of sea level retrievals close to the coast.

Thanks to X-TRACK/ALES and the use of 20-Hz measurements, the generated coastal sea level data record reaches a distance of 1.2–4 km to the coast. This data record is validated with tide gauges, obtaining an average value of 0.77 in terms of Pearson's correlation coefficient.

Besides the sea level trend analysis, the X-TRACK/ALES data record available from the CCI Sea Level project can be used to map ocean geostrophic current variability up to 5 km to the coast. Moreover, it has been already used to successfully detect storm surges in the Adriatic Sea, showing that the spatial, and implicitly temporal, variability of the fields is much higher than what is shown by models (Cavaleri et al. 2021).

### New sea level data sets for North Sea and Baltic Sea

In 2021, a comprehensive data set of regional sea level variations in the North Sea and the Baltic Sea has been created, including coastal areas and regions covered by sea ice. The two new data sets, named *North SEAL* and *Baltic SEAL* provide insights into long-term and seasonal sea level changes over the past quarter century. This information is of vital importance for planning protective measures and for understanding dynamic processes in the oceans and the climate system.

Especially near the coast, where many cities and industry facilities are located, the quality and quantity of the data collected by the satellites are compromised by strong perturbation of the radar signal. Another problem is sea ice, which covers parts of the oceans in winter and is impenetrable to radar. To improve the applicability of sea level data in such environments, advanced solutions for pre- and post-processing of altimetry observations have been developed within the **ESA Baltic+ Sea Level (Baltic SEAL) project**. This project, led by DGFI-TUM, was successfully completed in 2021.

Hundreds of millions of radar measurements taken between 1995 and 2019 were processed in a newly developed multi-stage process that includes the identification of radar reflections of water along cracks and fissures in ice-covered ocean regions, the development of new computational methods to achieve better quality of sea level data close to land, and finally the calibration and combination of measurements from various satellite missions.

The analysis of these data for the Baltic Sea shows that the sea level has risen at an annual rate of 2-3 millimeters in the south, on the German and Danish coasts, as compared to 6 millimeters in the north-east, in the Bay of Bothnia (Passaro et al., 2021a). The developed method has also been applied to the North Sea, where the sea level is rising by 2.6 millimeters per year, and by 3.2 millimeters in the German Bight (Dettmering et al., 2021).

The North SEAL and Baltic SEAL data sets provide monthly sea level anomalies as well as information on linear trend and annual signals and are freely available from open repositories for public use. They open up numerous possibilities for investigating the relationships and causes of sea-level change in these areas; see below.

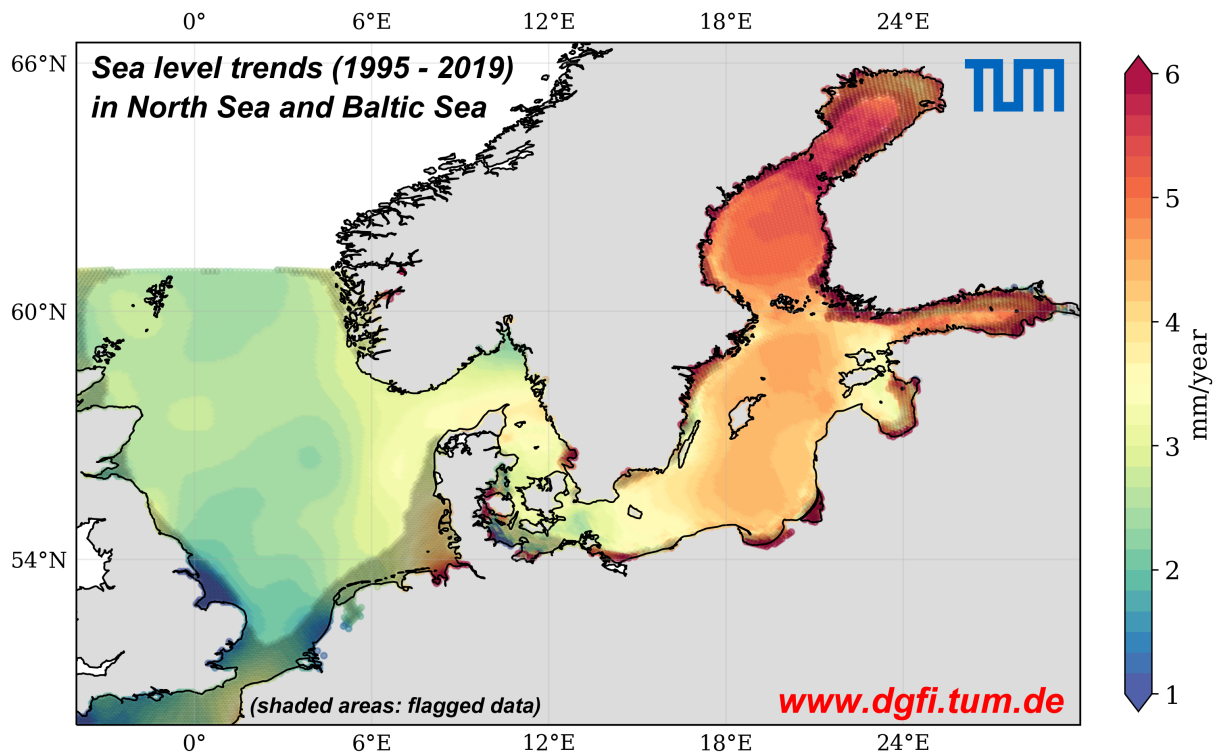


**Figure 2.2:** Sea level trends in North Sea and Baltic Sea between 1995 and 2019. Gray shading indicates areas with high statistical uncertainty.

### Analysis of Baltic Sea level trends

Monthly gridded sea level anomalies (SLA) from the Baltic SEAL data record between 1995 and 2019 were analyzed to provide new insights into sea level variability and trends. Figure 2.2 shows the map of sea level trends in the Baltic Sea. The measurements show that sea level has been rising in absolute terms throughout the region. The rate of sea level rise is increasing from the south-west of the Baltic Sea to the Gotland Basin and from the Gotland Basin to the Bay of Bothnia and the Gulf of Finland. By using specially developed classification methods and signal analysis techniques to measure sea level even in areas with sea ice cover in winter, we were able to extend the analysis to areas characterized by seasonal sea ice cover, i.e. the Bay of Bothnia and the Gulf of Finland. This major advantage of the Baltic SEAL dataset makes it possible to investigate seasonal processes that determine sea level fluctuations in the entire Baltic Sea area.

To explain the overall enhanced sea level trends (compared to global mean sea level rise) and the observed strong trend gradients across the area, the potential underlying driving mechanisms were investigated (Passaro et al., 2021a). In particular, the response of sea level to large-scale atmospheric variability in the region was analyzed. Previous studies have shown that the North Atlantic Oscillation (NAO), as the leading mode of atmospheric circulation in the region, strongly influences sea level variability in the Baltic Sea<sup>2 3</sup>. Figure 2.3a), which displays the point-by-point correlation of winter (DJF) sea level with the NAO index, confirms a largely uniform sea level response throughout the area except for the southwestern Baltic Sea. The opportunity provided by the Baltic SEAL dataset to observe local sea level changes in winter in areas covered with sea ice allowed a basin-wide comparison of the Bay of Bothnia with the southwestern Baltic Sea, which showed the largest deviations in the linear trends. Figure 2.3b) shows a high correlation between the time series of sea level difference (Bay of Bothnia - southwestern Baltic Sea) in the winter months and the NAO index.

From the comparison it is seen that positive NAO phases are associated with winters in which SLA are higher in the Bay of Bothnia than in the southwest. This connection was found to be related to the action of stronger southerly and westerly winds during positive NAO phases, which push the water north and east of the basin through Ekman transport. The intensity of the NAO phase thus drives the differences in SLA at the sub-basin scale in the Baltic Sea, with interannual variations affecting the linear trend of sea level.

The analysis demonstrates how dedicated coastal altimetry data records can help to identify forcing mechanisms in such challenging areas. This motivates further development and application of coastal altimetry to improve the understanding of the often small-scale and complicated dynamics of sea level in the coastal zone.

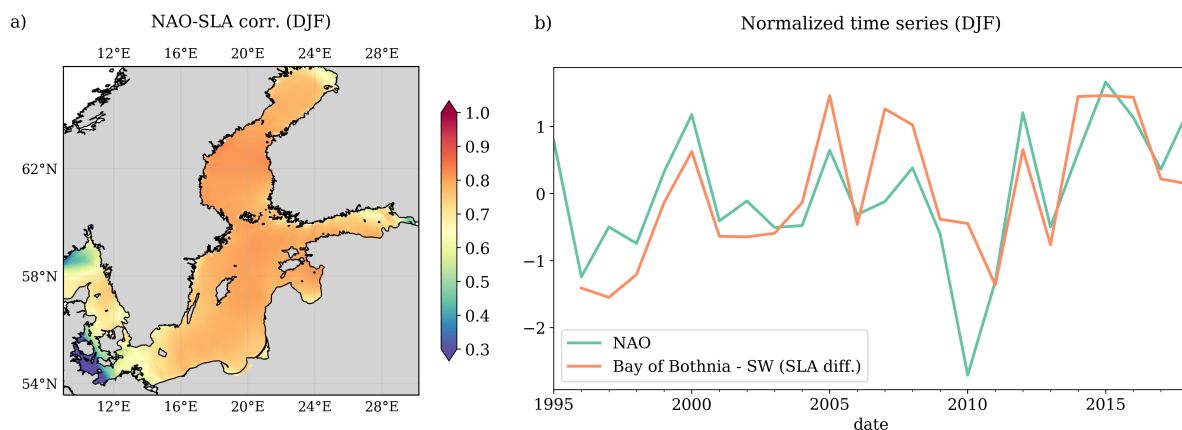


**Figure 2.3:** (a) Correlation of the NAO index with sea level anomalies from Baltic SEAL. (b) Normalized time series of NAO index (green) and SLA difference between the Bay of Bothnia and southwestern Baltic Sea (orange). Each point represents the time average of the quantities of the winter months December, January, and February (DJF).

<sup>2</sup>Jevrejeva, S., et al.: *Influence of large-scale atmospheric circulation on European sea level: results based on the wavelet transform method.* Tellus A, doi:[10.3402/tellusa.v57i2.14609](https://doi.org/10.3402/tellusa.v57i2.14609), 2005

<sup>3</sup>Stephenson, D., et al.: *North Atlantic Oscillation response to transient greenhouse gas forcing and the impact on European winter climate: a CMIP2 multi-model assessment.* Climate Dynamics, doi:[10.1007/s00382-006-0140-x](https://doi.org/10.1007/s00382-006-0140-x), 2006

## Arctic Ocean Surface Circulation

Two years ago, DGFI-TUM created a new dataset for monitoring sea surface currents in the northern Nordic Seas<sup>4</sup>. This dataset is based on the combination of satellite altimetry along-track dynamic ocean topography (DOT) heights with a numerical ocean model and was developed within the completed DFG project NEG-Ocean. In 2021, this combined dataset was analyzed to detect and characterize spatial and temporal changes in surface currents and circulation patterns, which are usually covered by a fragmented sea ice layer (Müller, 2021).

The studies performed so far, however, cover only about one sixth of the Arctic Ocean (Fig. 2.4). Within the new **IGSSE project AROCCIE** (Arctic Ocean Surface Circulation in a Changing Climate and its Possible Impact on Europe) the area will now be extended to the entire Arctic Ocean. AROCCIE is a joint project of DGFI-TUM and DTU Space (Danish Technical University) and is funded by TUM's International Graduate School of Science and Engineering (IGSSE).

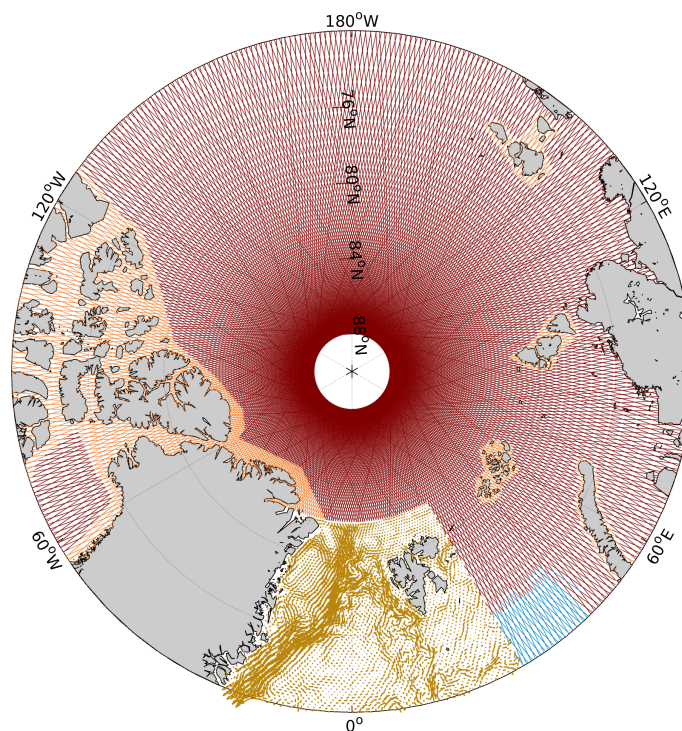


**Figure 2.4:** Geostrophic surface currents (yellow) in the northern Nordic Seas (1995-2012) and CryoSat-2 ground tracks of different acquisition modes (SAR, red; SARIn, orange; LRM, blue) in the Arctic Ocean.

Based on methods and experience from NEG-Ocean, a combined dataset of geostrophic ocean currents will be created. It will cover more than 25 years and allow investigations of the surface circulation under the effects of long-term changes in sea level. AROCCIE will investigate the possible impact of observed changes in surface currents on climatic conditions in Europe. Furthermore, AROCCIE aims to improve the Arctic marine gravity field and to study the influence of wind stress and freshwater inflow. Beside satellite altimetry and ocean modeling, observations from in-situ sensors and campaigns, as well as data from new technologies such as the CryoSat-2 SARIn and SWOT (Surface Water and Ocean Topography) will be incorporated. The project started in 2021 with the extension of the unsupervised open water detection developed in NEG-Ocean<sup>5</sup> to SARIn observations (Fig. 2.4, orange CryoSat-2 tracks).

<sup>4</sup>Müller F.L., et al.: *Geostrophic currents in the northern Nordic Seas from a combination of multi-mission satellite altimetry and ocean modeling*. Earth System Science Data, doi:[10.5194/essd-11-1765-2019](https://doi.org/10.5194/essd-11-1765-2019), 2019

<sup>5</sup>Müller F.L., et al.: *Monitoring the Arctic Seas: How Satellite Altimetry Can Be Used to Detect Open Water in Sea-Ice Regions*. Remote Sensing, doi:[10.3390/rs9060551](https://doi.org/10.3390/rs9060551), 2017

## Arctic Thin Ice Detection

Large parts of the north polar seas are seasonally covered by sea ice. This creates a difficulty for satellite altimetry, since the sea level can only be observed through openings in the sea ice, called leads or polynyas. The detection of these ice-free areas is decisive to obtain information about the sea level during the winter months in the Arctic Ocean. For this purpose, an open water detection approach based on an unsupervised classification has been developed for conventional altimetry (e.g. Envisat) in the DFG project NEG-Ocean and successfully extended for Delay Doppler radar observations (e.g. CryoSat-2)<sup>5,6</sup>. This classification is currently applied to all available altimeter missions within the IGSSE project AROCCIE (see above). Briefly summarized, the algorithm assigns altimetry radar echoes (waveforms) to certain sea surface conditions, such as open ocean, leads/polynyas and sea ice without the necessity of pre-known training data. In particular, the approach is based on an unsupervised waveform clustering (K-medoids), applied to a large sample of different waveform-derived power and shape features. In a second step, the generated reference model is used to classify all remaining waveforms from a mission by K-nearest neighbor.

With this approach, not only open water regions can be identified, but also thin ice layers. Thin ice can reach a thickness of up to 30 cm and forms mainly in polynyas, leads and the marginal ice zone (transition zone between open ocean and compact sea ice). It plays an important role in the heat exchange between the upper ocean and the atmosphere and has a significant influence on the salt flux into the lower ocean. From a satellite altimetry perspective, thin ice shows similar reflectivity characteristics to lead and polynyas, but the waveforms reflected from thin ice are characterized by a weaker maximum power and a slightly wider waveform than those from pure lead. Therefore, the previously assigned sea ice clusters are analyzed again for their reflection behavior and reassigned as thin ice if appropriate.

This reassignment was performed for ESA's CryoSat-2 mission in the entire Arctic Ocean. Figure 2.5 displays the seasonal evolution of the sea ice (except thin ice), thin ice (only) and open water coverage in percentage for the Arctic Ocean. Generally, a seasonal cycle is clearly visible in all three time series. Gray shaded sections indicate summer months when the surface type determination tends to increase uncertainty due to the occurrence of melt ponds and very specular sea ice surfaces. The maximum sea ice cover is in March, the minimum in September. Thin ice reaches its maximum in the melting period between June and July. A second subordinate peak can be spotted in the freezing period during November/December. A clear trend in the time series is not detectable, which can be mainly addressed to the short CryoSat-2 sample period of 10 years.

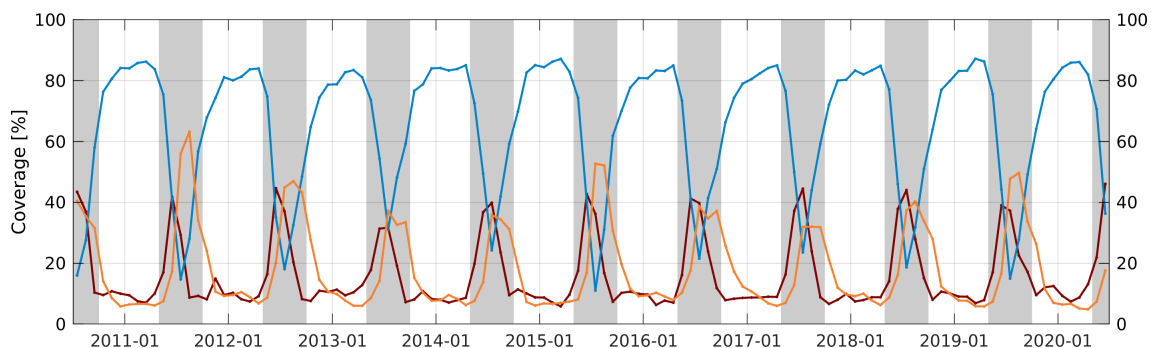


**Figure 2.5:** Temporal evolution of sea ice (blue), thin ice (red) and open water (orange) for the Arctic Ocean derived from the unsupervised classification applied to CryoSat-2 SAR waveforms. Gray shaded sections indicate summer months with an increased misclassification level.

<sup>6</sup>Dettmering D., et al.: *Lead Detection in Polar Oceans - A Comparison of Different Classification Methods for CryoSat-2 SAR Data*. Remote Sensing, doi:10.3390/rs10081190, 2018



In a further analysis, the CryoSat-2 classification results were averaged monthly into a triangle mesh with a spatial resolution of about 120 km to spatially estimate the seasonal phase of sea ice cover (including thin ice) and thin ice (only), shown as the day of the year (DOY) of the maximum in Figure 2.6. The left graph shows a sea ice maximum in January/February, while thin ice (right) is most visible in July in the central Arctic Ocean. In the Laptev Sea and partly also in the Kara Sea, which are marginal seas of the Arctic Ocean in northern Siberia, thin ice is observed mainly during the freezing period between December and February. In other regions (e.g. the northern Arctic Ocean and the Chukchi Sea) thin ice mainly occurs after the sea ice maximum at the end of March/April.

In cooperation with the Alfred Wegener Institute (AWI), Helmholtz Centre for Polar and Marine Research, further analyses and comparisons with external data sets (Sentinel-1 and MODIS) are currently being carried out.

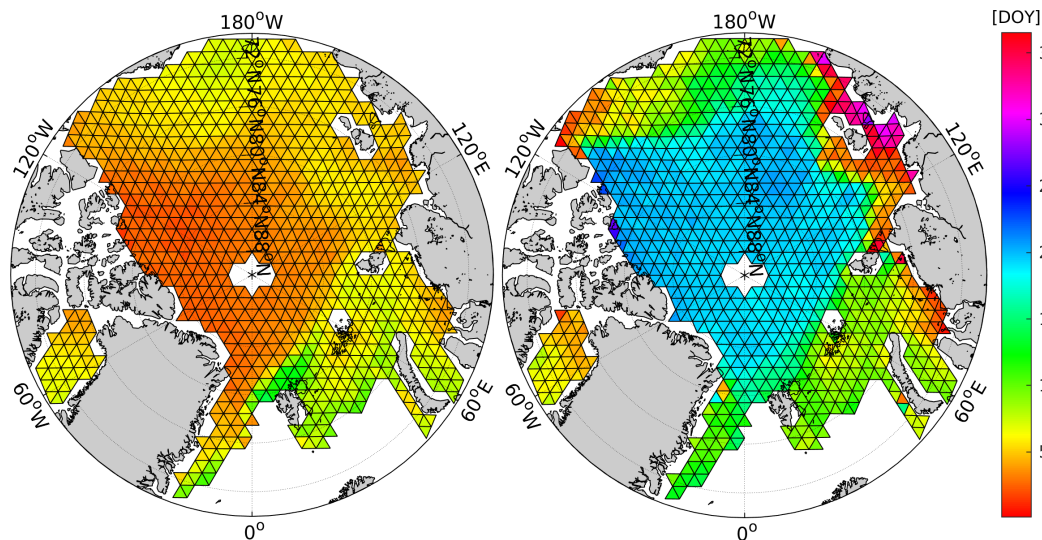


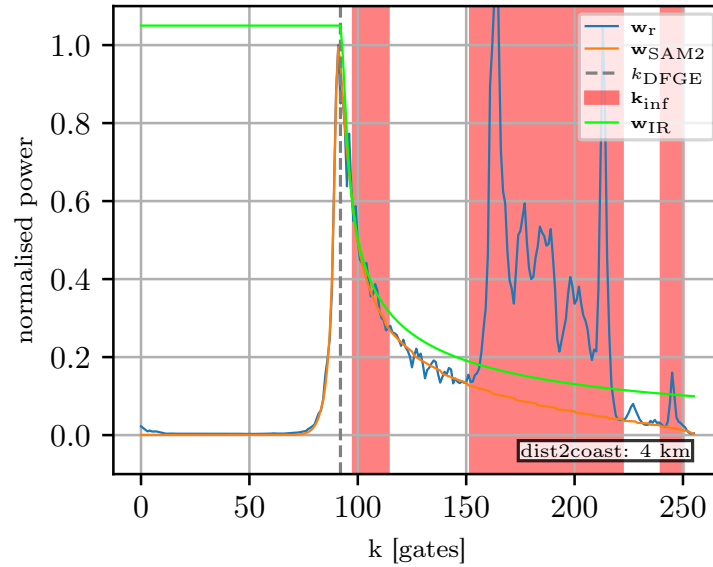
**Figure 2.6:** Day of year (DOY) of the annual maximum per cell for CryoSat-2 sea ice (including thin ice; left) and thin ice (only, right) classification between 2010 and 2020. Areas without CryoSat-2 SAR observations (e.g. pole, coasts) and a general sea ice concentration <10% are cut out.

## Significant wave height

Sea state, which is the state of the ocean due to the effect of wind, waves and swell, is one of the Essential Climate Variables (ECV) and thus a key quantity for recording and studying climate change processes. An important sea state parameter is the Significant Wave Height (SWH), which can be measured by satellite altimetry.

DGFI-TUM has a key role in the **ESA Climate Change Initiative (CCI) Sea State project** launched in June 2018 by leading the Algorithm Development Team for the satellite altimetry part. The main objective of the study is to estimate and exploit consistent time series of climate-quality SWH across different satellite missions. One of the focal points of the project is the coastal zone, as the performance of standard altimetry products decreases as the land is approached and sea state has a significant impact in this area.

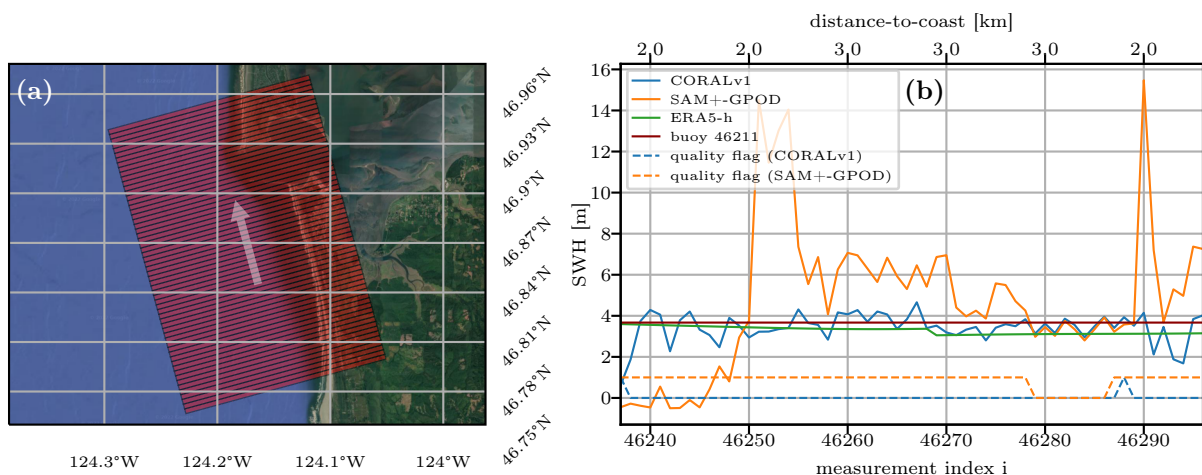
In 2021, a novel coastal retracking algorithm COastal Retracker for SAR ALtimetry Version 1.0 (CORALv1) was developed to estimate SWH in the coastal zone (Schlembach et al., 2022). The estimation can be quite difficult due to spurious signals that may emanate from highly reflective targets within the irradiated footprint. The blue curve in Figure 2.7 shows the received power return echo with interference originating from the immediate vicinity of the coastline and



**Figure 2.7:** Received (multilooked) power return echo waveform with spurious interference in the trailing edge (blue line); fitted, idealized, modeled power return echo waveform (orange); interference reference waveform, with which spurious interference is detected (green); detected interference range bins (red area).

located in the trailing edge of the waveform. CORALv1 takes this into account and detects spurious signals and excludes them during the iterative fitting process. It fits the idealized modeled waveform (orange curve) to the distorted waveform, extracting geophysical variables such as the SWH, sea surface height and wind speed. The range bins of the waveform that are detected as spurious interference are marked in red and are excluded from the fitting. In this way, both the quality and quantity of the SWH recordings are improved.

The altimeter radar footprint refers to the area on the ground illuminated by the radar altimeter and used to estimate SWH (as well as other parameters such as range). The SAR altimeter on board Sentinel-3A has an increased along-track resolution of 300 m due to its delay-Doppler processing. Its (simplified) footprint therefore looks like a rectangle measuring 7 km by 300 m.



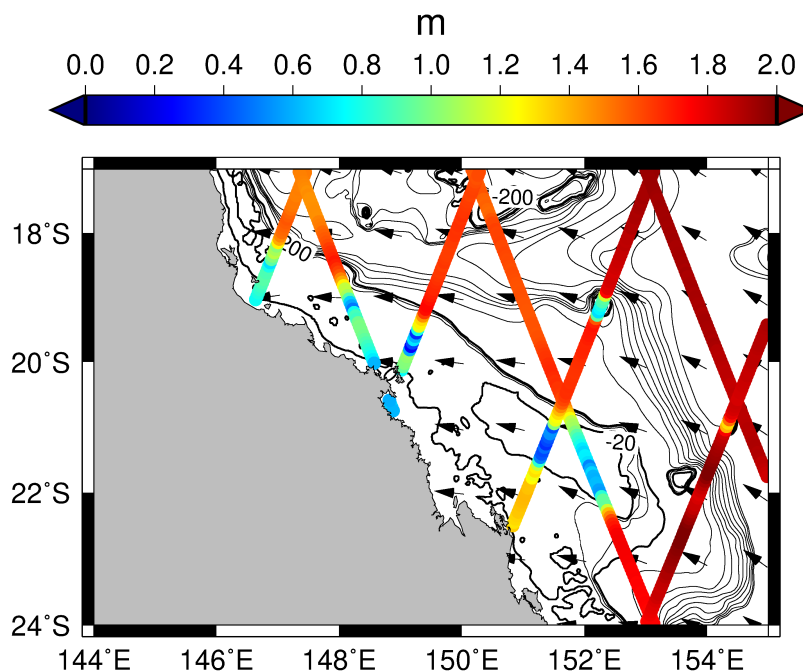
**Figure 2.8:** (a) Series of (simplified) radar footprints associated to measurements of a satellite track of Sentinel-3A in a coastal area along the western coast of the United States (46.87° N, 124.17° W) (image taken from Esri); (b) corresponding SWH estimates of the two coastal retrackerers CORALv1 and SAM+-GPOD, and the collocated ERA5-h wave model and the in-situ buoy record. The quality flag that indicates the validity of the records of CORALv1 and SAM+-GPOD are shown in dashed blue and orange (0 is good, 1 is bad).

Figure 2.8 shows the series of radar footprints associated to measurements of satellite track of Sentinel-3A along the western coast of the United States. The marked area in Figure 2.8 (a) is the footprint of an individual measurement that is affected by the coastline. Figure 2.8 (b) compares the series of the corresponding SWH records of the two coastal retracker CORALv1 and SAM+-GPOD with estimates from the ERA5-h wave model and in-situ data. The quality flag that indicates the validity of the records of CORALv1 and SAM+-GPOD are shown in dashed blue and orange (0 is good, 1 is bad). It can be seen that CORALv1 outperforms the SAM+-GPOD retracker in both quality and quantity of measurements and shows very good agreement with the ERA5-h wave model and buoy measurements.

### Global assessment of coastal waves

Knowledge of ocean wave heights at the coast is essential for several operational applications, ranging from coastal protection to energy exploitation. In this context, the Significant Wave Height (SWH) is one of the most general quantitative parameters that describe the sea state at a particular location. SWH, representing the average height of the highest waves, can be measured from satellites using radar altimeters. Over the open ocean, such measurements are routinely used, for example, for ocean weather predictions. In the coastal zone however, the radar measurements were not considered reliable. As an alternative, in-situ buoys or high-resolution ocean models are employed. While the network of in-situ buoys is very sparse and can only provide data at specific locations, appropriate ocean models are computationally very expensive and not globally available, besides requiring constant validation.

Led by DGFI-TUM, an international team has now analyzed reprocessed data from radar altimetry, specifically tailored to improve the quality and quantity of coastal measurements. The results provide a global picture of the average wave climate when going from offshore (about 30 km) to the coast, up to 3 km from land (Passaro et al., 2021b). The typical attenuation of



**Figure 2.9:** Examples of coastal change of mean SWH along the altimetry tracks (color scale) in the Great Barrier Reef region of eastern Australia. Bathymetry contours are plotted at intervals of 60 m from -20 m until -200 m depth and every 200 m until -2000 m depth. The mean wave direction computed from the ECMWF ERA5 reanalysis is shown with black arrows.

the waves when approaching the coast, for example due to the shading effect from the land, is quantified to be about 20% of the wave height reached offshore. As a consequence, the energy flux transported by the waves is calculated to decline by about 40% on a global average. This result is paramount for coastal assessments, which until now are often based on models with validation relative to offshore satellite altimetry data.

While the study provides global statistics, the interest lies in the possibility to observe the average wave climate at specific sites to understand how the local conditions influence the SWH. One example is provided in Figure 2.9, located in eastern Australia in the region of the Great Barrier Reef. Here, the SWH attenuation caused by the reef (visible by the bathymetric contour at -20 m depth) is counteracted by additional growth on the landward side of the reef.

The possibility to observe coastal gradients in wave height is given by the refitting of the altimetry signals with specific algorithms, in this case by the ALES retracker<sup>7</sup>. The same dataset has been also used by Violante-Carvalho et al. (2021) to observe the diffraction of ocean waves, i.e. the gradient of wave height perpendicular to the dominant direction of propagation, typically due to the presence of an emerged obstacle (in this case, an island). These observations were possible thanks to a synergetic approach involving in-situ buoys and model data.

## Empirical Ocean Tide Model EOT

In 2021, building on the regional studies and developments of the Empirical Ocean Tide (EOT) presented in previous reports, the latest global EOT model was developed, validated and published. The new model, named **EOT20** (Hart-Davis et al., 2021a), was the culmination of several years of research and development. The EOT20 model was developed with the main objective to improve the coastal representation of ocean tides, relying on recent developments in coastal altimetry such as the incorporation of the ALES retracker<sup>7</sup>.

EOT20 presents global atlases of the amplitudes and phases of 17 tidal constituents, presented on a 1/8 degree grid (Figure 2.10). Data obtained from OpenADB for eleven satellite altimetry missions were used to perform the residual tidal analysis using the FES2014b ocean tide model as a reference tide model. The result was validated using tide gauges from the TICON dataset<sup>8</sup> and an ocean bottom pressure sensor dataset<sup>9</sup>. Additional validation was conducted using gridded sea level variance analysis by comparing the resultant tidal corrections provided by EOT20 with the corrections from its predecessor EOT11a and from FES2014b for the Jason-1, Jason-2 and SARAL altimetry missions.

Error reductions were seen compared to the tide gauge and ocean bottom pressure sensor data for all major tidal constituents compared to EOT11a. Furthermore, EOT20 showed an overall lower error compared to the major ocean tide models for the full dataset. The datasets themselves were then divided into coastal, shelf and open ocean regions. In the coastal region, EOT20 showed the strongest performance, particularly in reducing the errors for the M2 tidal constituent. In the shelf and open ocean regions, expectedly the models showed similar errors compared to the observations with EOT20, FES2014b and DTU16 having the lowest errors. The differences between these models rarely exceed 1 mm. For the gridded sea level variance analysis, EOT20 produced an overall reduction in sea level variance compared to EOT11a and FES2014b for the three altimetry missions studied. The biggest reduction was once again seen in the coastal region.

<sup>7</sup>Passaro M., et al.: *ALES: A multi-mission adaptive subwaveform retracker for coastal and open ocean altimetry*. Remote Sensing of Environment, doi:10.1016/j.rse.2014.02.008, 2014

<sup>8</sup>Piccioni G., et al.: *TICON: Tidal CONstants based on GESLA sea-level records from globally located tide gauges*. Geoscience Data Journal, doi:97-104,10.1002/gdj3.72, 2019

<sup>9</sup>Stammer D., et al.: *Accuracy assessment of global barotropic ocean tide models*. Reviews of Geophysics, doi:10.1002/2014RG000450, 2014

The results of the validation of EOT20 provide strong motivation for the use of the model as a tidal correction for along-track satellite altimetry. Furthermore, a first estimation of the residual uncertainty of tidal estimations was done in this model version. Although a first look, these uncertainty estimates provide valuable insights into potential avenues of development for the model. The development of the EOT model will be continued and further updates are planned for the upcoming years.

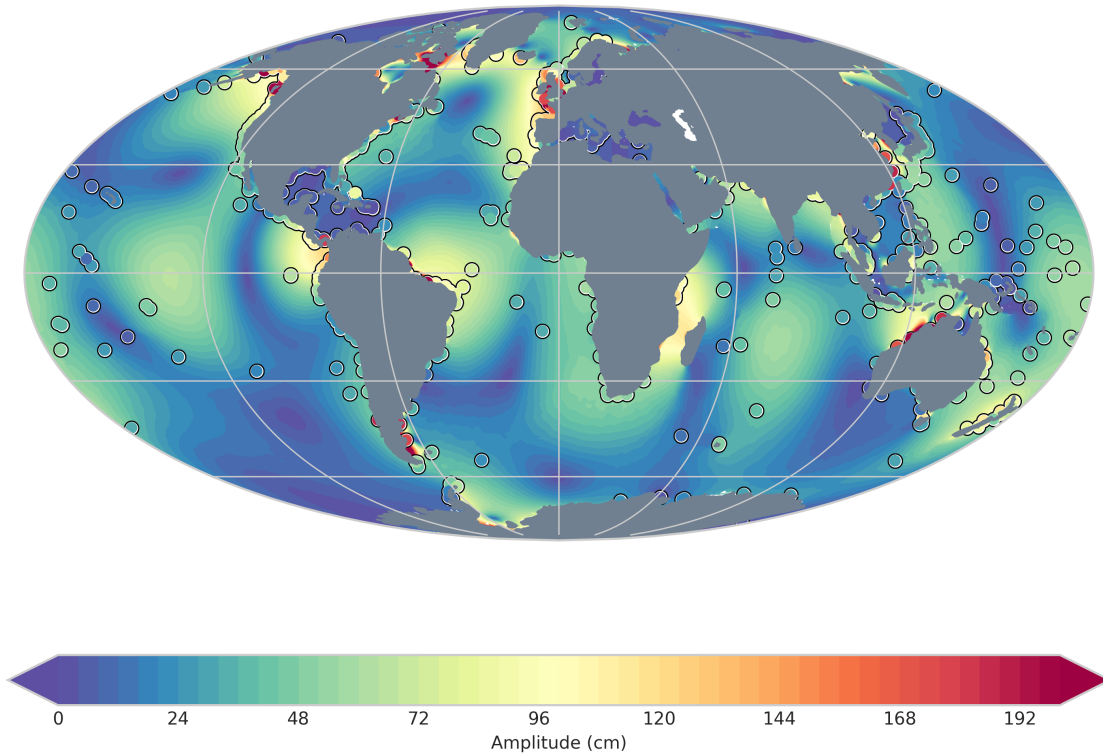


**Figure 2.10:** Amplitude of the M2 tidal constituent (in cm) as represented by EOT20. Dots show the M2 amplitude of TICON.

## Minor ocean tides

Investigations on smaller tidal constituents were continued as part of the **DFG project TIDUS** within the Research Unit 2736, NEROGRAV (New Refined Observations of Climate Change from Spaceborne Gravity Missions). Within TIDUS, regional assessments of the EOT model focused on improving the estimations of ocean tides from multi-mission satellite altimetry for the application in gravity field modeling.

Particular focus was placed on understanding the different techniques of estimating minor tidal constituents and the implications these techniques have on the ocean tidal correction used for along-track satellite altimetry. Minor tides are historically difficult to estimate from along-track altimetry due to their relatively small signals, especially compared to the larger signals of major constituents. Furthermore, the repeat orbits of satellite altimetry, about 10 days for the Jason missions for example, result in tidal aliasing meaning that a large number of samples from the altimetry are required in order to properly estimate these tides.

In order to combat these difficulties, a regular strategy to get estimations of these minor tides is to apply linear admittance theory. The concept of admittance, the relation of the tidal height with respect to the amplitude of the corresponding tide generating potential for a specific tidal wave,

is assumed to be a smooth function of frequency<sup>10</sup>. Simply put, this allows for the inference of certain minor constituents from the already estimated major constituents. This concept is commonly used in the estimation of the ocean tidal correction for along-track altimetry observations as well as in the GRACE processing.

To understand the accuracy of minor tide estimations for eight constituents, regional experiments were conducted to compare model derived estimations with admittance inferred estimations. The model derived estimations were obtained from a regional version of the EOT model (EOT-R), the data assimilative hydrodynamic model (FES2014b) and a purely hydrodynamic model (TiME)<sup>11</sup>. The same tides were also inferred (EOT-I) from the global EOT20 model. The models were compared to the TICON dataset<sup>8</sup> in three different regions: New Zealand (Figure 2.11), Australia and the Yellow Sea.

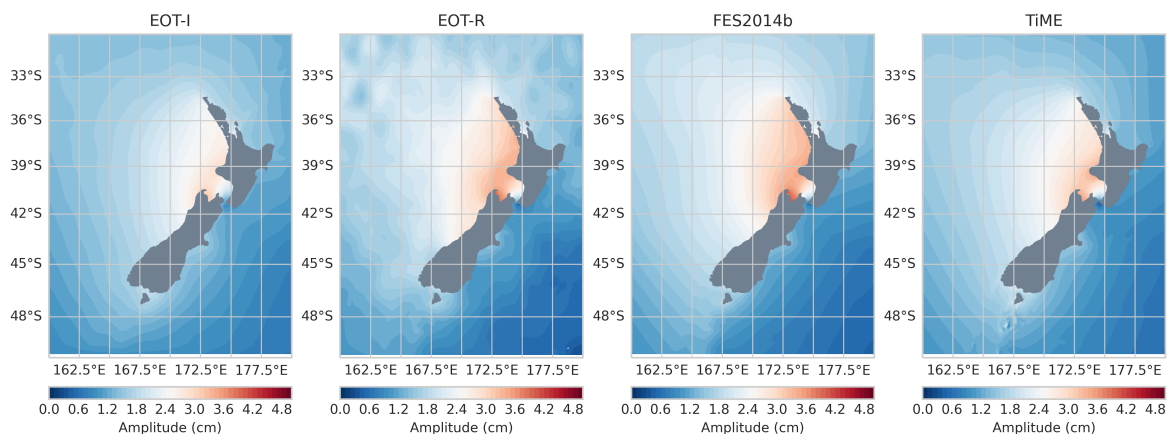


**Figure 2.11:** Amplitude of the L2 tidal constituent (in cm) in the region of New Zealand as represented by EOT-I, EOT-R, FES2014b and TiME.

The results of this regional study concluded that for the eight studied minor constituents, four should be directly estimated from the model ( $J_1$ ,  $L_2$ ,  $\mu_2$  and  $\nu_2$ ) and four should be inferred from the major constituents ( $2N_2$ ,  $\varepsilon_2$ ,  $MSF$  and  $T_2$ ) (Hart-Davis et al., 2021b). This approach yielded the best results when applied to the tidal correction for the Jason-2 mission for all the regions studied. An insight obtained from this study is that for some constituents the hydrodynamical model TiME outperformed the empirical estimations of EOT-R and EOT-I. Therefore, it can be suspected that an approach that combines the strengths of empirical estimations, especially for major constituents, with the strengths of numerical estimates, namely the ability to accurately estimate a large number of minor constituents, would be the best approach for estimating the tidal correction for satellite altimetry and GRACE processing. Investigations on this are currently in progress within the the Research Unit NEROGRAV.

### Coastal vertical land motion

Sea level change relative to the coast depends on two factors: The absolute sea level change and the vertical land motion (VLM). VLM is caused by different processes acting on a wide range of spatial and temporal scales. While mechanisms such as Glacial Isostatic Adjustment (GIA) are associated with large-scale VLM fingerprints that persist over millennia, other

<sup>10</sup>Munk W.H., Cartwright D.E.: *Tidal spectroscopy and prediction*. Philos. Trans. R. Soc. Lond. Ser. A Math. Phys. Sci., 259, 533–581, 1966.

<sup>11</sup>Sulzbach R., et al.: *High-Resolution Numerical Modeling of Barotropic Global Ocean Tides for Satellite Gravimetry*. Journal of Geophysical Research: Oceans, doi:10.1029/2020JC017097, 2021

processes such as tectonic activity, changes in surface loading or human activity can cause responses with much smaller spatial scales and non-linear temporal behavior.

Determining the spatio-temporal effects of the superposition of these processes is also a key challenge for sea level research, mainly due to the inhomogeneous distribution of direct VLM measurements (e.g. GNSS observations) and the non-uniform availability of data in time. As a result, many previous sea level studies were based on limited assumptions about the spatial and temporal characteristics of VLM, as they often rely on GIA models (which exclude non-GIA processes) or interpolated VLM trends (which neglect non-linear VLM effects).

To overcome these problems, a global VLM reconstruction for the present (1995-2020) has been created within the **DFG project VLAD** (Vertical Land Movement by Satellite Altimetry and Tide Gauge Difference). It maximizes the temporal and spatial resolution of the observed VLM processes in a Bayesian framework and is based on a comprehensive database of more than 10,000 GNSS, altimetry and tide gauge (TG) time series. The reconciliation between TG and satellite altimetry is based on the zone-of-influence (ZOI) approach (Oelsmann et al., 2021). A thorough pre-processing of the data was carried out, for which the semi-automatic Bayesian approach *DiscoTimeS* was developed to detect discontinuities and trend changes<sup>12,13</sup>. The VLM reconstruction provides estimates of the underlying secular trends together with VLM fingerprints representing the non-linear interannual to decadal components of the variability. The dataset will help shed light on the role of VLM and its uncertainties in past (1900-2000), present (1995-2020) and future (to 2150) coastal relative sea level changes.

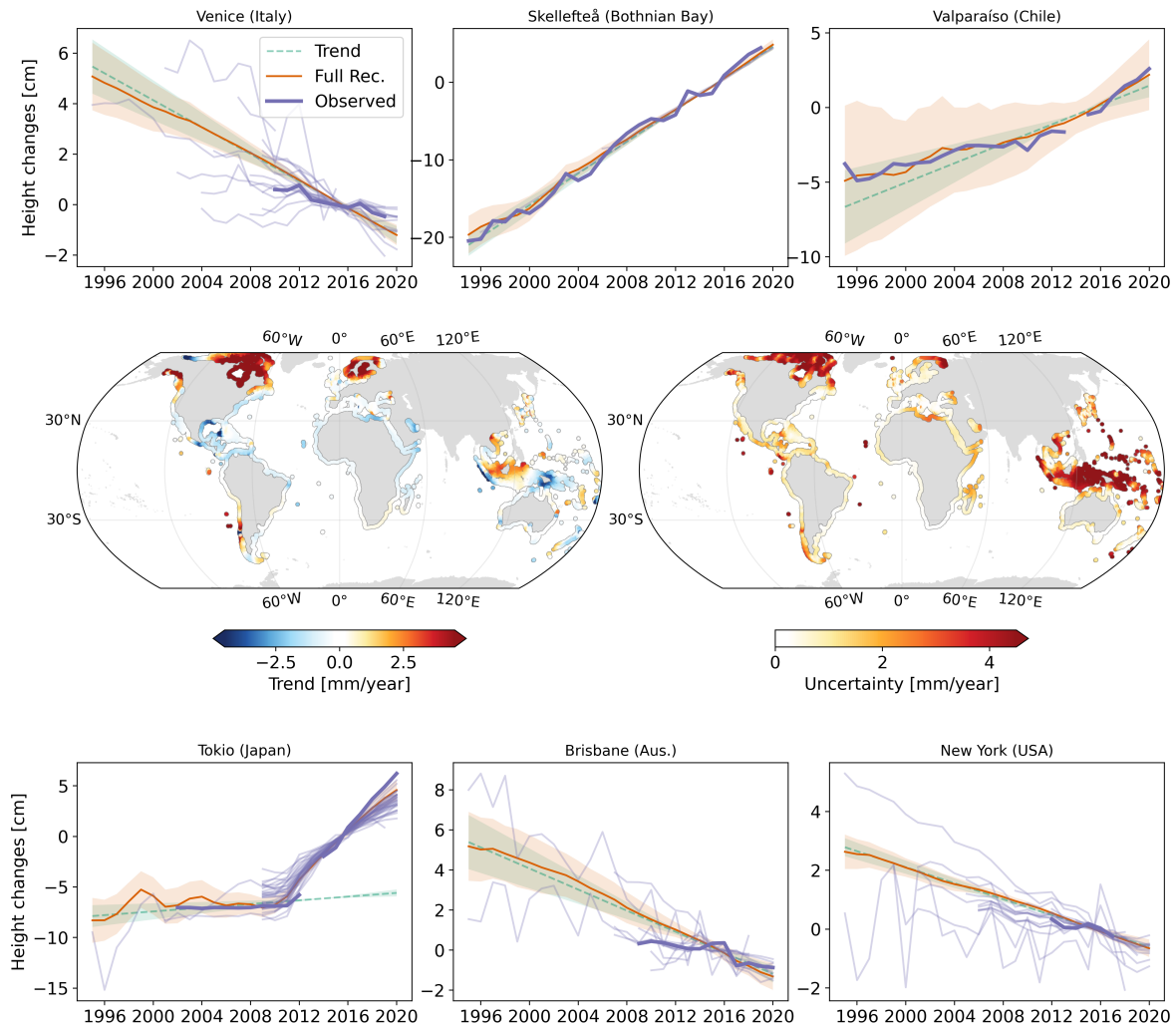
In a second step, a Bayesian principal component analysis (BPCA) was applied to the (spatially and temporally) inhomogeneously distributed and sampled data, to disentangle common VLM signatures and background trends. Explicitly, a linear trend component was modeled along with a set of principal components and empirical orthogonal functions (EOFs). The BPCA allows to re-evaluate the trend of height changes and their uncertainties at each observation epoch over the period 1995-2020. The estimated spatial patterns of EOFs and trends were interpolated in space using a Bayesian transdimensional analysis. Using the 3D reconstruction, the effects of non-GIA and non-linear VLM on relative sea level change was estimated by incorporating sea level reconstructions, projections and observations.

Figure 2.12 shows the derived secular trends and uncertainties as well as the time series for various selected regions. The time series illustrate the estimated trend component (and uncertainty, in green) and the full reconstruction (and uncertainty, in red) to separate the effects of secular motion and interannual variability. In addition to the observed VLM at the site (purple, solid lines), time series obtained in nearby locations were added (purple, translucent) to illustrate the apparent spatial variability and magnitude of the VLM.

The VLM reconstruction provides valuable estimates of the extent of VLM changes in time and space. The most pronounced observed feature is the characteristic GIA VLM signature in North America and Fennoscandia. This signature is overlaid by non-GIA effects that are due to regional natural or anthropogenic causes. Several key regions can be identified that are particularly vulnerable due to land subsidence and enhanced relative sea level change. Sub-continental subsidence is most evident along the coasts of the Gulf of Mexico (~1-5 mm/year), which has been shown to be primarily due to fluid withdrawal and tectonic downwarping. There are also regions affected by subsidence on much smaller spatial scales, such as Veneto (Italy), which benefit from a relatively high coverage of observations that allow us to resolve such processes. The presence of highly localized and small spatial scales of VLM in this area is also underlined by the large scatter of different observed VLM time series near the locations shown.

<sup>12</sup><https://github.com/oelsmann/discotimes>

<sup>13</sup>Oelsmann J., et al.: *Bayesian modeling of piecewise trends and discontinuities to improve the estimation of coastal vertical land motion*. Journal of Geodesy, submitted



**Figure 2.12:** VLM reconstruction over 1995-2020 based on observations. Shown are time series of observed VLM at different locations (purple and solid), together with the estimated trend (green) and the full reconstruction (red). Translucent purple time series indicate observed VLM in close proximity to the location shown to highlight the spatio-temporal variability in the observations. The interpolated linear trend estimates and uncertainties show the long-term VLM along most global coastlines.

While subsidence rates, e.g. in the Veneto region, are relatively stable over the observed period (1995-2020), other regions are affected by a high variability of the VLM, as shown by the observed and reconstructed time series for Valparaiso and Tokyo. The VLM in Tokyo is dominated by the effects of the Tohoku earthquake and subsequent post-seismic deformation, which are captured by the modeled time-varying components of the BPCA. Here we were able to separate the secular background trend from these components by assimilating the non-linear signatures of the earthquake. It is one of the advantages of BPCA that the secular background trend can be separated from the earthquake dynamics, which has often been neglected in previous studies. Knowledge of the secular motion is particularly important for temporal extrapolation of the VLM to study contemporary and projected relative sea-level change.



## 2.3 Inland Altimetry

### Database for Hydrological Time Series of Inland Waters (DAHITI)

DGFI-TUM has been working on new methods and advanced approaches for deriving various satellite-based hydrological datasets for almost a decade. All results are freely available in the institute's Database for Hydrological Time Series of Inland Waters (DAHITI) (see Section 4.6). The main result of DAHITI are water level time series from satellite altimetry<sup>14</sup>. Since 2019, DAHITI is being extended to include additional hydrological parameters derived from optical imagery, such as surface area time series, water occurrence masks, and land-water masks<sup>15</sup>. Furthermore, volume changes of lakes and reservoirs are provided, which are obtained from the combination of satellite altimetry and optical remote sensing<sup>16</sup>.

In 2021, the number of satellite altimeter missions used was expanded by IceSat-2 and Sentinel-6A to extend existing water level time series and include new targets. In addition, river discharge was added as a new parameter to DAHITI<sup>17</sup>. Work is also ongoing to improve the existing DAHITI data sets. A refined approach to derive more accurate water levels is being developed, and the existing river discharge approach is evolved towards a multi-station algorithm to provide more accurate time series.



**Figure 2.13:** Distribution of the more than 5900 virtual stations of DAHITI as of December 2021

In total, DAHITI provides nine different hydrological parameters derived from satellite altimetry and optical imagery for about 5900 globally distributed locations (virtual stations) by the end of 2021. Their global distribution can be seen in Fig. 2.13. Time series of water levels are available for 584 lakes/reservoirs and 5318 river crossings. Surface area time series, water occurrence masks and land-water masks are available for 198 lakes and reservoirs. Time series of volume changes, bathymetry and hypsometry models are available for 70 lakes and reservoirs.

<sup>14</sup>Schwatke C., et al.: *DAHITI - an innovative approach for estimating water level time series over inland waters using multi-mission satellite altimetry*. Hydrology and Earth System Sci., doi:10.5194/hess-19-4345-2015, 2015

<sup>15</sup>Schwatke C., et al.: *Automated Extraction of Consistent Time-Variable Water Surfaces of Lakes and Reservoirs Based on Landsat and Sentinel-2*, Remote Sensing, doi:10.3390/rs11091010, 2019

<sup>16</sup>Schwatke C., et al.: *Volume variations of small inland waters from a combination of satellite altimetry and optical imaging*. Remote sensing, doi:10.3390/rs12101606, 2020

<sup>17</sup>Scherer D., et al.: *Long-Term Discharge Estimation for the Lower Mississippi River Using Satellite Altimetry and Remote Sensing Images*. Remote Sensing, doi:10.3390/rs12172693, 2020

### Water level time series for narrow rivers

DGFI-TUM is developing new algorithms and methods for an automated and fast generation of water level series at the highest possible accuracy for all major inland water bodies on a global scale. This research is performed in the framework of the **DFG projects WALESA and ARISAS**, part of the Research Unit 2630 (GlobalCDA: Understanding the global freshwater system by combining geodetic and remote sensing information with modelling using a calibration/data assimilation approach).

The overall goal of GlobalCDA is to improve the understanding of global freshwater resources and to obtain better estimates of continental water fluxes and water storage. For this purpose, new virtual stations are continuously added to DAHITI (see above). Before transferring the calibration and data assimilation (C/DA) approach to a global scale, a special focus is set by the partners on selected target areas: The Mississippi, Amazon, Ganges, Congo, Euphrat, and Tigris river basins as well as France, Germany, and the Tibetan Plateau. A total number of 1722 stations were added within these areas. Most of the new stations are located along the Amazon, Mississippi and Congo, resulting from the addition of the Sentinel-3A/B altimeter missions. The number of stations in France, Germany, and the Tibetan Plateau is limited by the ground track geometry of the missions available.

One challenge when adding new stations to DAHITI is to decide whether the measured data is useful when judged only by the derived hydrograph, which does not have a strong signal due to lack of seasonal variation or a high degree of flow regulation. Therefore, in-situ data from different sources is continuously acquired and added to an internal validation database. In 2021, in-situ data from the Republic Hydrometeorological Service of Serbia, the Arctic Great Rivers Observatory, the Hydro-Geochemistry of the Amazonian Basin Observatory, Hydropor-tail by Eaufrance, the Murray-Darling Basin Authority, the United States Geological Survey, the Gewässerkundlicher Dienst Bayern, and the Bundesanstalt für Gewässerkunde were added.

### River surface slope from ICESat-2 observations

Within the project ARISAS, DGFI-TUM is also working on the exploitation of data from new satellites such as ICESat-2, Sentinel-6, or the upcoming SWOT mission, each of which carrying a unique and novel instrument. These data offer a wide variety of new possibilities and applications, but they also require the development of new analysis procedures.

The ATLAS instrument onboard ICESat-2 is a photon-counting LiDAR sensor, synchronously measuring along three parallel pairs of beams spaced 3 km apart. Compared to classical radar altimeters, each beam of the LiDAR instrument has a much smaller footprint (17 meters vs. several kilometers in the case of classical radar systems). Therefore, the water level in narrow rivers can be measured with high precision and accuracy. However, the photons cannot penetrate clouds, which leads to data gaps, and the temporal resolution is low because ICESat-2 is placed on a relatively long-repeat orbit of about 91 days.

Although ICESat-2 has limited performance for estimating continuous water level time series at virtual stations, its unique measurement geometry with six parallel observations and its high precision can be used to derive the water surface slope (WSS) of rivers, for which two methods are currently under development at DGFI-TUM: The along-track WSS and the across-track WSS estimation. For the along-track WSS, a line is fitted to the subsequent water level observations within an intersection of the river. The slope of the fitted line is projected onto the river centerline. For the across-track slope, a reference elevation is estimated for each intersection based on the standard DAHITI approach<sup>14</sup>. The WSS is then calculated from the elevation and crossing position differences of all intersections of the ATLAS beams and a river reach. First

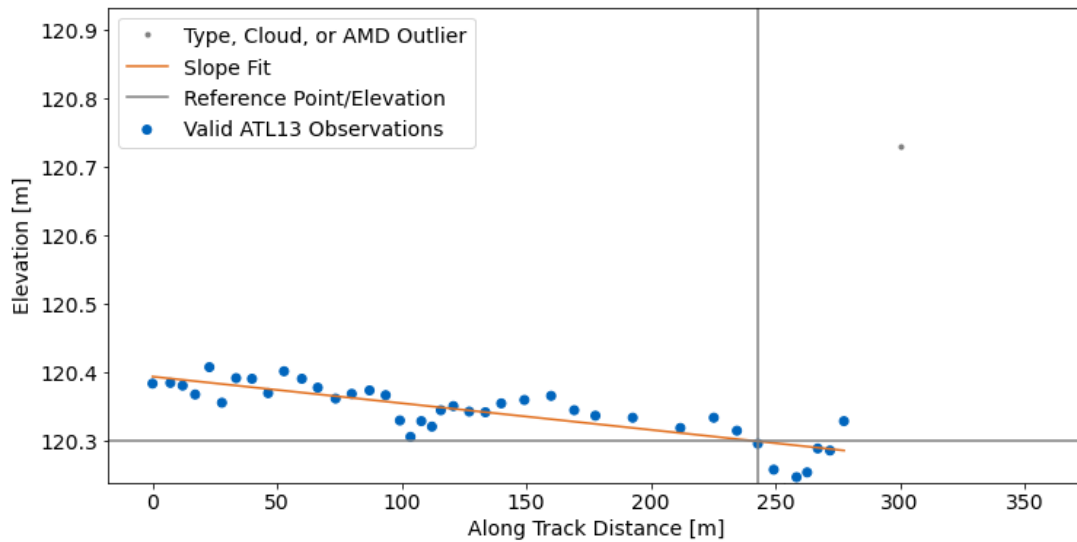


**Figure 2.14:** ICESat-2 observations from the intersection of one beam with the river Loire (13 Sept. 2020). The gray and blue dots show the outlier and valid observations, respectively, that are used to estimate the along-track WSS and water level at the reference point (i.e. the centerline intersection, gray lines).

results for 292 reaches within the Mississippi River basin show a median absolute error of 31 mm/km (across-track) and 70 mm/km (along-track) of the instantaneous WSS estimates w.r.t. in-situ gauge data.

Classical short-repeat orbit altimetry missions have an orbit repeatability of +/-1 km at the equator crossing. Thus, steep WSS can have an impact on the quality of the hydrograph derived for virtual stations, depending on the intersection angle and river morphology. Using the mean WSS derived from ICESat-2 observations as a correction at selected virtual stations can improve the RMSE by up to 69% (33 cm). However, even with mean in-situ WSS as a correction, the RMSE may degrade by 24% (4 cm) especially at virtual stations affected by off-nadir effects or with ambiguous crossing positions.

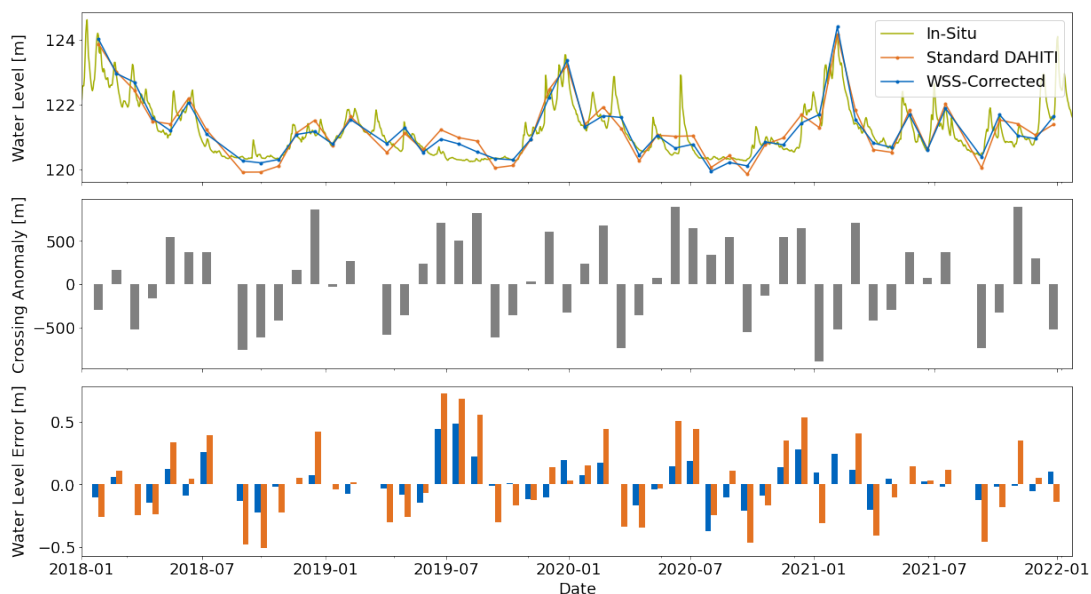


**Figure 2.15:** Top: DAHITI standard, WSS-corrected and in-situ water level time series. Center: Crossing anomaly which is multiplied with the estimated slope to obtain the WSS correction. Bottom: Standard DAHITI and WSS-corrected water level errors w.r.t. in-situ gauge data.

Figure 2.14 shows the instantaneous along-track WSS fitted to ICESat-2 observations of a beam intersection with the Loire River on September 13, 2020. The intersection angle of the beam ground track with the centerline is about 33 degrees with a resulting instantaneous along-track WSS of 467 mm/km. The mean of all daily along-track and across-track WSS is 430 mm/km, which only slightly differs from the mean in-situ WSS of 455 mm/km measured between a pair of upstream and downstream gauges.

Sentinel-3A intersects the respective reach at a virtual station. However, due to orbit repeatability tolerance of about 1 km, the river is actually crossed at different locations. The mean WSS is multiplied with this crossing anomaly to obtain a WSS correction. This correction is applied to the water level time series observed at the virtual station. Figure 2.15 shows the DAHITI standard, the WSS-corrected, and the in-situ water level series, as well as the crossing anomalies and errors w.r.t. gauge data. By applying the WSS correction, the RMSE is reduced by 0.15 m (49.46%).

## Related publications

- Birol F., Léger F., Passaro M., Cazenave A., Niño F., Calafat F.M., Shaw A., Legeais J.-F., Gouzenes Y., Schwatke C., Benveniste J.: *The X-TRACK/ALES multi-mission processing system: New advances in altimetry towards the coast*. Advances in Space Research, doi:[10.1016/j.asr.2021.01.049](https://doi.org/10.1016/j.asr.2021.01.049), 2021
- Cavaleri L., Bertotti L., Ferrarin C., Passaro M., Pezzutto P., Pomaro A.: *Synergic use of altimeter and model sea level data in inner and coastal seas*. Remote Sensing of Environment, doi:[10.1016/j.rse.2021.112500](https://doi.org/10.1016/j.rse.2021.112500), 2021
- Dettmering D., Müller F.L., Oelsmann J., Passaro M., Schwatke C., Restano M., Benveniste J., Seitz F.: *North SEAL: a new dataset of sea level changes in the North Sea from satellite altimetry*. Earth System Science Data, doi:[10.5194/essd-13-3733-2021](https://doi.org/10.5194/essd-13-3733-2021), 2021
- Dettmering D., Schwatke C.: *Ionospheric corrections for satellite altimetry - impact on global mean sea level trends*. Earth and Space Science, doi:[10.1029/2021EA002098](https://doi.org/10.1029/2021EA002098), 2022
- Hart-Davis M.G., Dettmering D., Sulzbach R., Thomas M., Schwatke C., Seitz F.: *Regional Evaluation of Minor Tidal Constituents for Improved Estimation of Ocean Tides*. Remote Sensing, doi:[10.3390/rs13163310](https://doi.org/10.3390/rs13163310), 2021
- Hart-Davis M.G., Piccioni G., Dettmering D., Schwatke C., Passaro M., Seitz F.: *EOT20: a global ocean tide model from multi-mission satellite altimetry*. Earth System Science Data, doi:[10.5194/essd-13-3869-2021](https://doi.org/10.5194/essd-13-3869-2021), 2021a
- Oelsmann J., Passaro M., Dettmering D., Schwatke C., Sánchez L., Seitz F.: *The zone of influence: matching sea level variability from coastal altimetry and tide gauges for vertical land motion estimation*. Ocean Science, doi:[10.5194/os-17-35-2021](https://doi.org/10.5194/os-17-35-2021), 2021
- Müller F.L.: *Improved polar geostrophic surface currents from satellite altimetry*. Dissertation, Technische Universität München und Reihe C der Deutschen Geodätischen Kommission, ISBN 978-3-7696-5278-9, 2021
- Passaro M., Müller F.L., Oelsmann J., Rautiainen L., Dettmering D., Hart-Davis M.G., Abulaitijiang A., Andersen O.B., Høyer J., Madsen K., Ringgaard I., Särkkä J., Scarrott R., Schwatke C., Seitz F., Tuomi L., Restano M., Benveniste J.: *Absolute Baltic Sea Level Trends in the Satellite Altimetry Era: A Revisit*. Frontiers in Marine Science, doi:[10.3389/fmars.2021.647607](https://doi.org/10.3389/fmars.2021.647607), 2021a

Passaro M., Hemer M., Quartly G.D., Schwatke C., Dettmering D., Seitz F.: *Global coastal attenuation of wind-waves observed with radar altimetry*. Nature Communications, doi:[10.1038/s41467-021-23982-4](https://doi.org/10.1038/s41467-021-23982-4), 2021b

Schlembach F., Passaro M., Dettmering D., Bidlot, J., Seitz F.: *Interference-sensitive coastal SAR altimetry retracking strategy for measuring significant wave height*. Remote Sensing of Environment, doi:[10.1016/j.rse.2022.112968](https://doi.org/10.1016/j.rse.2022.112968), 2022

Violante-Carvalho N., Arruda W.Z., Carvalho L.M., Rogers W.E., Passaro M.: *Diffraction of irregular ocean waves measured by altimeter in the lee of islands*. Remote Sensing of Environment, doi:[10.1016/j.rse.2021.112653](https://doi.org/10.1016/j.rse.2021.112653), 2021

### 3 Cross-Cutting Research Topics

*The three overarching research topics Atmosphere, Regional Gravity Field, and Standards and Conventions are closely interlinked with the DGFI-TUM Research Areas Reference Systems and Satellite Altimetry.*

*The atmosphere (Section 3.1) is crucial for the analysis of all space-geodetic observations. Satellite orbits are perturbed by atmospheric drag, and measurement signals are affected by refraction and signal delay. These effects must be adequately taken into account in precise orbit determination and geodetic data analysis, and optimizing the corresponding correction models is an important research task. Conversely, space-geodetic observations provide valuable information about the state and dynamics of the atmosphere. This information can be used to study atmospheric processes as well as the effects of space weather and is also of great interest to other disciplines. In recent years, space weather has attracted increasing attention as an emerging field, especially from policy makers and scientists, as it can severely damage modern infrastructures such as navigation systems, power supply and communication facilities. Crucial conclusions about space weather can be drawn from changes in the upper atmosphere, i.e. the sub-compartments magnetosphere, ionosphere, plasmasphere and thermosphere. Over the past years, DGFI-TUM has built up strong expertise in modeling and predicting global and regional structures of electron and neutral density in the Earth's upper atmosphere through the joint analysis of space geodetic observations using problem-adapted data representations and estimation techniques. DGFI-TUM is strongly involved in space weather research in Germany and has cooperated closely with the German Space Situational Awareness Center (Weltraumlagezentrum) and DLR for many years. At the international level, DGFI-TUM has chaired the Focus Area on Geodetic Space Weather Research (FA-GSWR) of the Global Geodetic Observing System (GGOS) under the umbrella of the IAG since 2017.*

*For various applications in geodesy, precise knowledge of the Earth's gravity field (Section 3.2) is of great importance. The realization and unification of height systems and the determination of high-precision satellite orbits are examples of these applications. The latter are a prerequisite for the calculation of accurate reference frames or for reliable estimates of water heights from satellite altimetry. Furthermore, the geoid represents the reference surface for ocean circulation. Temporal changes in the gravity field contain information on mass transports in the Earth system and are of great interest, for example, for the investigation of dynamic processes in the Earth's interior or in the hydrosphere. DGFI-TUM primarily focuses on theoretical and practical aspects of regional gravity field determination. The aim is to create high-resolution and high-precision potential fields for delimited areas by combining various data types, such as space- and airborne gravity measurements, satellite altimetry, and terrestrial and ship gravimetry.*

*To ensure the highest possible consistency of parameters and data products, the definition and application of uniform standards and conventions (Section 3.3) is essential. At the international level, DGFI-TUM is deeply involved in the activities of the relevant bodies for the definition of standards in geodesy and the monitoring of their implementation. DGFI-TUM chairs the GGOS Bureau of Products and Standards (BPS) and operates it jointly with several partners. Within the framework of the United Nations Global Spatial Information Management (UN-GGIM), DGFI-TUM provides the IAG representative for the key area "Data Sharing and Development of Standards" to the UN-GGIM Subcommittee "Geodesy".*

### 3.1 Atmosphere

The Earth's atmosphere can be divided into different layers depending on physical parameters such as temperature or charge state. With regard to the charge state, a distinction is essentially made between the neutral atmosphere up to an altitude of about 50 km and the ionosphere roughly between 50 km and 1000 km altitude. The plasmasphere is located above the ionosphere. Both the plasmasphere and the ionosphere can be characterized by the number of free electrons, i.e. the electron density, and therefore play a key role in monitoring space weather.

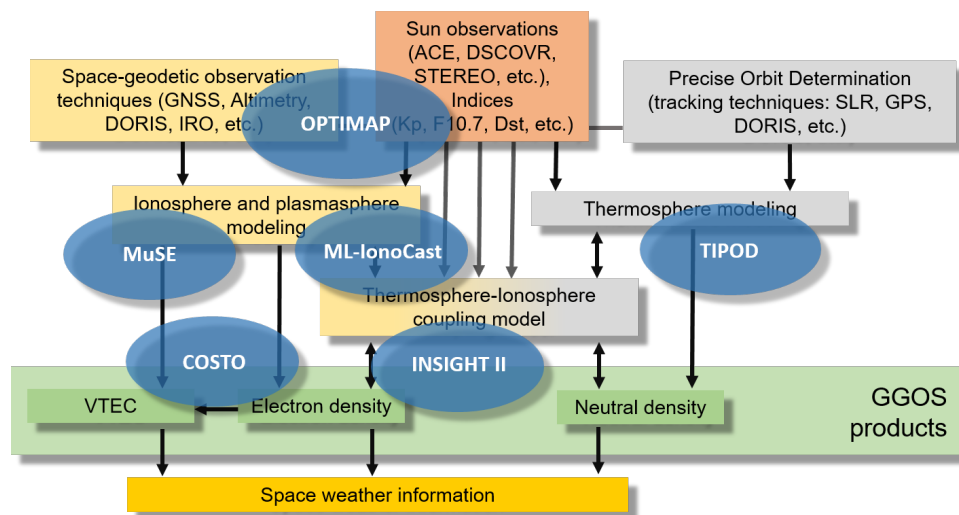


**Figure 3.1:** Work structure of the research topic 'Atmosphere' in 2021: the blue colored oval areas visualize the third-party funded projects running at DGFI-TUM in 2021 (project acronyms written in white letters). The location of such an oval area reflects the scientific content of the project and demonstrates its role in the structure of the research topic.

Figure 3.1 gives an overview about the 2021 project collection of DGFI-TUM in the frame of atmosphere modeling. The blue colored oval areas in Fig. 3.1 indicate the altogether six third-party funded projects. In the recent years, we have reported comprehensively on the scientific work within the OPTIMAP (Operational Tool for Ionospheric Mapping And Prediction) project funded by the Bundeswehr GeoInformation Center (Zentrum für Geoinformationswesen der Bundeswehr, ZGeoBW). On 31 October 2021, the second phase of OPTIMAP was successfully completed. The three projects MuSE (Multi-Satellite ionosphere-plasmasphere Electron density reconstruction), INSIGHT-II (Interactions of Low-orbiting Satellites with the Surrounding Ionosphere and Thermosphere) and TIPOD (Development of High-precision Thermosphere Models for Improving Precise Orbit Determination of Low-Earth-Orbiting Satellites), are all funded by the German Research Foundation (DFG) within the SPP 1788 Dynamic Earth. The ESA project COSTO (Contribution of Swarm data to the prompt detection of tsunamis and other natural hazards) was completed at the beginning of 2021. A final article reporting about the results of COSTO has been published by Jarmołowski et al. (2021). The project ML-lonoCast (Machine Learning for Forecasting the Ionospheric Total Electron Content) is funded by the scholarship programme 'Research grants for doctoral programmes in Germany' of the DAAD (German Academic Exchange Service).

In the following, we present (1) a real-time global model of the vertical total electron content (VTEC) developed in the framework of OPTIMAP, (2) machine learning studies for VTEC forecasting carried out in the framework of ML-lonoCast, and (3) a comparison of thermospheric density scaling factors obtained from SLR and accelerometer measurements in the framework of TIPOD.

### Real-time global VTEC model considering nowcasted B-spline coefficients

Monitoring and modeling VTEC is becoming more and more important for modern applications such as autonomous driving and space weather event detection. Therefore, several analysis centers have made efforts to estimate VTEC in real time using different approaches. In the framework of the **ZGeoBW project OPTIMAP**, DGFI-TUM has developed a real-time global VTEC model with high spectral resolution from GNSS data, based on B-spline functions and Kalman filtering (Erdogan et al. 2021). The model is the core of a complex software system that DGFI-TUM has been developing since 2014 for operational use in real-time space weather monitoring at the German Space Situational Awareness Center (Weltraumlagezentrum; since 2021 Weltraumkommando der Bundeswehr) in Uedem.

For real-time applications, GNSS data have been usually transmitted from GNSS receivers to users by casters through the Networked Transport of RTCM via Internet Protocol (NTRIP). NTRIP is a data transfer protocol that enables the streaming of GNSS data to stationary or mobile users via Internet. The open-source software BNC, provided by the Federal Agency for Cartography and Geodesy (BKG) as an NTRIP Client, can be executed to download data from the GNSS constellations. The downloaded data set includes carrier-phase observations from the L1 and L2 signals of GPS as well as the E1 and E5a signals of GALILEO. The challenging task in real-time modeling is to deal with high-rate raw GNSS data. Most receivers in the IGS caster provide data at a 1Hz sampling rate. Since accomplishing the data processing and estimation steps in real-time in less than a second might not be possible in practice, a proper down-sampling is typically applied by considering the computational resources. Here, we set the down-sampling rate for the raw data to 10 seconds.

After the data download, the real-time pre-processing step is carried out. First, the geometry-free ionosphere combination  $L_{r,k}^s = \Phi_{r,f_1,k}^s - \Phi_{r,f_2,k}^s$  of the carrier-phase observations  $\Phi_{r,f_1}^s$  and  $\Phi_{r,f_2}^s$  is calculated in the unit meter, obtained from GNSS signals transmitted at a satellite  $s$  and received at a station  $r$  with the two signal carrier frequencies  $f_1$  and  $f_2$  at time stamp  $k$ . These ionosphere combinations are collected for each receiver-satellite pair in an arc container. A cycle-slip detection algorithm is separately applied to each arc to detect jumps in the signals. The algorithm utilizes the first-order time difference

$$\Delta L_{r,k}^s = (L_{r,k}^s - L_{r,k-1}^s) / \Delta t_k \quad (3.1)$$

of the carrier-phase ionosphere combination; it amplifies the jumps and therefore increases the possibility to detect them. The division by the time difference  $\Delta t_k = t_k - t_{k-1}$  aims at avoiding a false jump detection due to a missing observation. From the time series  $\Delta L_{r,k-n}^s, \dots, \Delta L_{r,k}^s$  along an arc, the predicted value of  $\Delta L_{r,k+1}^s$  for the time moment  $t_{k+1}$  is calculated. The prediction is performed using a second-order polynomial function, and the coefficients of the polynomials are computed via a curve-fitting approach using the last, e.g., 15 consecutive data points. If the difference between the real observation  $\Delta L_{r,k+1}^s$  and the predicted value of  $\Delta L_{r,k+1}^s$  exceeds the threshold  $\varepsilon$ , the data point on the arc at  $t_{k+1}$  is marked as a jump. Moreover, a data gap threshold of 120 seconds is also applied to mark time differences exceeding the threshold. It should be noted that a detected cycle-slip is not repaired; instead, a new arc is initiated. After the jump detection and the marking procedures, the ionosphere combinations  $L_{r,k}^s$  are converted to TECU and then stored in a database.

In our approach the Kalman filter is carried out as a sequential estimator for real-time VTEC modeling. The geometry-free ionosphere combination  $L_{r,k}^s$  eliminates the non-dispersive effects, including the geometric line of sight distance between the satellite  $s$  and the receiver  $r$  as well as the receiver and satellite clock offsets, and can be written as

$$L_{r,k}^s + e_k = STEC_k + B_{r,k} + B_k^s + B_{A_s^s,k} \quad (3.2)$$



where  $STEC_k$  is the slant total electron content,  $B_{r,k}$  and  $B_k^s$  refer to the frequency-dependent receiver and satellite inter-frequency biases (IFB). Furthermore,  $B_{A_{r,k}^s}$  denotes the combined ambiguity bias of a carrier-phase observation and  $e_k$  stands for the measurement error. Applying the Single Layer Model (SLM) in Eq. (3.2)  $STEC_k$  can be replaced by  $STEC_k = m(z_{r,k}^s) \cdot VTEC_k$ , where the mapping function  $m$  is depending on the satellite zenith angle  $z_{r,k}^s$ . Consequently, we obtain from the ionosphere combination (3.2) the observation equations

$$y_{GPS,k} + e_{GPS,k} = m(z_{r,k}^s) \cdot VTEC_k + C_{r,GPS,k}^s, \quad (3.3a)$$

$$y_{GAL,k} + e_{GAL,k} = m(z_{r,k}^s) \cdot VTEC_k + C_{r,GAL,k}^s, \quad (3.3b)$$

where  $y_{GPS}$  and  $y_{GAL}$  are the ionospheric observations  $L_{r,k}^s$  for GPS and GALILEO. The quantities  $C_{r,GPS,k}^s$  and  $C_{r,GAL,k}^s$  refer to the total phase biases and consist of the IFBs and the carrier-phase ambiguity biases as given in Eq. (3.2) and are defined as

$$C_{r,GNSS,k}^s = B_{r,k} + B_k^s + B_{A_{r,k}^s}. \quad (3.4)$$

As already presented in the previous Annual Reports, we model  $VTEC(\varphi, \lambda)$  globally as a series expansion

$$VTEC_k = VTEC(\varphi, \lambda, t_k) = \sum_{k_1=0}^{K_{J_1}-1} \sum_{k_2=0}^{K_{J_2}-1} d_{k_1,k_2}^{J_1,J_2}(t_k) N_{J_1,k_1}^2(\varphi) T_{J_2,k_2}^3(\lambda), \quad (3.5)$$

in terms of two-dimensional (2D) tensor products of polynomial B-spline functions  $N_{J_1,k_1}^2(\varphi)$  of degree 2 depending on the geomagnetic latitude  $\varphi$  and trigonometric B-spline functions  $T_{J_2,k_2}^3(\lambda)$  of order 3 depending on the geomagnetic longitude  $\lambda$ . In Eq. (3.5) the time-dependent B-spline coefficients  $d_{k_1,k_2}^{J_1,J_2}(t_k)$  are the unknown parameters and have to be determined, e.g. from the GNSS observation equations (3.3a) and (3.3b).

The parameters  $k_1$  and  $k_2$  in Eq. (3.5) refer to the geometrical positions of the knot locations on the sphere and demonstrate the localizing feature of the 2D tensor product B-spline basis functions. The spatial resolution of the expansion (3.5) is controlled by the levels  $J_1$  and  $J_2$ . The number of polynomial B-spline functions in latitude direction is given by  $K_{J_1} = 2^{J_1} + 2$ , and  $K_{J_2} = 3 \cdot 2^{J_2}$  refers to the number of trigonometric B-splines in the longitude direction. Accordingly, the total number of B-spline coefficients reads  $K_{J_1} \cdot K_{J_2}$ .

The global VTEC representation (3.5) requires a properly handling of constraints to preserve spherical geometry. Two sets of constraint equations, namely the pole equality and the pole continuity, are introduced for the B-spline model representing a function defined on the sphere. Accordingly, the overall constraint equation reads

$$\mathbf{X}_{d_{MC,k}} \mathbf{d}_k = \mathbf{y}_{MC,k} \quad (3.6)$$

where  $\mathbf{X}_{d_{MC,k}}$  is a known matrix,  $\mathbf{y}_{MC,k}$  equals to the zero vector and the vector  $\mathbf{d}_k$  comprises the B-spline coefficients.

Data gaps due to the heterogeneous GNSS data distribution and the large size of unknown parameters typically make estimators vulnerable to numerical problems, such as ill-conditioning and filter instability. The global real-time approach is extended by supplementary information to keep the Kalman filter numerically stable and to enhance the estimation quality at regions suffering from large data gaps. This supplementary information can be considered as a background ionosphere model providing homogeneous observations to support the real-time model over the oceans where the filter usually suffers from a lack of enough observations. Moreover, it feeds the estimator in case of interruptions in the real-time data streams, e.g., due to loss of the connection to data providers. The supplementary information is obtained in the form of

B-spline coefficients from the ultra-rapid global VTEC product of DGFI-TUM with a delay of less than 3 hours<sup>1</sup>. Because of its dissemination latency, the supplementary information has to be transferred into real-time modeling via a nowcast model.

The nowcast model comprises a stochastic and a deterministic part. A linear trend (LT) model and a trigonometric series (TS) are chosen to represent the deterministic part in the time series of B-spline coefficients. For the stochastic part, an ARMA process is run consisting of an autoregressive polynomial of order  $p$  and a moving average polynomial of order  $q$ . The overall nowcast model reads

$$\begin{aligned}
 d_{k_1, k_2, \text{NC}}^{J_1, J_2}(t_k) &= \{c_0 + c_1 \cdot t_k\}_{k_1, k_2}^{\text{LT}} \\
 &+ \left\{ \sum_{i=1}^N (a_i \cdot \cos(\omega_i t_k) + b_i \cdot \sin(\omega_i t_k)) \right\}_{k_1, k_2}^{\text{TS}} \\
 &+ \left\{ Z_{t_k} + \sum_{m=1}^q (\phi_k \cdot Z_{t_{k-m}}) + \sum_{l=0}^p (\theta_k \cdot X_{t_{k-l}}) \right\}_{k_1, k_2}^{\text{AR}}, \quad (3.7)
 \end{aligned}$$

where the first term refers to the LT model consisting of the coefficients  $c_0$  and  $c_1$ . The term  $\{\cdot\}_{k_1, k_2}^{\text{TS}}$  refers to the TS model including the series coefficients  $a_1, \dots, a_N$  and  $b_1, \dots, b_N$  with the known periods  $T_i = 2\pi/\omega_i$ . The term  $\{\cdot\}_{k_1, k_2}^{\text{AR}}$  stands for the ARMA process including the coefficients  $\phi_1, \dots, \phi_p$  and  $\theta_1, \dots, \theta_q$  of the auto-regressive part and the moving average part, respectively. Moreover, the parameters  $X_{t_k}$  and  $Z_{t_k}$  are the residual signal and the error term.

The coefficients of the nowcast model are determined for each B-spline coefficient independently. Firstly, the linear trend and the trigonometric series coefficients are computed by fitting the deterministic model  $\{\cdot\}_{k_1, k_2}^{\text{LT}} + \{\cdot\}_{k_1, k_2}^{\text{TS}}$  to the input time series of a B-spline coefficient. Next, the residual signal, which is obtained by subtracting the deterministic signal from the input signal, is used to compute the coefficients of the ARMA model  $\{\cdot\}_{k_1, k_2}^{\text{AR}}$ . The overall estimation procedure is repeated every hour to keep the parameters of the nowcast model up to date. Once the coefficients are estimated, the nowcasted B-spline coefficients  $\mathbf{d}_{\text{NC}, k}$  are obtained by extrapolating (3.7) to the present time. The nowcasted coefficients are considered in real-time modeling as a vector of supplementary observations  $\mathbf{y}_{\text{NC}, k}$  given as

$$\mathbf{y}_{\text{NC}, k} = \mathbf{d}_{\text{NC}, k}. \quad (3.8)$$

The measurement model of the Kalman filter is constructed from the observation equations (3.3a) and (3.3b) for each GNSS satellite, the constraint equation (3.6), and the supplementary information derived from the nowcast model (3.8). The measurement model reads

$$\mathbf{y}_k + \mathbf{e}_k = \mathbf{X}_k \boldsymbol{\beta}_k, \quad (3.9)$$

where  $\mathbf{X}_k$  is the design matrix,  $\boldsymbol{\beta}_k$  denotes the vector of the B-spline coefficients, and  $\mathbf{e}_k$  is the error vector. The measurement vector  $\mathbf{y}_k$  comprises the sub-vectors  $\mathbf{y}_{\text{GPS}, k}$ ,  $\mathbf{y}_{\text{GAL}, k}$ ,  $\mathbf{y}_{\text{NC}, k}$  and  $\mathbf{y}_{\text{MC}, k}$ . The constraint equation (3.6) is handled by the method of perfect measurements and therefore the sub-vector  $\mathbf{y}_{\text{MC}, k}$  is considered as measured. The state vector  $\boldsymbol{\beta}_k$  consists of the sub-vector  $\mathbf{d}_k = (d_{k_1, k_2}^{J_1, J_2}(t_k))$  of the unknown B-spline coefficients  $d_{k_1, k_2}^{J_1, J_2}(t_k)$  and the sub-vectors  $\mathbf{c}_{r, \text{GPS}, k}^s$  and  $\mathbf{c}_{r, \text{GAL}, k}^s$  of the arc biases (3.4). The design matrix  $\mathbf{X}_k$  in (3.9) is given as

$$\mathbf{X}_k = \begin{bmatrix} \mathbf{X}_{\text{yGPS}, k} \\ \mathbf{X}_{\text{yGAL}, k} \\ \mathbf{X}_{\text{yNC}, k} \\ \mathbf{X}_{\text{yMC}, k} \end{bmatrix} = \begin{bmatrix} \mathbf{X}_{d\text{GPS}, k} & \mathbf{X}_{C\text{GPS}, k} & \mathbf{0} \\ \mathbf{X}_{d\text{GAL}, k} & \mathbf{0} & \mathbf{X}_{C\text{GAL}, k} \\ \mathbf{X}_{d\text{NC}, k} & \mathbf{0} & \mathbf{0} \\ \mathbf{X}_{d\text{MC}, k} & \mathbf{0} & \mathbf{0} \end{bmatrix}. \quad (3.10)$$

<sup>1</sup>Goss A., et al.: *High-resolution vertical total electron content maps based on multi-scale B-spline representations*. *Annales Geophysicae*, doi:10.5194/angeo-37-699-2019, 2019

Herein,  $\mathbf{X}_{d_{GPS},k}$  and  $\mathbf{X}_{d_{GAL},k}$  are the design sub-matrices for GPS and GALILEO w.r.t. the vector  $\mathbf{d}_k$  of the unknown B-spline coefficients. The design sub-matrices for the arc biases of GPS and GALILEO are  $\mathbf{X}_{C_{GPS},k}$  and  $\mathbf{X}_{C_{GAL},k}$ . The matrix  $\mathbf{X}_{d_{NC},k}$  refers to the design matrix of the nowcasted observation and is equivalent to the identity matrix.  $\mathbf{X}_{d_{MC},k}$  stands for the design matrix of the constraint equation (3.6). For more details concerning the Kalman filter implementation, see Erdogan et al. (2021).

The flowchart in Fig. 3.2 summarizes the different steps of the presented real-time modeling approach. The overall procedure can be split into three main categories highlighted by different colors in Fig. 3.2, namely (1) the ultra-rapid VTEC product generation, (2) the nowcasting of the global VTEC, and (3) the real-time VTEC modeling.

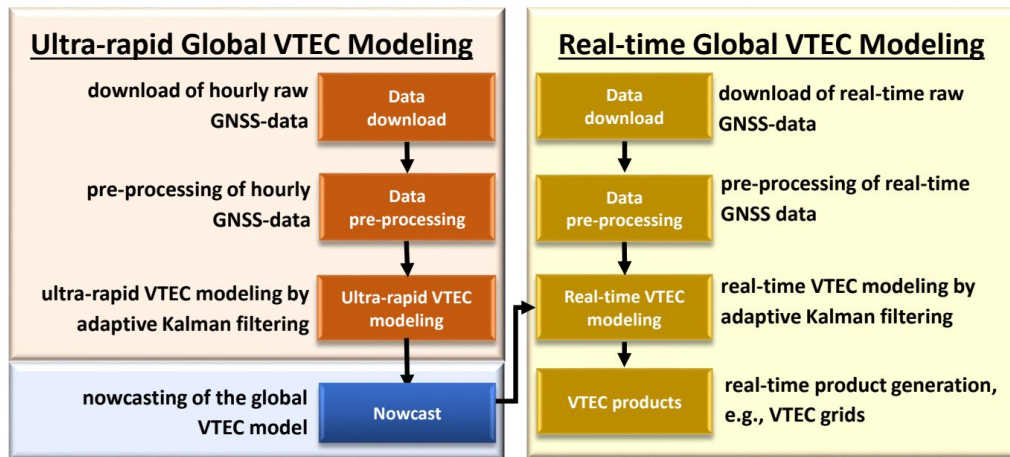


**Figure 3.2:** Overall flowchart of the developed real-time modeling approach (Erdogan et al., 2021).

In parallel to the ultra-rapid product generation and the nowcasting processes, real-time GNSS data are continuously downloaded in the RTCM format. As mentioned earlier, 10 seconds of data sampling are applied to download raw GNSS data. In the real-time data processing step, carrier-phase observations are extracted from the raw data set. Phase-continuous arcs between receivers and satellites are constructed by checking cycle slips and data gaps. Then the ionosphere combination of carrier-phase observations (3.2) is computed.

In the next step, the real-time VTEC modeling, the validity of each carrier-phase bias in the state vector is checked in the data editing process before incorporating the observations into the filter; outdated bias parameters are removed, and new biases are introduced into the filter state vector and its covariance matrix. After that, the ionospheric target parameters consisting of the B-spline coefficients and the carrier-phase biases are estimated sequentially using the real-time adaptive Kalman filter. It should be noted that the filter temporal step size is set to 30 seconds by taking computational resources into account, though the data download rate and the pre-processing step size are set to 10 seconds.

Figure 3.3 presents the real-time global VTEC map for April 28, 2019 at 00:00 UT (top right). The top left panel depicts DGFITUM's ultra-rapid global VTEC result 'othg' for the same time. Whereas in the real-time case the latency is around 30 to 60 seconds, the corresponding value of the ultra-rapid product is given by 2-3 hours. The standard deviations shown in the two bottom panels are in the same range and show a similar behavior. Deviations are mainly caused by the different global distribution of GNSS stations providing either hourly and/or real-time data. For both the ultra-rapid and the real-time model, the criteria for selecting the resolution levels  $J_1$  and  $J_2$  are essentially based on the distribution of the input data, the computational load, and the desired level of smoothness for the B-spline representation embedded into a

Kalman filter<sup>2</sup>. Accordingly, we chose for the example in Fig. 3.3 the B-spline level values  $J_1 = 5$  and  $J_2 = 3$ , leading to a total number of 816 time-dependent B-spline coefficients updated at each cycle of the filter.

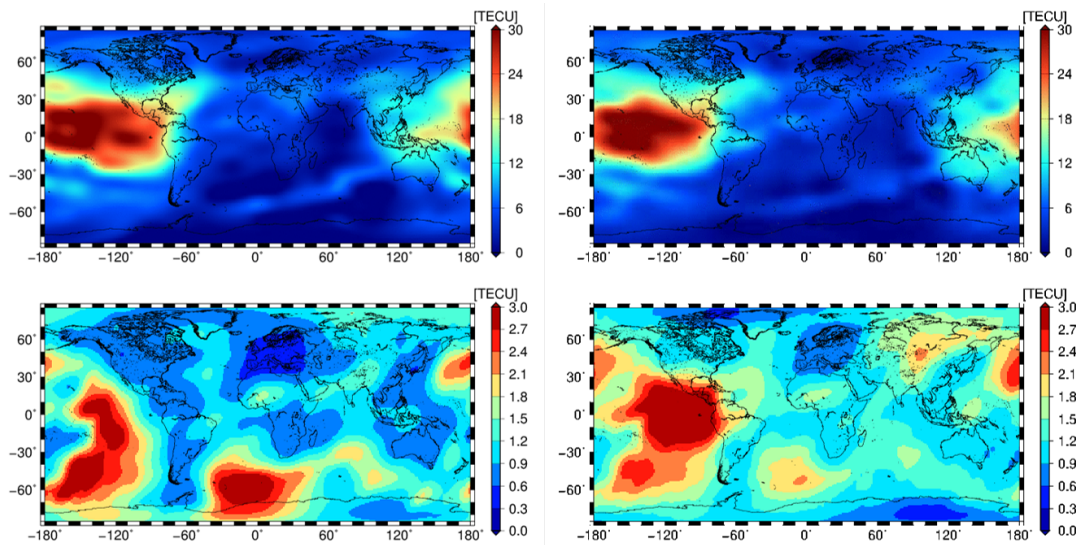


**Figure 3.3:** High resolution ultra-rapid global VTEC product 'othg' (top left) versus the real-time global VTEC model (top right) generated according to the developed real-time modeling approach presented in Fig. 3.2 for April 28, 2019, 00:00 UT ; the two bottom panels show the corresponding standard deviation maps.

### Machine Learning for Vertical Total Electron Content Forecasting

In another study within the OPTIMAP project, we aimed to improve VTEC forecasting during a geomagnetic storm by including solar and magnetic indices as exogenous variables in the ARMA model (3.7). However, this so-called ARIMAX model did not show significant improvements, since it cannot represent the non-linear relationship between VTEC and the exogenous variables, e.g. the disturbance storm time (Dst) index.

As an alternative, machine learning methods can be used for modeling complex and non-linear relationships between input and output variables. However, the development of a VTEC forecast model that includes a space weather component and can describe non-linear relationships between VTEC and, e.g. magnetic field variations is still a major challenge, but also a task of high interest to the GNSS community and to space weather services, e.g. for providing early warning information in case of space weather events. To consider space weather effects, the complete chain of physical processes between the Sun, the interplanetary magnetic field, the Earth's magnetic field and the ionosphere must be studied. The main objective of the **DAAD project ML-IonoCast** is to develop a model for VTEC forecast, taking into account physical processes and using state-of-the-art machine learning techniques, in order to better describe and understand the complex and non-linear relationships on the basis of appropriate data sets.

In 2021, we applied supervised learning to develop a model driven by a set of input variables, e.g. the solar wind and geomagnetic field information, to predict (estimate) output variables such as VTEC. To achieve this goal, a training set of observations  $(x_i, y_i)$  with time stamp  $i = 1, \dots, N$  for the period 01/2015 - 12/2016 was pre-processed with a time sampling of 1 hour. While the input variables  $x_i$  can be considered as predictors or independent variables, the output variables  $y_i = f(x_i)$  are called responses or dependent variables. Since we need a

<sup>2</sup>Erdogan E., et al.: *Adaptive Modeling of the Global Ionosphere Vertical Total Electron Content*. Remote Sensing, doi:10.3390/rs12111822, 2020

long time series of VTEC values in our study, we could not use DGFI-TUM's global ionosphere maps (GIM) from the OPTIMAP project, but took the corresponding GIMs from the Center for Orbit Determination in Europe (CODE) in Bern; cf Fig. 3.4. The other input data, such as the F10.7 time series (cf. the top panel in Fig. 3.8], were obtained from NASA OmniWeb.

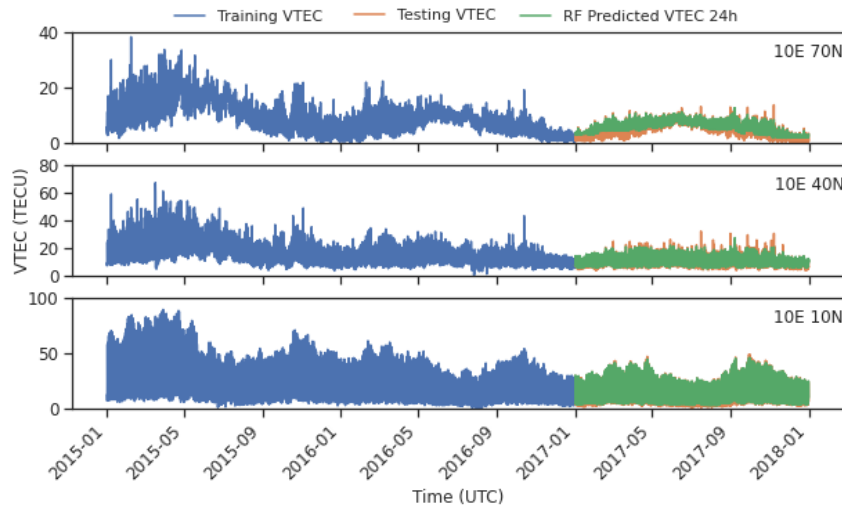


**Figure 3.4:** VTEC time series (blue) for three locations in different regions (from bottom to top: low-, mid- and high-latitude) is used to train the model for the period 01/2015 to 12/2016; the 24 hour forecasted VTEC model values (green) using Random Forest (RF) are compared with the testing VTEC data (orange) for the entire year 2017.

A machine learning algorithm aims to generate optimal prediction (estimation) rules to determine an approximation function  $\hat{y}_i = \hat{f}(x_i)$  that satisfies given optimisation criteria. In doing so, the learning algorithm changes the input-output relationship according to the differences  $y_i - \hat{f}(x_i)$  between the original and the predicted (estimated) output. This process means a learning by example and is called the training phase. When the learning process is completed, the approximation function  $\hat{f}(x)$  represents the predictive relationship between input and output, i.e. the desired model.

As mentioned before, the machine learning based VTEC model to be developed is trained using solar, geomagnetic and VTEC data from the past. In doing so, the training data should be representative of as many cases as possible that occur in practice. The quality of the data is crucial, e.g., outliers should be eliminated and data gaps should be filled in a pre-processing step. Since it is also advisable not to choose too much correlated input data, a correlation map, as shown in Fig. 3.5, may help. Consequently, a precise machine learning based VTEC forecast model requires a suitable combination of input and output variables.

Two machine learning algorithms have been applied in this study, namely Regression Tree (RT) and Random Forest regression (RF). A tree-based method is simple and easy to interpret but has a lower prediction accuracy. However using many decision trees, like in RF, the predictive performance of the trees can be significantly improved<sup>3</sup>.

Each training data pair  $(x_i, y_i)$  consists of the vector  $x_i = [x_{i,0}, x_{i,1}, \dots, x_{i,p}, \dots, x_{i,p-1}]^T$  of the  $P$  input variables  $x_{i,p}$  with  $p = 0, 1, \dots, P - 1$  at time stamp  $i$  and the response value  $y_i = f(x_i)$ . Whereas the vectors  $x_i$  can be interpreted as the rows of the  $N \times P$  predictor matrix  $\mathbf{X} = [\mathbf{X}_0, \mathbf{X}_1, \dots, \mathbf{X}_p, \dots, \mathbf{X}_{p-1}]$ , the components  $x_{i,p}$  of the  $N \times 1$  column vector  $\mathbf{X}_p = [x_{1,p}, x_{2,p}, \dots, x_{i,p}, \dots, x_{N,p}]^T$  represent a time series of the  $p$ th input variable. To generate a RT, the input predictor space, i.e. the set of possible values for the matrix  $\mathbf{X}$  is divided into

<sup>3</sup>Breiman, L.: *Random forests*. Machine Learning, doi:10.1023/A:1010933404324, 2001

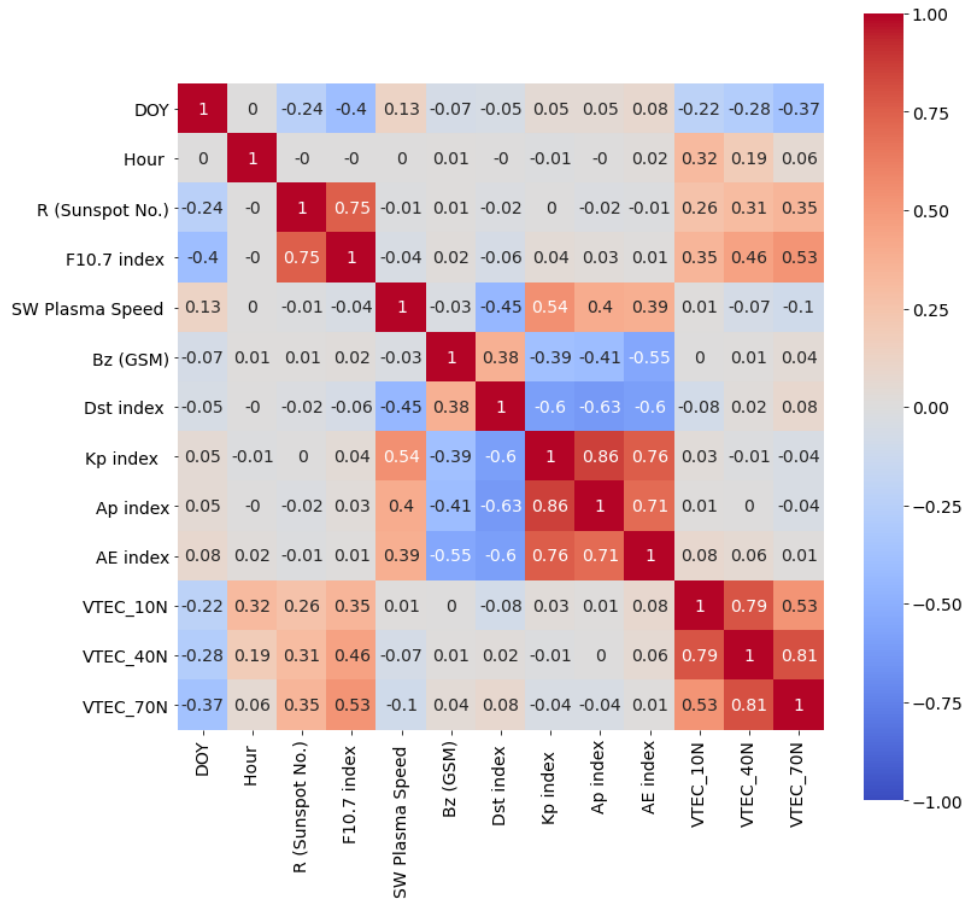


**Figure 3.5:** Correlations between different input data sets and VTEC for the period 01/2015 to 12/2016: the largest correlations between VTEC and other data sets occur in relation to the F10.7 index, the sunspot number R, the hour of day (Hour) and the day of year (DOY).

$J$  distinct and non-overlapping regions  $R_1, R_2, \dots, R_j, \dots, R_J$ , represented as high-dimensional rectangles or boxes, which are found by minimizing the empirical risk

$$\hat{\Theta} = \arg \min_{\Theta} \sum_{j=1}^J \sum_{i \in R_j} (y_i - \gamma_j)^2 \quad (3.11)$$

with  $\Theta = \{\gamma_j, R_j\}_{j=1}^J$ ; in Eq. (3.11) the quantity  $\gamma_j$  is the mean value of the training observations  $y_i$  falling into the region  $R_j$ <sup>4</sup>.

In our study, a RT was generated from training data by recursive binary splitting. For simplicity, a small RT of depth 3 is shown in Fig. 3.6. The tree is generated for VTEC nowcasting solely based on solar and magnetic activity and temporal information. The approach starts at the top of the tree in the root node, where all observations belong to a single region spanned by the considered predictors; in the case of Fig. 3.6 we have three predictors with  $p = 0, 1, 3$ . Subsequently, the predictor space is successively split, i.e. a node is divided into two sub-nodes by the statement "true" or "false". At each splitting step, the predictor vector  $\mathbf{X}_p = (x_{i,p})$  and the split point value  $s$  are chosen such that the resulting two sub-regions (sub-nodes) for  $x_{i,p} \leq s$  and  $x_{i,p} > s$  lead to the largest possible reduction of the minimisation problem (3.11). A tree ends when a node has less than a minimum number of observations. Such a terminal node is also called a leaf.

<sup>4</sup>Hastie, T., et al.: *The elements of statistical learning: data mining, inference, and prediction*. Springer, doi: 10.1007/978-0-387-84858-7, 2009

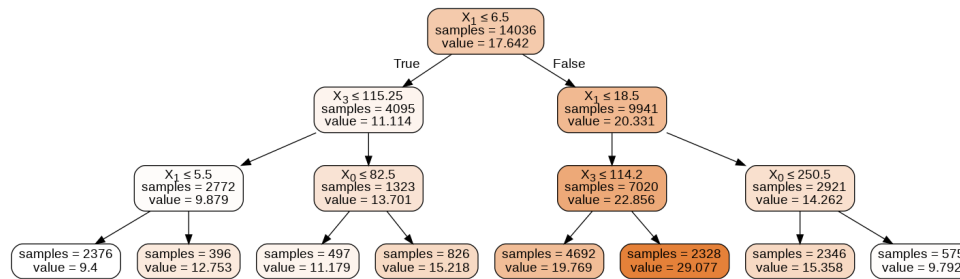


**Figure 3.6:** Example of a small decision tree with a depth of 3 for predicting VTEC at a geographical location with  $10^\circ$  longitude and  $10^\circ$  latitude. As predictors, i.e. input variables, we chose the day of year (DOY,  $p = 0$ ), the hour of day (Hour,  $p = 1$ ) and the F10.7 index ( $p = 3$ ). Since the tree is small, it was only created from input data highly correlated to VTEC; cf. Fig. 3.5.

As Fig. 3.6 shows, a single decision tree is highly interpretable. It can be easily visualized by a simple two-dimensional graph of a binary tree. However, due to its simplicity, a decision tree can be unstable, i.e. a small change in the input data can lead to a completely different splitting chain and thus a completely different tree. Another limitation of trees is the lack of smoothness of the prediction.

On the other hand, RF uses a combination of multiple regression trees, improving the stability and prediction accuracy at the expense of some loss in interpretation. In an example to forecast VTEC based on RF we consider a random sample of  $m = 6$  predictors as split candidates from a full set of  $P = 11$  predictors. As predictors we chose the first 10 input variables in Fig. 3.5 and add for  $p = P - 1 = 10$  one single VTEC time series for the selected latitude ( $10^\circ$ ,  $40^\circ$  or  $70^\circ$ ) to forecast VTEC for the next day. In this approach altogether 300 trees are used with a maximum depth set to 10. Thus, the final output means an average over these 300 trees.

However, when creating a large combination of trees an easy interpretation can be lost. Therefore, other parameters need to be defined to interpret the results, such as the relative importance of the input variables as shown in Fig. 3.7. It is often useful to study the relative importance or contribution of each input variable in predicting the response. As explained above, at each node in a tree, one of the predictors is used to split a region (node) into two sub-regions (sub-nodes) providing a maximum improvement in the minimization problem (3.11). The relative importance of one single predictor is then estimated as the sum of such squared improvements over all internal nodes for which it was chosen as the splitting variable.

The approach is discussed in Natras et al. (2022b) alongside with other machine learning methods for VTEC forecasting including adaptive boosting and extreme gradient boosting methods. The application of a feed-forward artificial neural network for spatio-temporal regional ionosphere modeling for Southeast Europe, based on regional ionosphere parameters estimated from CORS GNSS observations, as well as solar and geomagnetic parameters is presented by Natras et al. (2022a).

### Comparison of scale factors for the thermospheric density

The knowledge of the thermospheric density is of crucial importance not only for precise orbit determination (POD) of low Earth orbiting (LEO) satellites at altitudes below 1000 km, but also for re-entry predictions, for maneuver and satellite lifetime planning, as well as for many geo-scientific applications such as remote sensing, satellite gravimetry and satellite altimetry. Several empirical thermospheric models, such as the NRLMSISE-00 or the JB 2008 model, provide the thermospheric density among other parameters. Since these models are based on different input data sets, they can give quite different results, especially for strong space

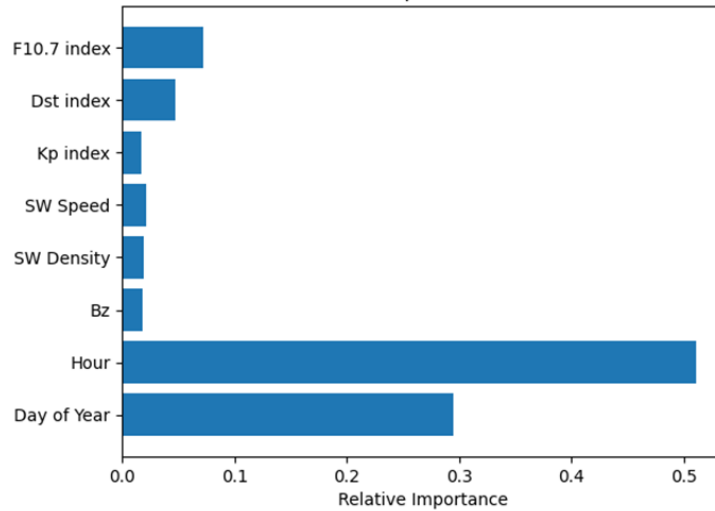


**Figure 3.7:** Bar plot of the estimated relative importance of various input variables to VTEC nowcast from a model based on RF with a maximum depth set to 10 for a location at mid-latitude  $40^\circ$ . We consider random samples of  $m = 6$  predictors from altogether  $P = 11$  input variables. The hour of day (Hour) and the day of year (DOY) show with 50% and 30% the largest relative importance values followed by the F10.7 and the Dst index.

weather events. Since LEO satellites are sensitive to atmospheric drag, appropriate on-board instrumentation (accelerometers, trackers, reflectors, etc.) can be used to derive density information. As satellites above 550 km are usually not equipped with accelerometers, an important question arises when modeling the thermosphere from SLR measurements:

*Do SLR measurements to LEO satellites provide a suitable complement to accelerometer measurements to obtain thermospheric density information?*

In the **DFG project TIPOD**, we have addressed this question in collaboration with our partners from the Institute of Geodesy and Geoinformation (IGG) at the University of Bonn. The results are published in the article of Zeitler et al. (2021). We distinguish between two approaches: the first one utilizes the POD of LEO satellites to estimate scale factors of the thermospheric density from SLR tracking measurements<sup>5</sup>. The second approach consists in the calculation of scale factors of the thermospheric density from the evaluation of the aerodynamic acceleration using satellite accelerometer measurements<sup>6</sup>.

In the equation of motion of a satellite the aerodynamic acceleration is defined as

$$\mathbf{a}_{\text{aero}} = -\frac{1}{2} \frac{A_{\text{ref}}}{m} \mathbf{c}_{\text{aero}} \rho_M v_{\text{rel}}^2, \quad (3.12)$$

where  $\mathbf{c}_{\text{aero}}$  is a dimensionless force coefficient vector depending on the geometry and orientation of the satellite,  $A_{\text{ref}}$  is the effective cross-section of the satellite interacting with the atmosphere,  $m$  means the total satellite mass,  $\rho_M$  is the thermospheric density and  $v_{\text{rel}}$  means the velocity of the satellite relative to the atmosphere.

The first of the two aforementioned approaches is typically applied to spherical LEO satellites. In this case, we obtain from Eq. (3.12) with  $\mathbf{a}_{\text{aero}} \approx \mathbf{a}_D$  the drag acceleration

$$\mathbf{a}_D = -\frac{1}{2} f_{s,\text{SLR}} \frac{A_{\text{ref}}}{m} C_D \rho_M v_{\text{rel}}^2 \mathbf{x}, \quad (3.13)$$

<sup>5</sup>Panzetta F., et al.: *Absolute thermospheric density estimation from SLR observations of LEO satellites - A case study with ANDE-Pollux satellite*. Journal of Geodesy, doi:10.1007/s00190-018-1165-8, 2018

<sup>6</sup>Vielberg K., et al.: *Comparison of Accelerometer Data Calibration Methods Used in Thermospheric Neutral Density Estimation*. Annales Geophysicae, doi:10.5194/angeo-36-761-2018, 2018



where  $\mathbf{x}$  is the along-track unit vector and  $C_D$  means the dimensionless aerodynamic drag coefficient, computed analytically following physical principles considered in a gas-surface interaction model. Assuming that the quantities  $A_{\text{ref}}$ ,  $m$ ,  $C_D$  and  $v_{\text{rel}}$  are precisely known, the time-dependent scale factor  $f_{s,\text{SLR}}$  can be interpreted as a pure scaling of the thermospheric density  $\rho_M$  provided by a thermosphere model. In our numerical investigations, we used the empirical model NRLMSISE-00, which describes the neutral temperature and density from the Earth surface to the lower exosphere, i.e. between 0 km and 1000 km. Applying a POD, the scale factor  $f_{s,\text{SLR}}$  estimated from SLR measurements has to be interpreted as the mean value resulting from the integration along the orbit during a time interval of 24 hours up to 6 hours<sup>7</sup>. We chose the four spherical LEO satellites Starlette (mean altitude: 957 km), WESTPAC (835 km), Stella (798 km) and Larets (681 km) and verified the reliability of the estimated scale factors by using the two POD software packages DOGS-OC of DGFITUM and GROOPS operated at IGG Bonn.

In the second approach, space-borne accelerometry was used to provide in-situ thermospheric density data along the satellite orbit with a high temporal resolution of, e.g., 10 seconds for GRACE. An accelerometer measures the non-gravitational acceleration acting on a spacecraft. Since the atmospheric drag is the largest non-gravitational acceleration for LEO satellites, there is a direct relation between the density at the position of the satellite and the measured acceleration. Solving Eq. (3.12) for  $\rho_M =: \rho_{\text{ACC}}$  we obtain the thermospheric density

$$\rho_{\text{ACC}} = \frac{-2 \cdot m \cdot \mathbf{x}^T \mathbf{a}_{\text{aero}}}{A_{\text{ref}} \cdot \mathbf{x}^T \mathbf{c}_{\text{aero}} \cdot v_{\text{rel}}^2} \quad (3.14)$$

from accelerometer measurements. In case of a non-spherical satellite, the geometry and the attitude of the complex-shaped satellite surface and its interaction with atmospheric particles have to be taken into account, i.e. both a high-quality macro model and an attitude realization have to be used. For more details concerning Eq. (3.14) and its evaluation we refer to the aforementioned publication of Vielberg (2018) as well as Forootan et al. (2021). Finally, the time-dependent scale factor

$$f_{s,\text{ACC}} = \frac{\rho_{\text{ACC}}}{\rho_M}. \quad (3.15)$$

can be calculated as the quotient of the density (3.14) and the density  $\rho_M$  of the NRLMSISE-00 model. Our colleagues from IGG Bonn applied this procedure to CHAMP (mean altitude: 454 km) and GRACE (500 km).

To compare the scale factors  $f_{s,\text{SLR}}$  and  $f_{s,\text{ACC}}$  obtained from SLR and accelerometers, the temporal resolution was fixed to 12 hours, i.e. the integration interval within the POD was set to the same value as the time interval for averaging the accelerometer results. Additionally, we compared our scale factors with fitted thermospheric density ratios (FDR) which have also been used to scale the modelled thermospheric density provided by the NRLMSISE-00 model<sup>8</sup>.

Figure 3.8 visualises the time series of the scale factors  $f_{s,\text{SLR}}$ ,  $f_{s,\text{ACC}}$  and  $f_{\text{FDR}}$  after performing a noise reduction using a 10-day moving average filter. It can be seen that at low solar activity (cf. the time series of the F10.7 index in the upper panel) the scale factors fluctuate by  $\pm 30\%$  around the value 1. At high solar activity, on the other hand, the scale factors vary sometimes dramatically, e.g. in case of Starlette they deviate by up to  $\pm 70\%$  from the value 1, especially in the years 1999 to 2003.

In general, the estimated scale factors indicate by how much the thermospheric density values calculated from the NRLMSISE-00 model deviate from those estimated using the two geodetic

<sup>7</sup>Rudenko S., et al.: *Calibration of empirical models of thermospheric density using satellite laser ranging observations to near-Earth orbiting spherical satellites*. IAG Symposia, doi:10.1007/1345\_2018\_40, 2018

<sup>8</sup>Emmert J., et al.: *A Globally Averaged Thermospheric Density Data Set Derived From Two-Line Orbital Element Sets and Special Perturbations State Vectors*. Journal of Geophysical Research: Space Physics, doi:10.1029/2021JA029455, 2021

observation techniques. Since NRLMSISE-00 underestimates or overestimates the density at different solar activity levels significantly, the calculated thermospheric density must be multiplied by the determined time- and altitude-dependent scale factors.

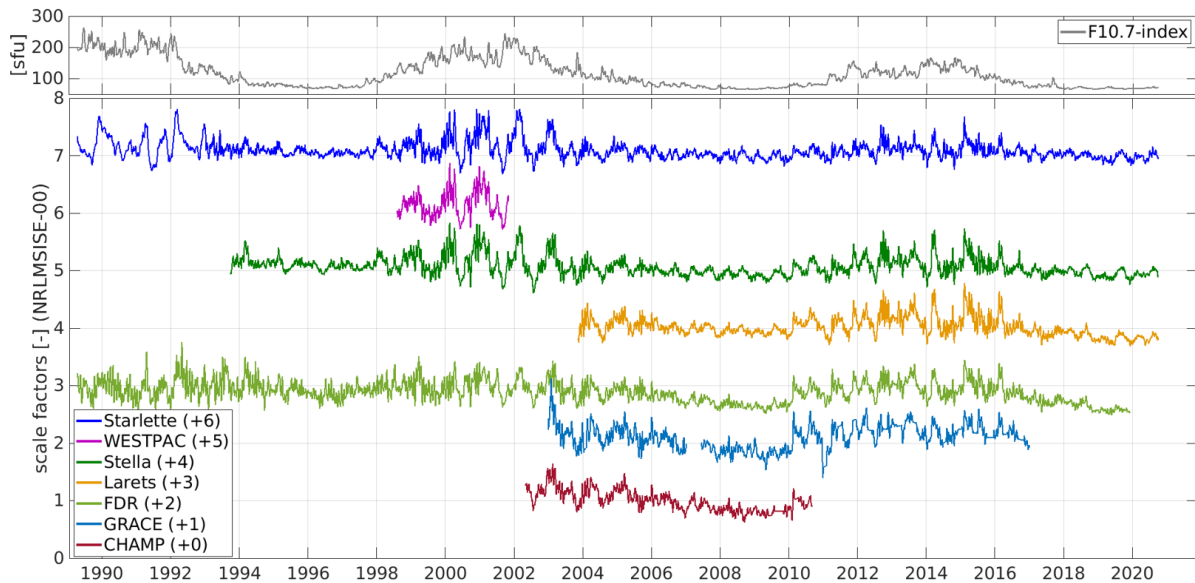


**Figure 3.8:** Filtered scale factors  $f_{s,SLR}$  from SLR (using DOGS-OC),  $f_{s,ACC}$  of accelerometer measurements from CHAMP and GRACE and of the fitted density ratios  $f_{FDR}$  in an averaged altitude of 575 km compared to the F10.7 solar activity index (top; in solar flux unit, sfu). Scale factor time series are shifted against each other by +1 according to their mean altitude to make them more distinguishable (Zeitler et al., 2021).

Table 3.1 lists the mean values and standard deviations of the scale factor time series for both low and high solar activity. In the first case, the scale factors generally increase with increasing satellite altitude, while for the latter case they decrease with increasing altitude. Therefore, on average, the NRLMSISE-00 model overestimates the thermospheric density at low solar activity and needs to be downscaled using the estimated scale factors, while the model underestimates the thermospheric density at high solar activity and therefore needs to be upscaled.

**Table 3.1:** Mean values and standard deviations (STD) of estimated scale factors  $f_{s,SLR}$  and  $f_{s,ACC}$  for various satellite altitudes from SLR measurements and from GRACE and CHAMP accelerometer measurements. The same quantities are given for the scale factors  $f_{FDR}$  at the average altitude of 575 km. All values refer to low (01.01.2006 - 03.09.2010) and high (01.01.2011 - 31.12.2016) solar activity conditions.

Solar activity	Statistics	Starlette	Stella	Larets	FDR	GRACE	CHAMP
Low	Mean	1.01	0.96	0.99	0.74	0.95	0.89
	STD	0.07	0.08	0.09	0.12	0.16	0.11
High	Mean	1.10	1.12	1.12	0.96	1.20	-
	STD	0.12	0.17	0.19	0.16	0.16	-

Table 3.2 shows the correlations between the time series of scale factors estimated from different satellite solutions and the external FDR data set. These values are calculated at overlapping time intervals for each pair of scale factor time series. They vary between 0.70 and almost 1. The three numbers highlighted in yellow in Tab. 3.2 signify the largest correlations. These are (1) with the value 0.98 the SLR comparison between WESTPAC and Stella, (2) with the value 0.81 a mixed SLR/accelerometer solution between Larets and GRACE: and (3) with the value 0.89 a pure accelerometer solution between GRACE and CHAMP. It is noticeable that the correlation coefficients become larger with a decreasing altitude difference between the satellites. The correlation coefficients of the FDR time series confirm a high agreement with the other derived scale factor time series.

**Table 3.2:** Correlations between scale factor time series estimated from different satellite solutions and the external FDR data set. The highest SLR-only, accelerometer-only and mixed SLR-accelerometer correlation values are highlighted in yellow (Zeitler et al., 2021).

	Starlette	WESTPAC	Stella	Larets	FDR	GRACE	CHAMP
Starlette	1	0.96	0.90	0.86	0.73	0.71	0.70
WESTPAC	0.96	1	0.98	-	0.83	-	-
Stella	0.90	0.98	1	0.93	0.84	0.77	0.75
Larets	0.86	-	0.93	1	0.93	0.81	0.74
FDR	0.73	0.83	0.84	0.93	1	0.89	0.92
GRACE	0.71	-	0.77	0.81	0.89	1	0.89
CHAMP	0.70	-	0.75	0.74	0.92	0.89	1

In this study it was shown that time-averaged scale factors from in-situ accelerometer measurements on board CHAMP and GRACE fit well to arcwise scale factors estimated from SLR measurements to spherical satellites. Therefore, we can answer the above question positively, i.e. yes, SLR measurements on LEO satellites are a very well suited complement to accelerometer measurements to obtain information on the thermospheric density.

### Related publications

- Erdogan E., Schmidt M., Goss A., Görres B., Seitz F.: *Real-time monitoring of ionosphere VTEC using Multi-GNSS carrier-phase observations and B-splines*. Space Weather, doi: [10.1029/2021sw002858](https://doi.org/10.1029/2021sw002858), 2021
- Forootan E., Farzaneh S., Kosary M., Schmidt M., Schumacher M.: *A simultaneous calibration and data assimilation (C/DA) to improve NRLMSISE00 using thermospheric neutral density (TND) from space-borne accelerometer measurements*. Geophysical Journal International, doi:[10.1093/gji/ggaa507](https://doi.org/10.1093/gji/ggaa507), 2021
- Jarmołowski W., Belehaki A., Hernández Pajares M., Schmidt M., Goss A., Wielgosz P., Yang H., Krypiak-Gregorczyk A., Tsagouri I., Paouris E., Monte-Moreno E., García-Rigo A., Milanowska B., Erdogan E., Graffigna V., Haagmans R.: *Combining Swarm Langmuir probe observations, LEO-POD-based and ground-based GNSS receivers and ionosondes for prompt detection of ionospheric earthquake and tsunami signatures: case study of 2015 Chile-Illapel event*. Journal of Space Weather and Space Climate, doi:[10.1051/swsc/2021042](https://doi.org/10.1051/swsc/2021042), 2021
- Natras, R., Magnet N., Halilovic D., Goss A., Schmidt M., Weber R., Mulic M.: *Regional ionosphere delay models based on CORS data and machine learning*. NAVIGATION, Wiley, 2022a, submitted
- Natras R., Soja B., Schmidt M.: *Ensemble Machine Learning of Random Forest, AdaBoost and XGBoost for Forecasting Vertical Total Electron Content of the Ionosphere*. Journal of Geodesy, 2022b, submitted
- Zeitler L., Corbin A., Vielberg K., Rudenko S., Löcher A., Bloßfeld M., Schmidt M., Kusche J.: *Scale factors of the thermospheric density: a comparison of Satellite Laser Ranging and accelerometer solutions*. Journal of Geophysical Research: Space Physics, doi:[10.1029/2021JA029708](https://doi.org/10.1029/2021JA029708), 2021

## 3.2 Regional Gravity Field

Gravity field determination is a major topic in geodesy, supporting applications from Earth system sciences, orbit determination, and the realization of the International Height Reference System (IHRs). Local high-resolution gravity measurements (e.g., terrestrial, airborne, and shipborne) can be combined with medium-resolution data (e.g. inferred from satellite altimetry missions) and low-resolution global data provided by satellite gravity missions, such as the Gravity Recovery and Climate Experiment (GRACE) and the Gravity Field and Steady-State Ocean Circulation Explorer (GOCE) for regional gravity field refinement. The optimal combination of different types of gravity observations with varying spatial and spectral resolution is the key to obtain a high-resolution and high-precision regional gravity model. In current studies based on spherical radial basis functions (SRBFs), a single-level approach is commonly applied, which combines all the data types at the maximum degree of expansion. Although promising results have been reported from numerous studies<sup>9</sup>, it has been suspected that this approach may fail to extract the full information contained in the gravity data<sup>10</sup>. To take the spectral sensitivity of each observation technique into consideration, a spectral combination based on SRBFs is realized through the multi-resolution representation (MRR) in the framework of the **DFG Project ORG4Heights**.

### Multi-resolution representation

The fundamental idea of the MRR as applied in ORG4Heights is that a given gravity signal is decomposed into an expansion in terms of spherical harmonics for the long-wavelength part, and a number of frequency-dependent detail signals each represented in terms of wavelet functions for the medium and the high frequency part<sup>11</sup>. The spectral domain is discretized into multiple frequency bands indicated by the level values  $i = i', i' + 1, \dots, I - 1, I$ , which include a certain number of spectral degree values (see Fig. 3.9). The MRR of a gravity functional  $F(\mathbf{x})$  can be expressed as

$$F(\mathbf{x}) = \bar{F}(\mathbf{x}) + \sum_{i=i'}^I G_i(\mathbf{x}) + r(\mathbf{x}) \quad (3.16)$$

where  $\bar{F}(\mathbf{x})$  is a reference model, i.e., usually the long-wavelength component from a global gravity model (GGM), and it is used as the background model within the remove-compute-restore (RCR) procedure.  $G_i(\mathbf{x})$  are the detail signals of the resolution levels  $i = i', 1, \dots, I - 1, I$ , and  $r(\mathbf{x})$  is the truncation error. The detail signal  $G_i(\mathbf{x})$  of level  $i$  in Eq. (3.16) is defined as

$$G_i(\mathbf{x}) = \sum_{k=1}^{K_i} d_{k,i} \Psi_i(\mathbf{x}, \mathbf{x}_{k,i}). \quad (3.17)$$

Herein, the position vectors  $\mathbf{x}_{k,i}$  with  $k = 1, 2, \dots, K_i$  are related to the level- $i$  grid points where the spherical wavelet functions  $\Psi_i(\mathbf{x}, \mathbf{x}_{k,i})$  are centered and where the corresponding series coefficients  $d_{k,i}$  are located. Note, as point grids we chose in the sequel always Reuter grids.

The resolution levels  $i = i', 1, \dots, I - 1, I$  of the MRR are connected to each other by the pyramid algorithm, which is successfully realized in this work. It determines the coefficients of the lower resolution levels from the coefficients of the higher levels by successive low-pass filtering.

<sup>9</sup>Liu Q., et al.: *Determination of the regularization parameter to combine heterogeneous observations in regional gravity field modeling*. Remote Sensing, doi:10.3390/rs12101617, 2020

<sup>10</sup>Klees R., et al.: *A methodology for least-squares local quasi-geoid modelling using a noisy satellite-only gravity field model*. Journal of Geodesy, doi:10.1007/s00190-017-1076-0, 2018

<sup>11</sup>Schmidt M., et al.: *Regional gravity modeling in terms of spherical base functions*. Journal of Geodesy, doi:10.1007/s00190-006-0101-5, 2007

$i$	1	2	3	4	5	6	7	8	9	10	11	...
$n_i = 2^i - 1$	1	3	7	15	31	63	127	255	511	1023	2047	...
$\rho_i = \frac{\pi R}{n_i}$ [km]	20000	6667	2857	1333	645	317	157	78	39	20	10	...
	satellite gravimetry											
	satellite altimetry											
								terrestrial, air-/shipborne				

Figure 3.9: Numerical values for the spectral degree  $n_i$  and the spatial resolution  $\rho_i$  of the resolution levels  $i$  within the MRR (top); resolution levels covered by different gravity field observation techniques (bottom).

### The MRR based on the pyramid algorithm

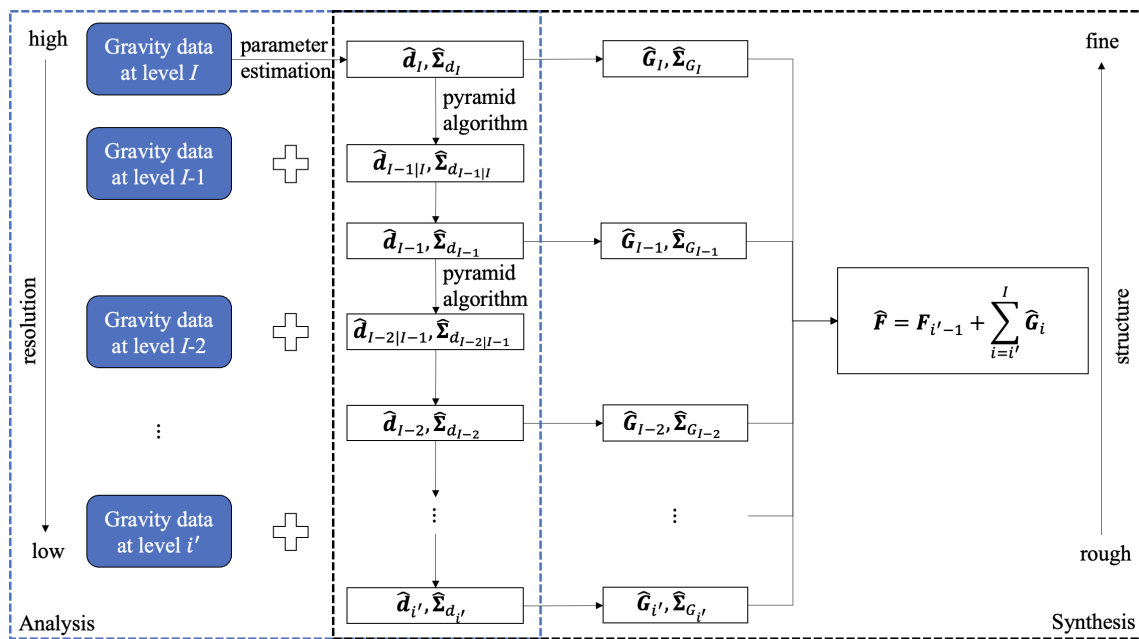
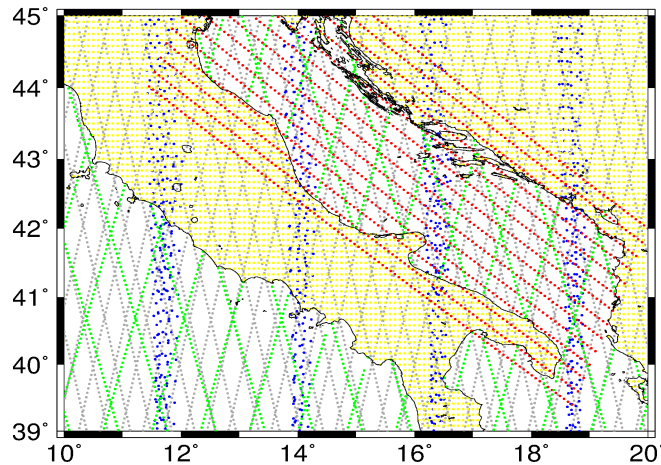


Figure 3.10: Flowchart for visualizing the MRR based on the pyramid algorithm

As shown from Fig. 3.9, gravity data from different observation techniques are sensitive to different frequency bands and can be classified according to their spectral resolution. To benefit from the individual strengths of each data set optimally, an MRR scheme is developed based on the pyramid algorithm, in connection with sequential parameter estimation. This approach, visualized in Fig. 3.10, allows different data types to be introduced to the estimation model at the spectral level of their highest sensitivity. Within the procedure the coefficients are in the first step estimated at the highest resolution level  $I$  using only the high-resolution data set(s). Then they are transformed to the next lower level  $I - 1$  by applying low-pass filtering, i.e., the pyramid algorithm. At the lower level, the coefficient vector is updated by the lower-resolution data set(s) introduced at this level. Direct combination of coefficients from the pyramid algorithm and new data is realized through a parameter estimation procedure<sup>12</sup>. The updated coefficient vector is then used in combination with the corresponding wavelet functions to calculate the detail signal (Eq. (3.17)). Continuing this process until the lowest level  $i'$  of the MRR, all data sets are introduced into the scheme at different resolution levels and the coefficient vectors, the detail signals as well as all their covariance matrices are obtained.

<sup>12</sup>Liu Q., et al.: Regional gravity field refinement for (quasi) geoid determination based on spherical radial basis functions in Colorado. Journal of Geodesy, doi:10.1007/s00190-020-01431-2, 2020

Numerical investigations are conducted to compare the performance of the MRR based on the pyramid algorithm with the single-level SRBF approach. As shown in Fig. 3.11 five types of gravity observations have been simulated from the global gravity model GECO. They are used along with simulated observation noise for calculating the gravity models. The terrestrial, airborne, altimetry, GOCE, and GRACE data are included in the estimation model at the levels 11, 10, 9, 8, and 7, respectively.



**Figure 3.11:** The study area and the simulated gravity data, including terrestrial (yellow dots), airborne (red dots), altimetry (green dots), GOCE (grey dots), and GRACE (blue dots) data

Figure 3.12 (cf. Liu et al. 2022) visualizes the estimated coefficients at each resolution level. At level 11 (first row), only terrestrial observations are involved. Consequently, additional gravity information with respect to the background model is captured in the onshore area, where the terrestrial data are available (see Fig. 3.11). From the second row (level 10) to the fifth row (level 7), the left plots show the scaling coefficients calculated directly from the pyramid algorithm, and the right ones are the updated coefficients after including the gravity data at this level  $i$ . The gravity observations used at each level insert additional gravity information in the region where they are located, and at the same time, the gravity signals captured from the previous level are preserved.

The calculated detail signals (left column) of the MRR as well as the gravity signal (right column) of each resolution level are presented in Fig. 3.13 (Liu et al. 2022). The gravity signal (in terms of disturbing potential) of level 6 (right column, last row) is the long wavelength component from the global gravity model GECO, which only contains very smooth information. The detail signals at different levels show the spectral information contained in the corresponding frequency ranges (see Fig. 3.9). When the resolution level increases from level 7 (fifth row) to level 11 (first row), more and more fine structures show up in both the detail signals and the gravity signals.

**Table 3.3:** Comparison between the single-level model and the MRR based on the pyramid algorithm, with respect to the validation data in terms of disturbing potential values (unit [ $\text{m}^2/\text{s}^2$ ])

	Min	Max	Mean	RMS	Corr.
Single-level model	-38.22	21.64	-1.83	5.48	0.97
MRR based on pyramid algorithm	-20.98	12.82	0.99	3.44	0.99

The gravity model calculated from the MRR based on the pyramid algorithm is evaluated by the validation data in terms of disturbing potential values, and their differences are given in

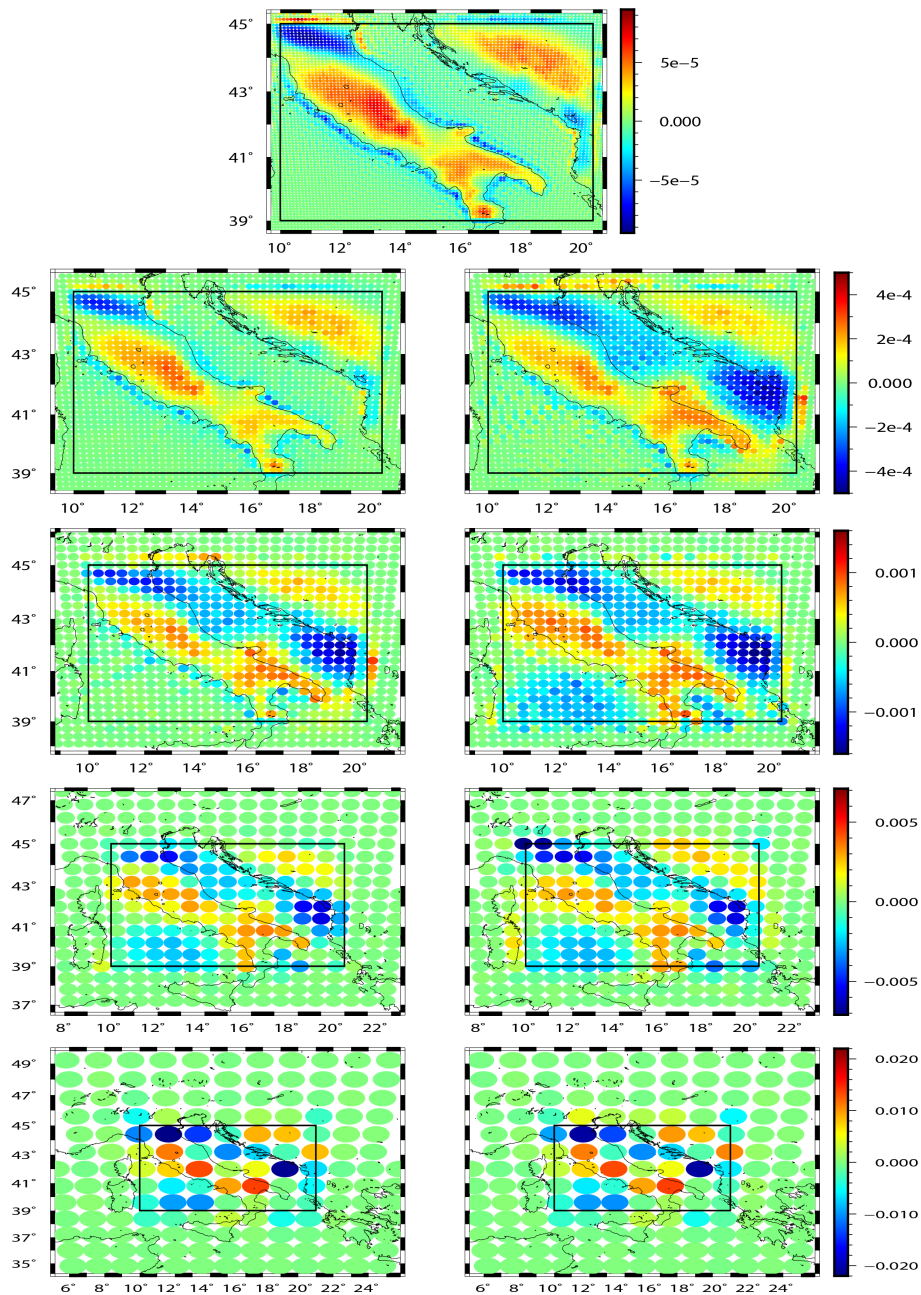


**Figure 3.12:** The estimated series coefficients at level 11 (first row), and levels 10, 9, 8, 7 (second to fifth row). From the second to the fifth row, the left column represents the coefficients estimated directly from the pyramid algorithm, and the right column represents the updated coefficients after including the new data at this level. The black rectangle inside each plot shows the observation area (see Fig. 3.11)

Fig. 3.14 (right). For comparison, the single-level gravity model is also computed, and Fig. 3.14 (left) shows its differences with respect to the validation data. The corresponding statistics are listed in Table 3.3 (Liu et al. 2022). Comparing to the validation data, the single-level model delivers small differences in onshore regions, where the terrestrial data are available. However, in offshore regions with no terrestrial data coverage, the differences are quite large. These results demonstrate that the single-level approach majorly recovers gravity information from the terrestrial observations, and the contribution of other measurements which are sensitive to lower spectral bands is not captured sufficiently. In case of the MRR based on the pyramid algorithm, as shown in Fig. 3.14 (right), the differences between the calculated gravity model and the validation data do not show a dependency on the distribution of certain types of

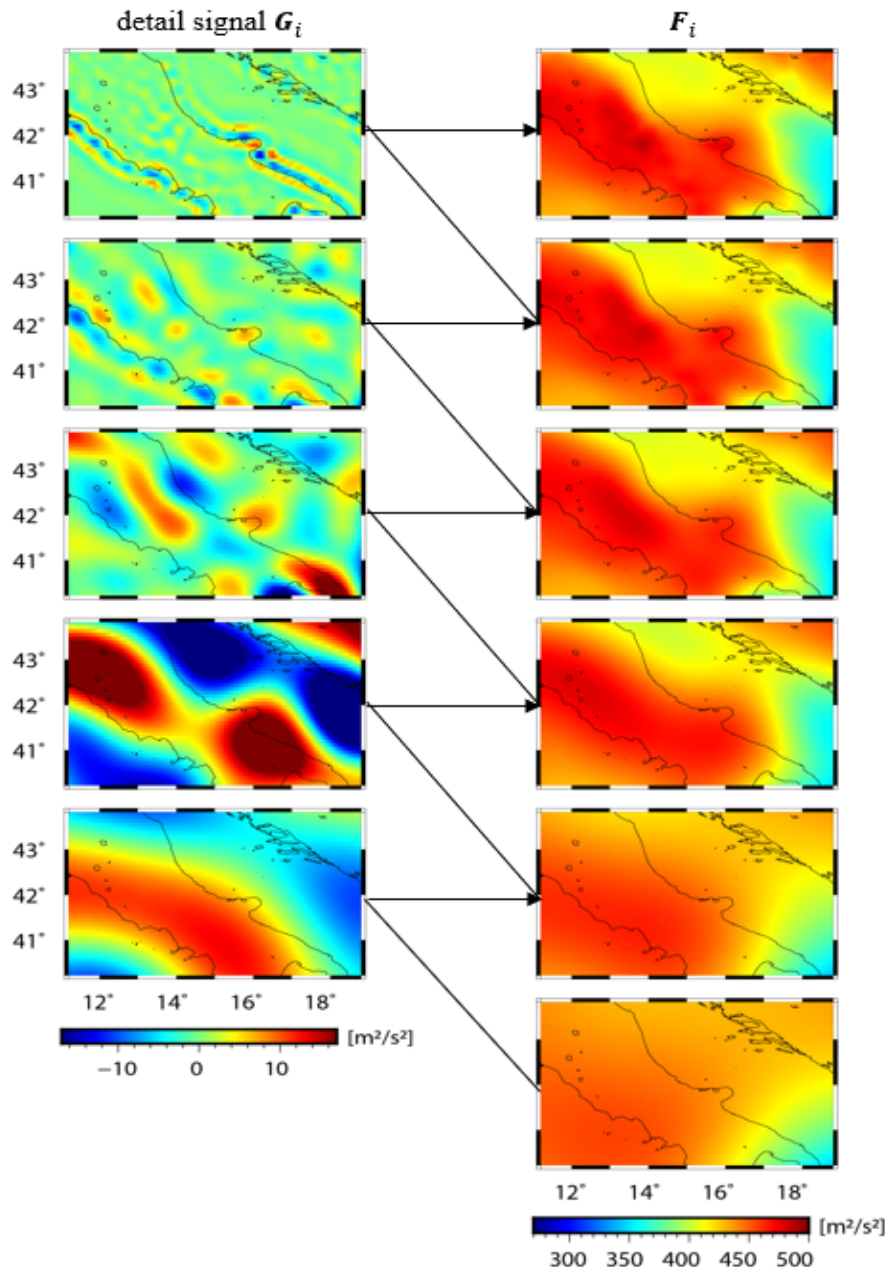


**Figure 3.13:** The detail signals  $G_i$  (left column) of the MRR based on the pyramid algorithm, as well as the modeled gravity signal (in terms of disturbing potential)  $F = \bar{F} + \sum_{i=7}^{11} G_i$  (right column) from level 11 (first row) to level 7 (fifth row), with  $\bar{F}$  (right column, last row) modeled from GECO

observations. It suggests that each observation type makes a contribution to the final result, and the MRR benefits from all measurements. This statement is supported by the fact that the RMS error obtained by the MRR based on the pyramid algorithm decreases by 35% with respect to the one delivered by the single-level approach. Large differences in the MRR based on the pyramid algorithm show up at the border of the high-resolution terrestrial data, which are caused by edge effects.

Next efforts concentrate on developing approaches to reduce edge effects and investigating the correlation between gravity observations acquired with different measurement techniques. It is planned to extend DGFI-TUM's SRBF/MRR method by the inclusion of a more complete stochastic model, e.g., the covariance information of the GGM and the correlation matrices between different observation techniques. The usage of this extended stochastic model will



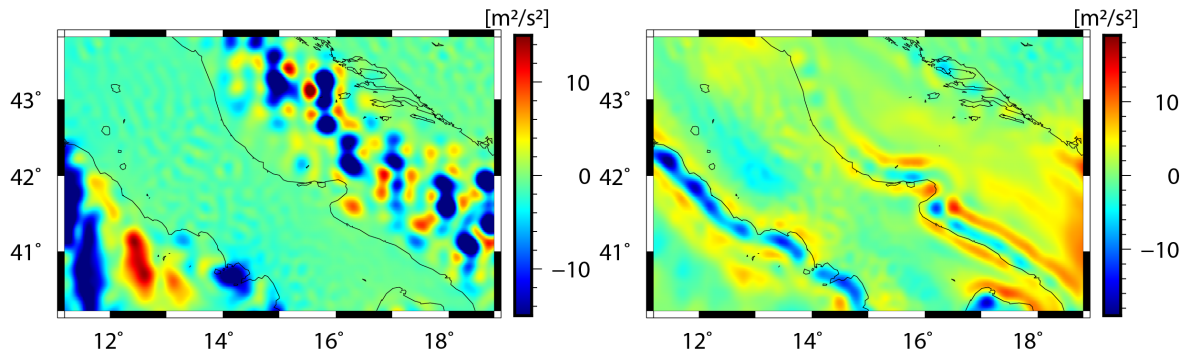


**Figure 3.14:** Differences between modeled disturbing potential and validation data, delivered by the single-level approach (left), and the MRR based on the pyramid algorithm (right)

lead to a more realistic assessment of the covariance information of the estimated parameters. Research activities in this regard are being faced within the **DFG Project Geo-H** (Enhanced geopotential field modeling as basis for the establishment of precise height systems) funded by the DFG for the term 2021 to 2024. Geo-H is a joint initiative of DGFI-TUM and TUM's Chair of Astronomical and Physical Geodesy (APG) and it is also set up as the perfect platform to continue supporting DGFI-TUM's research for the establishment of the International Height Reference Frame (IHRF).

### Related publication

Liu Q., Schmidt M., Sánchez L.: *Combination of different observation types through a multi-resolution representation of the regional gravity field using the pyramid algorithm and parameter estimation*. Journal of Geodesy, 2022, submitted

## 3.3 Standards and Conventions

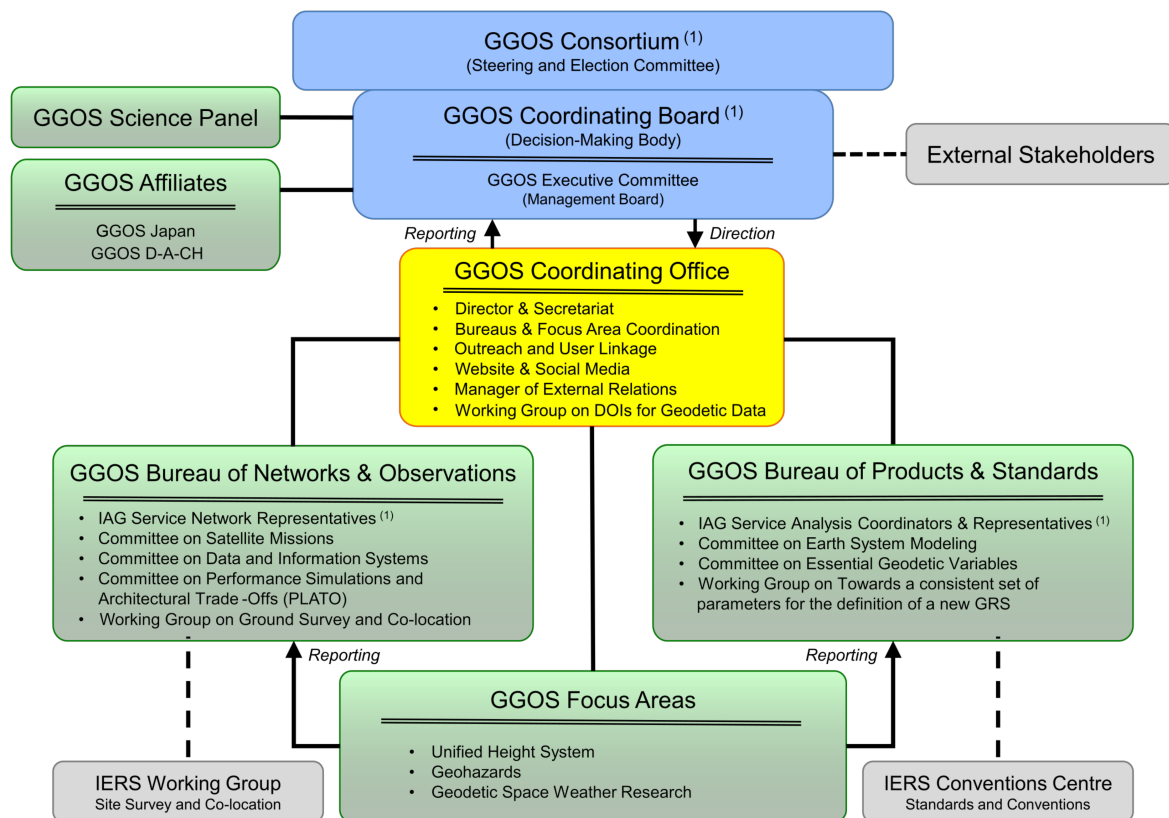
With the ongoing technological advancement of Earth observation systems, geodesy provides the potential to determine unambiguously and with utmost precision the geometric shape of land, ice and ocean surfaces as well as the rotation and gravity field of the Earth as global functions of space and time. Thus, geodesy provides the metrological basis for Earth system research and for reliably monitoring geodynamics and climate change phenomena. To ensure consistent results and to fully benefit from the high accuracy of geodetic observations, reliable reference frames as well as common standards, conventions and models are essential for the analysis of observations and the generation of meaningful scientific data products.

The IAG strives to provide geodetic results at the highest level of precision and consistency, which fundamentally requires that the processing and combination of the contributing geometric and gravimetric observations are based on uniform standards and conventions. The definition and implementation of uniform standards and conventions has played an important role in DGFI-TUM research for many years.

DGFI-TUM has taken on a central role in IAG's Global Geodetic Observing System (GGOS) for many years by hosting and chairing the Bureau for Products and Standards (BPS; Director: Dr. Detlef Angermann). The BPS evaluates the adopted standards and conventions across all IAG components used to generate the IAG scientific data products. The BPS is one of two GGOS bureaus, the second being the Bureau of Networks and Observations (BNO), chaired by the Harvard Smithsonian Center for Astrophysics, USA.

Furthermore, within GGOS, DGFI-TUM provides the GGOS Vice President (Dr. Laura Sánchez) and chairs two of the three GGOS Focus Areas (FA): The FA Unified Height System (Chair: Dr. Laura Sánchez; see Section 1.4) and the FA Geodetic Space Weather Research (Chair: Prof. Michael Schmidt, see Section 3.1). The third FA Geohazards is chaired by NASA.

In 2021, a second GGOS Affiliate *GGOS D-A-CH* has been established, encompassing the D-A-CH countries with the goal to bundle the GGOS-related activities of the national geodetic commissions of Germany (DGK), Austria (ÖGK) and Switzerland (SGK) in terms of science and infrastructure. The first GGOS Affiliate *GGOS Japan* was established in 2017. Figure 3.15 provides an overview about the organizational structure of GGOS.



<sup>(1)</sup> GGOS is built upon the foundation provided by the IAG Services, Commissions, and Inter-Commission Committees

**Figure 3.15:** Organizational structure of IAG's Global Geodetic Observing System (GGOS).

## GGOS Bureau of Products and Standards

The BPS is chaired by DGFI-TUM and operated jointly with TUM's Chair of Astronomical and Physical Geodesy within the Research Group Satellite Geodesy (Forschungsgruppe Satellitengeodäsie, FGS). Further involved partners are GFZ (German Research Centre for Geosciences, Potsdam) and DLR (German Aerospace Centre, Oberpfaffenhofen).

In its current structure, the following GGOS entities are associated to the BPS:

- Committee "Contributions to Earth System Modeling",
- Committee "Definition of Essential Geodetic Variables (EGVs)",
- Working Group "Towards a consistent set of parameters for the definition of a new Geodetic Reference System (GRS)".

The BPS supports GGOS in its goal to obtain consistent science data products describing the geometry, rotation and gravity field of the Earth. Key objectives of the BPS are to

- serve as coordinating point for the homogenization of IAG standards and products,
- keep track of adopted geodetic standards and conventions across all IAG components,
- stimulate the development of new geodetic products for Earth sciences and society,
- describe and promote geodetic results (see GGOS website, [www.ggos.org](http://www.ggos.org)).

The work of the BPS is primarily built on activities within the IAG Scientific Service related to data analysis, data combination and product generation. Thus, a close interaction with the IAG Analysis and Combination Centers regarding the homogenization of standards and products is required. The IAG Scientific Services and the other entities involved in standards and geodetic products have chosen representatives as associated members of the BPS. The Bureau comprises the staff members, the chairs of the associated GGOS components, the two committees and the working group as listed above, as well as representatives of the IAG Scientific Services, the International Astronomical Union (IAU) and other organizations; see Table 3.4.

**Table 3.4:** IAG Scientific Services and other international organizations represented in the BPS (status: December 2021).

International Earth Rotation and Reference Systems Service (IERS)
International GNSS Service (IGS)
International Laser Ranging Service
International VLBI Service for Geodesy and Astrometry (IVS)
International DORIS Service
International Gravity Field Service (IGFS)
Bureau Gravimetric International (BGI)
International Service for the Geoid (ISG)
International Center for Global Earth Models (ICGEM)
International Digital Elevation Model Service (IDEMS)
International Geodynamics and Earth Tide Service (IGETS)
IAU Commission A3
Control Body for ISO Geodetic Registry Network
IAG Communication and Outreach Branch
IAG Representative to ISO/TC211
Representative of gravity community

Figure 3.16 gives an overview and schedule of the BPS tasks as specified in the latest BPS Implementation Plan 2020–2022. The activities of the BPS are divided into three main categories: Coordination activities, specific tasks, and outreach activities.

**Coordination activities:** This category comprises GGOS Consortium meetings (annually), GGOS Coordinating Board meetings (twice per year) and monthly telecons of the GGOS Executive Community to ensure a regular exchange of information among the GGOS components and to manage the strategic planning. Furthermore, external and internal BPS meetings are regularly scheduled to coordinate and perform the operational Bureau work.

**Specific tasks:** A key objective of the BPS is to keep track and to foster homogenization of adopted geodetic standards and conventions across all components of the IAG as a fundamental basis for the generation of consistent geometric and gravimetric science products. Towards reaching these goals, the BPS has compiled an inventory of standards and conventions used for the generation of IAG products, which is regularly updated. The second version of this

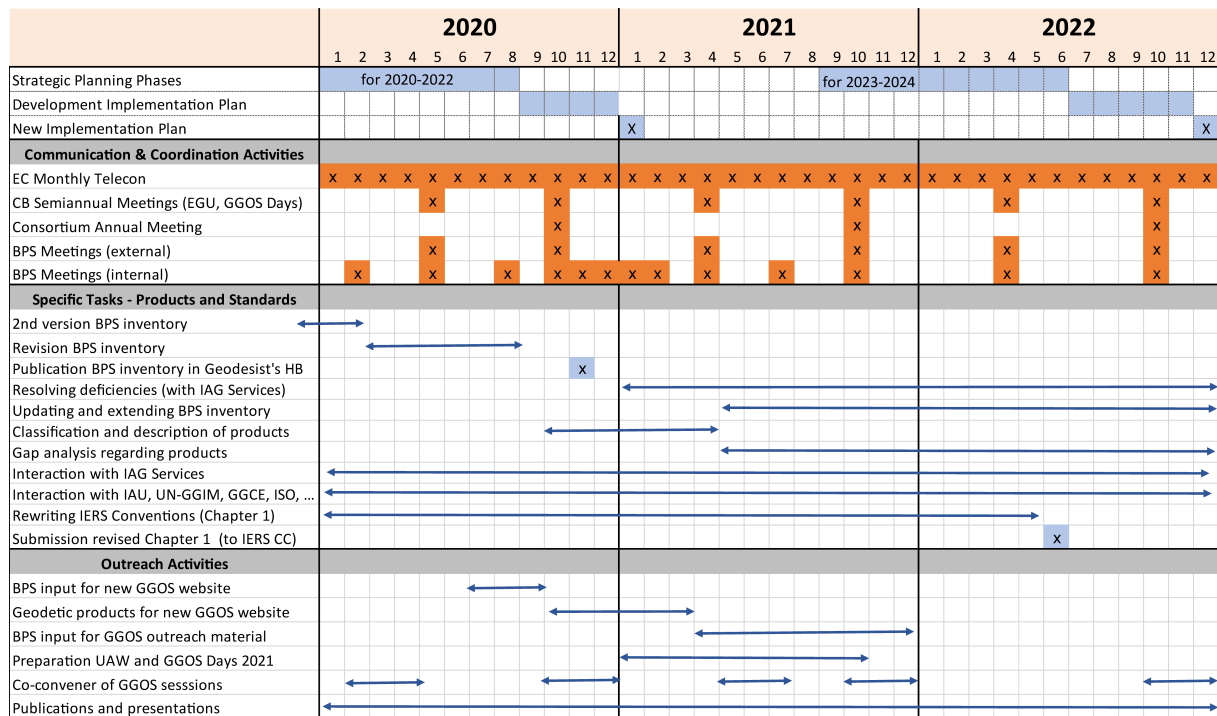


Figure 3.16: Overview and schedule of BPS activities.

document has been published in the Geodesist's Handbook (Journal of Geodesy) 2020<sup>13</sup>. This inventory presents the current status, identifies gaps and inconsistencies as well as interactions between different products. It also provides open issues and recommendations regarding standards and conventions used for the generation of IAG science products. In this way, the BPS supports IAG in its goal to deliver geodetic results of highest accuracy and consistency. Moreover, the Bureau contributes to the development of new geodetic products for Earth sciences and society. The tasks also comprise the interaction with IAG and other entities in the field of standards and conventions such as the contribution to the rewriting/revising of the IERS Conventions, mainly in the function as Chapter Expert for Chapter 1 "General definitions and numerical standards". Furthermore, the BPS director acts as representative to the International Organization for Standardization (ISO/TC 211) and to the United Nation Global Geospatial Information Management (UN-GGIM) Subcommittee on Geodesy (SCoG) Working Group "Data Sharing and Development of Geodetic Standards". The BPS also cooperates with the newly established Global Geodetic Centre of Excellence (GGCE) of UN and IAU.

**Outreach activities:** The various outreach activities include supporting the GGOS Coordinating Office concerning the renewing of the GGOS website ([www.ggos.org](http://www.ggos.org)). This new site now emphasizes more on the "Observing System" than on the GGOS organization itself. Therefore, the website was enhanced to provide an extensive information platform to bring the IAG observations, science products and services into the focus, and to provide a unique information platform as a central access point. In this context, the BPS contributions focused on the generation of illustrative and user-friendly descriptions of geodetic results (see below). The outreach also comprises the presentation of BPS activities and results at workshops, conferences, and its publication in scientific journals.

<sup>13</sup>Angermann D., et al., *GGOS Bureau of Products and Standards: Inventory of standards and conventions used for the generation of IAG products*. Journal of Geodesy, doi:10.1007/a00190-020-01434-z, 2020

## Description and representation of GGOS geodetic science products

In the framework of the renewing of the GGOS website ([www.ggos.org](http://www.ggos.org)), the BPS closely interacts with the GGOS Coordinating Office regarding the representation of geodetic science products. In cooperation with the IAG Scientific Services, other data providers and the GGOS Science Panel members, user-friendly data descriptions of 23 science products were generated until now. These products are classified into two categories (Fig. 3.17):

- **Geodetic themes:** Reference frames, surface geometry, Earth orientation, gravity field, positioning and applications.
- **Earth system components and space:** Outer and near space, atmosphere, hydrosphere, oceans, cryosphere, solid Earth.

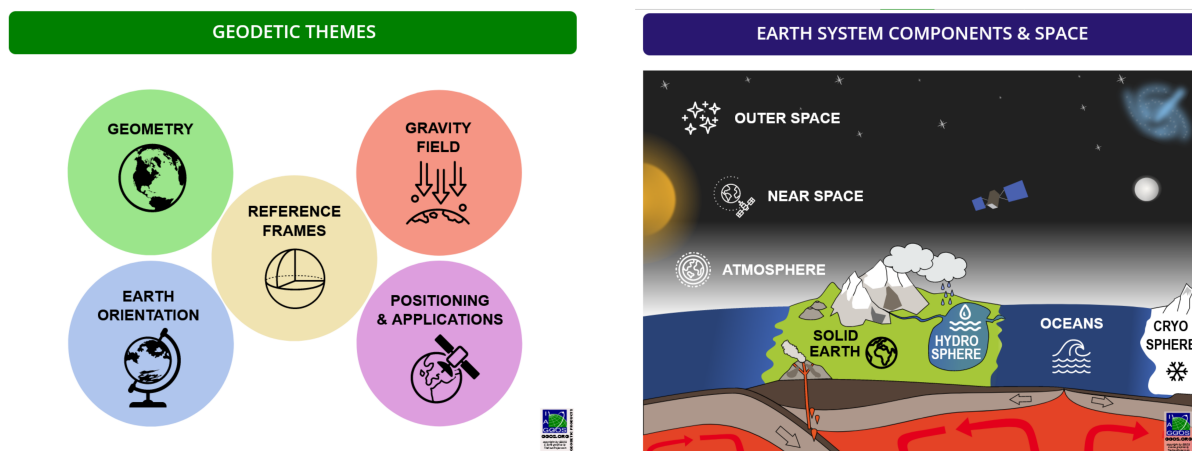


**Figure 3.17:** GGOS website providing geodetic science data for geodesy and Earth system research.

In addition to official IAG results, the GGOS website also offers related data of other institutions publicly available and thus provides a unique information platform and “entrance door” to geodetic data to support science and society. More information on the description and representation of geodetic products at the GGOS website is provided in Angermann et al., 2022.

### Related publication

Angermann D., Gruber T., Gerstl M., Heinkelmann R., Hugentobler U., Sánchez L., Steigenberger P., Gross R., Heki K., Marti U., Schuh H., Sehnal M., Thomas M.: *GGOS Bureau of Products and Standards: Description and promotion of geodetic products*. IAG Symposia, 2022, in press.

## 4 Scientific Transfer

*The transfer of knowledge, results and data within the scientific community and with the public is an essential element of scientific work. In the following, DGFI-TUM's efforts are outlined in relation to the most important instruments of information exchange: cooperation in scientific organizations and collaborative research programs at national and international level, scientific publications and presentations, participation in scientific meetings, visiting scientists and the operation of internet and data portals.*

*Section 4.1 contains a compilation of the positions and involvement of DGFI-TUM staff in national and international scientific organizations. The institute is intensively networked with other institutions worldwide, in particular through research activities within the International Union of Geodesy and Geophysics (IUGG), the International Astronomical Union (IAU), and the International Association of Geodesy (IAG). DGFI-TUM is a major player in the IAG's Global Geodetic Observing System (GGOS) (cf. Section 3.3) and operates research centers, analysis centers, and data centers, mostly on the basis of long-term commitments (cf. Section 1). Institute scientists participate in various collaborative projects, working groups, and study groups, and in line with DGFI-TUM's international strategy, institute staff members assume numerous key leadership and management positions to actively shape the future direction of international geodetic research.*

*Section 4.2 lists the scientific publications of the year 2021. Section 4.3 contains the list of posters and talks given by DGFI-TUM scientists at the numerous national and international conferences, symposia and workshops listed in Section 4.4. Guests who visited DGFI-TUM as part of research collaborations in 2021 are listed in Section 4.5. To share scientific information and exchange results and data with partners and the interested public, DGFI-TUM maintains several websites, public databases, and a Facebook page. An overview of the portals operated can be found in Section 4.6.*

### 4.1 Functions in Scientific Bodies

#### **United Nations Global Spatial Information Management (UN-GGIM)**

- Subcommittee Geodesy, Working Group for a Global Geodetic Reference Frame (GGRF),  
*IAG Representative for Key Area Data Sharing and Development of Standards:*  
*Angermann D.*

#### **International Astronomical Union (IAU)**

- Commission A.2, Rotation of the Earth,  
*President: Seitz F., Member: Seitz M.*
- Division A, Fundamental Astronomy,  
*Member of the Steering Committee: Seitz F.*
- Joint IAU CA.2/IAG/IERS Working Group Consistent Realization of TRF, CRF and EOP,  
*Vice-Chair: Seitz M., Member: Seitz F.*
- Joint IAU CA.2/IAG Working Group Improving Theories and Models of the Earth's Rotation,  
*Member: Seitz F.*

### **International Union of Geodesy and Geophysics (IUGG)**

- *Representative to the Panamerican Institute for Geodesy and History (PAIGH):*  
*Sánchez L.*

### **International Association of Geodesy (IAG)**

- Global Geodetic Observing System (GGOS),  
*Vice-President: Sánchez L.*
- Global Geodetic Observing System (GGOS) Executive Committee,  
*Member: Angermann D., Sánchez L.*
- Global Geodetic Observing System (GGOS) Coordinating Board,  
*Member: Angermann D., Sánchez L., Schmidt M.*
- Global Geodetic Observing System (GGOS) Bureau of Products and Standards,  
*Director: Angermann D., Member: Sánchez L.*
- Global Geodetic Observing System (GGOS) Focus Area Unified Height System,  
*Lead: Sánchez L.*
- Global Geodetic Observing System (GGOS) Focus Area Geodetic Space Weather Research,  
*Lead: Schmidt M.*
- Global Geodetic Observing System (GGOS) GGOS Bureau of Products and Standards, Working Group Towards a consistent set of parameters for the definition of a new GRS,  
*Member: Angermann D., IHRF representative: Sánchez L.*
- Global Geodetic Observing System (GGOS) Focus Area Unified Height System, Joint Working Group Implementation of the International Height Reference Frame (IHRF),  
*Chair: Sánchez L.*
- Global Geodetic Observing System (GGOS) Focus Area Geodetic Space Weather Research, Joint Working Group 1 Electron density modelling,  
*Member: Gerzen T., Goss A., Schmidt M.*
- Global Geodetic Observing System (GGOS) Focus Area Geodetic Space Weather Research, Joint Working Group 2 Improvement of thermosphere models,  
*Member: Schmidt M., Zeitler L.*
- Global Geodetic Observing System (GGOS) Focus Area Geodetic Space Weather Research, Joint Working Group 3 Improved understanding of space weather events and their monitoring by satellite missions,  
*Member: Dettmering D.*
- Global Geodetic Observing System (GGOS) Working Group on DOIs for Geodetic Data,  
*Member: Angermann D., Schwatke C.*
- Global Geodetic Observing System (GGOS) Working Group on Performance Simulations and Architectural Trade-Offs (PLATO),  
*Member: Bloßfeld M., Kehm A.*
- Global Geodetic Observing System (GGOS) Committee Essential Geodetic Variables (EGV),  
*Member: Angermann D.*
- IAG Symposia Series,  
*Assistant Editor-in-Chief: Sánchez L.*

- Commission 1, Sub-Commission 1.4 Interaction of celestial and terrestrial reference frames,  
*Member: Seitz M.*
- Commission 1, Working Group 1.2.1 Assessing impacts of loading on reference frame realizations,  
*Member: Seitz, M.*
- Commission 1, Working Group 1.4.2 Improving VLBI-based ICRF and comparison with Gaia-CRF,  
*Member: Seitz, M.*
- Commission 2, Joint Working Group 2.1.1 Establishment of the International Gravity Reference Frame,  
*Corresponding member, IHRF representative: Sánchez L.*
- Commission 2, Joint Working Group 2.2.2 Error assessment of the 1 cm geoid experiment,  
*Member: Liu Q., Sánchez L.*
- Commission 4, Sub-Commission 4.3 Atmosphere Remote Sensing,  
*Chair: Schmidt M.*
- Commission 4, Joint Working Group 4.3.1 Real-time Ionosphere Monitoring and Modeling,  
*Member: Erdogan E., Goss A.*
- Commission 4, Working Group 4.3.2 Prediction of ionospheric state and dynamics,  
*Vice-Chair: Erdogan E.*
- Commission 4, Working Group 4.3.3 Ionosphere Scintillations,  
*Member: Schmidt M.*
- Commission 4, Joint Working Group 4.3.4 Validation of VTEC models for high-precision and high resolution applications,  
*Member: Erdogan E., Goss A.*
- Inter-Commission Committee on Geodesy for Climate Research (ICCC), Joint Working Group C.1 Climate Signatures in Earth Orientation Parameters,  
*Member: Göttl F.*
- Inter-Commission Committee on Theory (ICCT), Joint Study Group T.26 Geoid/quasi-geoid modelling for realization of the geopotential height datum,  
*Member: Sánchez L.*
- Inter-Commission Committee on Theory (ICCT), Joint Study Group T.29 Machine learning in geodesy,  
*Member: Natras R.*
- Inter-Commission Committee on Theory (ICCT), Joint Study Group T.33 Time series analysis in geodesy and geodynamics,  
*Member: Schmidt M.*

#### **International Earth Rotation and Reference Systems Service (IERS)**

- Directing Board,  
*Associate member: Angermann D., Bloßfeld M.*
- ITRS Combination Center,  
*Chair: Seitz M., Member: Bloßfeld M.*
- Working Group on SINEX Format,  
*Member: Seitz M.*



- Working Group on Site Coordinate Time Series Format,  
*Member: Seitz M.*

#### **International Laser Ranging Service (ILRS)**

- Governing Board,  
*Member: Schwatke C.*
- Analysis Standing Committee,  
*Member: Bloßfeld M., Kehm A., Schwatke C.*
- EUROLAS Data Center (EDC),  
*Chair: Schwatke C.*
- Operations Center,  
*Chair: Schwatke C.*
- Data Formats and Procedures Standing Committee,  
*Chair: Schwatke C.*
- Networks and Engineering Standing Committee,  
*Member: Schwatke C.*
- Study Group on Data Format Update,  
*Member: Schwatke C.*
- Study Group on ILRS Software Library,  
*Member: Schwatke C.*

#### **International VLBI Service for Geodesy and Astrometry (IVS)**

- Operational Analysis Center,  
*Member: Glomsda M., Seitz M.*
- IVS Combination Center,  
*Member: M. Seitz*

#### **International DORIS Service (IDS)**

- Governing Board,  
*Member: Dettmering D.*
- Associate Analysis Center,  
*Member: Bloßfeld M., Rudenko S.*
- DORIS Analysis Working Group,  
*Member: Bloßfeld M., Rudenko S.*
- Working Group on NRT DORIS data,  
*Chair: Dettmering D., Member: Erdogan E., Schmidt M.*

#### **International GNSS Service (IGS)**

- Governing Board,  
*Network Representative: Sánchez L.*
- Regional Network Associate Analysis Center for SIRGAS,  
*Chair: Sánchez L.*
- Infrastructure Committee,  
*Member: Sánchez L.*

- Working Group Reference Frame,  
*Member: Sánchez L.*
- Ionosphere Working Group,  
*Member: Schmidt M.*

#### **International Service for the Geoid (ISG)**

- *Scientific Advisor: Sánchez L.*

#### **International Organization for Standardization (ISO)**

- ISO/TC211,  
*IAG Representative to ISO/TC211: Angermann D.*

#### **International Space Science Institute (ISSI)**

- Team Understanding the Connection Between Coastal Sea Level and Open Ocean Variability Through Space Observations,  
*Member: Oelsmann J., Passaro M.*

#### **European Commission (EC) / European Space Agency (ESA)**

- Copernicus POD Quality Working Group,  
*Member: Dettmering D.*

#### **European Space Agency (ESA)**

- Copernicus New Generation Topography Constellation Ad-Hoc Expert Group,  
*Member: Passaro M.*
- Copernicus Sentinel-3 Next Generation Topography Mission Advisory Group,  
*Member: Passaro M.*
- CryoSat Expert Group,  
*Member: Passaro M.*
- Coastal Altimetry Workshop Organizing Committee,  
*Member: Passaro M.*
- Scientific Committee of 4th Hydrospace-GEOGloWS 2021,  
*Member: Schwatke C.*

#### **European Space Agency (ESA) / European Organisation for the Exploitation of Meteorological Satellites (EUMETSAT)**

- Sentinel-3 Validation Team, Altimetry Sub-Group,  
*Member: Dettmering D.*
- Sentinel-6 Validation Team,  
*Member: Dettmering D., Oelsmann J., Passaro M., Schlembach F., Schwatke C.*

#### **Center National d'Etudes Spatiales (CNES) / National Aeronautics and Space Administration (NASA)**

- Ocean Surface Topography Science Team,  
*Member: Dettmering D., Oelsmann J., Passaro M., Schwatke C., Schlembach F.*
- SWOT Science Team,  
*Member: Dettmering D., Schwatke C.*

- SWOT Science Team Working Group Global Hydrology and Remote Sensing,  
*Member: Schwatke C.*
- SWOT Science Team Working Group River Science,  
*Member: Schwatke C.*
- SWOT Science Team Working Group Science for Lakes and Wetlands,  
*Member: Schwatke C.*

#### **Sistema de Referencia Geocéntrico para las Américas (SIRGAS)**

- Scientific Committee,  
*Member: Sánchez L.*
- SIRGAS Analysis Center,  
*Chair: Sánchez L.*

#### **Forschungsgruppe Satellitengeodäsie (FGS)**

- *Deputy Speaker: Seitz F.*
- Managing Board,  
*Member: Schmidt M., Seitz F.*

#### **Ausschuss Geodäsie der Bayerischen Akademie der Wissenschaften (Deutsche Geodätische Kommission, DGK)**

- *Member: Seitz F.*

#### **Deutsche Gesellschaft für Geodäsie, Geoinformation und Landmanagement (DVW)**

- Working Group 7: Experimentelle, Angewandte und Theoretische Geodäsie,  
*Member: Schmidt M., Seitz F.*

## **4.2 Publications**

Angermann D., Pail R., Seitz F., Hugentobler, U.: *Mission Erde - Geodynamik und Klimawandel im Visier der Satellitengeodäsie*, Springer, doi:[10.1007/978-3-662-62338-1](https://doi.org/10.1007/978-3-662-62338-1), 2021

Benveniste J., Andral A., Guitierrez A., Bates P., Bauer-Gottwein P., Brachet C., Crétaux J., Bohórquez C.I.G., Dias de Paiva R.C., Maisongrande P., Ouattara T., Unnayar S., Berry P., David C.H., Fleischmann A.S., Gao H., Güntner A., Huffman G., Lee H, Nielsen K., Papa F., Prigent C., Schwatke C., Tarpanelli A., Tourian M., Zaidi A.Z.: *Summary and Recommendations from the HYDROSPACE-GEOGloWS 2021 Workshop*. 4th HydroSpace-GEOGloWS 2021, doi:[10.5270/esa.hydroSpace-geogloWS-2021-report](https://doi.org/10.5270/esa.hydroSpace-geogloWS-2021-report), 2021

Birol F., Léger F., Passaro M., Cazenave A., Niño F., Calafat F.M., Shaw A., Legeais J.-F., Gouzenes Y., Schwatke C., Benveniste J.: *The X-TRACK/ALES multi-mission processing system: New advances in altimetry towards the coast*. Advances in Space Research, doi:[10.1016/j.asr.2021.01.049](https://doi.org/10.1016/j.asr.2021.01.049), 2021

Boergens E., Schmidt M., Seitz F.: *The use of B-splines to represent the topography of river networks*. International Journal on Geomathematics, 12(1), doi:[10.1007/s13137-021-00188-w](https://doi.org/10.1007/s13137-021-00188-w), 2021

- Cavaleri L., Bertotti L., Ferrarin C., Passaro M., Pezzutto P., Pomaro A.: *Synergic use of altimeter and model sea level data in inner and coastal seas*. Remote Sensing of Environment, 261, 112500, doi:[10.1016/j.rse.2021.112500](https://doi.org/10.1016/j.rse.2021.112500), 2021
- Deggim S., Eicker A., Schawohl L., Gerdener H., Schulze K., Engels O., Kusche J., Saraswati A.T., van Dam T., Ellenbeck L., Dettmering D., Schwatke C., Mayr S., Klein I., Longuevergne L.: *RECOG RL01: correcting GRACE total water storage estimates for global lakes/reservoirs and earthquakes*. Earth System Science Data, 2227-2244, doi:[10.5194/essd-13-2227-2021](https://doi.org/10.5194/essd-13-2227-2021), 2021
- Dettmering D., Müller F. L., Oelmann J., Passaro M., Schwatke C., Restano M., Benveniste J., Seitz F.: *North SEAL: a new dataset of sea level changes in the North Sea from satellite altimetry*. Earth System Science Data, 13(8), 3733-3753, doi:[10.5194/essd-13-3733-2021](https://doi.org/10.5194/essd-13-3733-2021), 2021
- Erdogan E., Schmidt M., Goss A., Görres B., Seitz F.: *Real-time monitoring of ionosphere VTEC using Multi-GNSS carrier-phase observations and B-splines*. Space Weather, doi:[10.1029/2021sw002858](https://doi.org/10.1029/2021sw002858), 2021
- Foortan E., Farzaneh S., Kosary M., Schmidt M., Schumacher M.: *A simultaneous calibration and data assimilation (C/DA) to improve NRLMSISE00 using thermospheric neutral density (TND) from space-borne accelerometer measurements*. Geophysical Journal International, 224(4), 1096–1115, doi:[10.1093/gji/ggaa507](https://doi.org/10.1093/gji/ggaa507), 2021
- Glomsda M., Bloßfeld M., Seitz M., Seitz F.: *Correcting for site displacements at different levels of the Gauss-Markov model - a case study for geodetic VLBI*. Advances in Space Research, doi:[10.1016/j.asr.2021.04.006](https://doi.org/10.1016/j.asr.2021.04.006), 2021
- Glomsda M., Seitz M., Angermann D., Gerstl M.: *DGFI-TUM Analysis Center Biennial Report 2019+2020*. In: Armstrong K, et al. (Eds.), International VLBI Service for Geodesy and Astrometry 2019+2020 Biennial Report, 2021
- Glomsda M., Seitz M., Bloßfeld M., Kehm A., Gerstl M., Angermann D.: *First VLBI-only TRF/CRF solution based on DGFI-TUM data for ITRF2020*. In: Haas R. (Ed.), Proceedings of the 25th EVGA Working Meeting, 2021
- Goss A.: *Generation of high-resolution global and regional multi-scale B-spline models of the vertical total electron content based on low-latency GNSS data*. Dissertation, Technische Universität München, Deutsche Geodätische Kommission, C886, 2021
- Göttl F., Groh A., Schmidt M., Schröder L., Seitz F.: *The influence of Antarctic ice loss on polar motion: an assessment based on GRACE and multi-mission satellite altimetry*. Earth, Planets and Space, 73(1), doi:[10.1186/s40623-021-01403-6](https://doi.org/10.1186/s40623-021-01403-6), 2021
- Hart-Davis M.G., Backeberg B.C.: *Towards a particle trajectory modelling approach in support of South African search and rescue operations at sea*. Journal of Operational Oceanography, 1-9, doi:[10.1080/1755876X.2021.1911485](https://doi.org/10.1080/1755876X.2021.1911485), 2021
- Hart-Davis M.G., Backeberg B.C.: *Preliminary assessment of the potential for particle trajectory modelling to support ocean search and rescue operations*. Proceedings of the Nansen-Tutu Centre 10th Anniversary Symposium, 2021
- Hart-Davis M.G., Dettmering D., Sulzbach R., Thomas M., Schwatke C., Seitz F.: *Regional Evaluation of Minor Tidal Constituents for Improved Estimation of Ocean Tides*. Remote Sensing, 13(16), doi:[10.3390/rs13163310](https://doi.org/10.3390/rs13163310), 2021

- Hart-Davis M.G., Piccioni G., Dettmering D., Schwatke C., Passaro M., Seitz F.: *EOT20: A global Empirical Ocean Tide model from multi-mission satellite altimetry (data)*. Deutsches Geodätisches Forschungsinstitut, München. SEANOE, doi:[10.17882/79489](https://doi.org/10.17882/79489), 2021
- Hart-Davis M.G., Piccioni G., Dettmering D., Schwatke C., Passaro M., Seitz F.: *EOT20: A global ocean tide model from multi-mission satellite altimetry*. Earth System Science Data, 13(8), 3869-3884, doi:[10.5194/essd-13-3869-2021](https://doi.org/10.5194/essd-13-3869-2021), 2021
- Herrnegger M., Stecher G., Schwatke C., Olang L.: *Hydroclimatic analysis of rising water levels in the Great rift Valley Lakes of Kenya*. Journal of Hydrology: Regional Studies, 36, 100857, doi:[10.1016/j.ejrh.2021.100857](https://doi.org/10.1016/j.ejrh.2021.100857), 2021
- Heye S., Krug M., Veitch J., Rouault M., Hart-Davis M.G.: *Impact of the Agulhas Current mesoscale variability on surface dispersion in the KwaZulu-Natal Bight*. Proceedings of the Nansen-Tutu Centre 10th Anniversary Symposium, 2021
- International Altimetry Team: Abdalla S., ... Dettmering D., ... Passaro M., ... Rudenko S., ..., Schwatke C.,... et al.: *Altimetry for the future: Building on 25 years of progress*. Advances in Space Research, doi:[10.1016/j.asr.2021.01.022](https://doi.org/10.1016/j.asr.2021.01.022), 2021
- Jarmołowski W., Belehaki A., Hernández Pajares M., Schmidt M., Goss A., Wielgosz P., Yang H., Krypiak-Gregorczyk A., Tsagouri I., Paouris E., Monte-Moreno E., García-Rigo A., Milanowska B., Erdogan E., Graffigna V., Haagmans R.: *Combining Swarm Langmuir probe observations, LEO-POD-based and ground-based GNSS receivers and ionosondes for prompt detection of ionospheric earthquake and tsunami signatures: case study of 2015 Chile-Illapel event*. Journal of Space Weather and Space Climate, 11, 28, doi:[10.1051/swsc/2021042](https://doi.org/10.1051/swsc/2021042), 2021
- Kleinschroth F., Mekuria W., Schwatke C., McCartney M.: *Ecosystem services in changing social-ecological systems*. In: Lautze J., et al. (Eds.), The Omo-Turkana Basin, Routledge, doi:[10.4324/9781003169338](https://doi.org/10.4324/9781003169338), 2021
- Müller F. L.: *Improved polar geostrophic surface currents from satellite altimetry*. Dissertation, Technische Universität München, Deutsche Geodätische Kommission, C866, 2021
- Müller F. L., Oelsmann J., Dettmering D., Passaro M., Schwatke C., Restano M., Benveniste J., Seitz F.: *North SEAL: Gridded Sea Level Anomalies and Trends for the North Sea from Multi-Mission Satellite Altimetry (data)*. Deutsches Geodätisches Forschungsinstitut, München. SEANOE, doi:[10.17882/79673](https://doi.org/10.17882/79673), 2021
- Natras R., Schmidt M.: *Machine Learning Model Development for Space Weather Forecasting in the Ionosphere*. Proceedings of the International Conference on Information and Knowledge Management 2021 Workshops (CIKMW 2021), 2021
- Oelsmann J., Passaro M., Dettmering D., Schwatke C., Sánchez L., Seitz F.: *The zone of influence: matching sea level variability from coastal altimetry and tide gauges for vertical land motion estimation*. Ocean Science, 17(1), 35–57, doi:[10.5194/os-17-35-2021](https://doi.org/10.5194/os-17-35-2021), 2021
- Passaro M., Hemer M., Quartly G.D., Schwatke C., Dettmering D., Seitz F.: *Global coastal attenuation of wind-waves observed with radar altimetry*. Nature Communications, 12, 3812, doi:[10.1038/s41467-021-23982-4](https://doi.org/10.1038/s41467-021-23982-4), 2021
- Passaro M., Müller F.L., Oelsmann J., Rautiainen L., Dettmering D., Hart-Davis M.G., Abulaitijiang A., Andersen O.B., Høyer J., Madsen K., Ringgaard I., Särkkä J., Scarrott R., Schwatke C., Seitz F., Tuomi L., Restano M., Benveniste J.: *Absolute Baltic Sea Level Trends in the Satellite Altimetry Era: A Revisit*. Frontiers in Marine Science, 8, doi:[10.3389/fmars.2021.647607](https://doi.org/10.3389/fmars.2021.647607), 2021

- Paul S., Huntemann M.: *Improved machine-learning-based open-water–sea-ice–cloud discrimination over wintertime Antarctic sea ice using MODIS thermal-infrared imagery*. *The Cryosphere*, 15(3), 1551-1565, doi:[10.5194/tc-15-1551-2021](https://doi.org/10.5194/tc-15-1551-2021), 2021
- Pavlis E.C., Pearlman M.R., Carabajal C.C., Rinklefs R., Schwatke C., Wilkinson M., Kirchner G., Luceri V., Otsubu T., Torre J.-M., Schreiber U.: *International Laser Ranging Service (ILRS)*. Reports 2019-2021 of the International Association of Geodesy (IAG), Travaux de l'AIG, 2021
- Piccioni G.: *Exploit satellite altimetry to improve coastal tide estimation*. Dissertation, Technische Universität München, 2021
- Piccioni G., Dettmering D., Schwatke C., Passaro M., Seitz F.: *Design and regional assessment of an empirical tidal model based on FES2014 and coastal altimetry*. *Advances in Space Research*, 68(2), 1013-1022, doi:[10.1016/j.asr.2019.08.030](https://doi.org/10.1016/j.asr.2019.08.030), 2021
- Qi L., Hernández-Pajares M., Lyu H., Goss A.: *Influence of temporal resolution on the performance of global ionospheric maps*. *Journal of Geodesy*, 95(3), doi:[10.1007/s00190-021-01483-y](https://doi.org/10.1007/s00190-021-01483-y), 2021
- Rudenko S., Bloßfeld M., Zeitlhöfler J.: *DGFI-TUM Associate Analysis Center*. In: Soudarin L. and Ferrage P. (Eds.), *International DORIS Service Activity Report 2019-2020*, 2021
- Sánchez L.: *Das neue Internationale Höhenreferenzsystem (IHR)*. *FORUM: Zeitschrift des Bundes der Öffentlich bestellten Vermessungsingenieure e.V.*, 3(3/2021), 4-13, 2021
- Sánchez L., Ågren J., Huang J., Wang Y.M., Mäkinen J., Pail R., Barzaghi R., Vergos G.S., Ahlgren K., Liu Q.: *Strategy for the realisation of the International Height Reference System (IHR)*. *Journal of Geodesy*, 95(3), doi:[10.1007/s00190-021-01481-0](https://doi.org/10.1007/s00190-021-01481-0), 2021
- Sánchez L., Kehm A.: *SIRGAS Regional Network Associate Analysis Centre (IGS RNAAC SIRGAS) Technical Report 2020*. International GNSS Service Technical Report 2020, 135-146, doi:[10.48350/156425](https://doi.org/10.48350/156425), 2021
- Seitz M., Bloßfeld M., Angermann D., Seitz F.: *DTRF2014: DGFI-TUM's ITRS realization 2014*. *Advances in Space Research*, 69(6), 2391-2420, doi:[10.1016/j.asr.2021.12.037](https://doi.org/10.1016/j.asr.2021.12.037), 2021
- Smirnov A., Shprits Y., Zhelavskaya I., Lühr H., Xiong C., Goss A., Prol F., Schmidt M., Hoque M., Pedatella N., Szabó-Roberts M.: *Intercalibration of the Plasma Density Measurements in Earth's Topside Ionosphere*. *Journal of Geophysical Research: Space Physics*, doi:[10.1029/2021ja029334](https://doi.org/10.1029/2021ja029334), 2021
- Violante-Carvalho N., Arruda W.Z., Carvalho L.M., Rogers W. E., Passaro M.: *Diffraction of irregular ocean waves measured by altimeter in the lee of islands*. *Remote Sensing of Environment*, 265, 112653, doi:[10.1016/j.rse.2021.112653](https://doi.org/10.1016/j.rse.2021.112653), 2021
- Wang Y.M., Sánchez L., Ågren J., Huang J., Forsberg R., Abd-Elmotaal H.A., Ahlgren K., Barzaghi R., Bašić T., Carrion D., Claessens S., Erol B., Erol S., Filmer M., Grigoriadis V.N., Isik M.S., Jiang T., Koç Ö., Krcmaric J., Li X., Liu Q., Matsuo K., Natsiopoulou D.A., Novák P., Pail R., Pitoňák M., Schmidt M., Varga M., Vergos G.S., Véronneau M., Willberg M., Zingerle P.: *Colorado geoid computation experiment: overview and summary*. *Journal of Geodesy*, 95(12), doi:[10.1007/s00190-021-01567-9](https://doi.org/10.1007/s00190-021-01567-9), 2021
- Zeitler L., Corbin A., Vielberg K., Rudenko S., Löcher A., Bloßfeld M., Schmidt M., Kusche J.: *Scale factors of the thermospheric density: a comparison of Satellite Laser Ranging and accelerometer solutions*. *Journal of Geophysical Research: Space Physics*, 126, e2021JA029708, doi:[10.1029/2021JA029708](https://doi.org/10.1029/2021JA029708), 2021

### 4.3 Presentations

- Angermann D.: *Bureau of Products and Standards*. GGOS Coordinating Board Meeting, online, 2021
- Angermann D., Gruber T., Gerstl M., Heinkelmann R., Hugentobler U., Sánchez L., Sehnal M., Steigenberger P.: *The role and activities of the GGOS Bureau of Products and Standards*. AGU Fall Meeting, online, 2021
- Angermann D., Gruber T., Gerstl M., Heinkelmann R., Hugentobler U., Sánchez L., Steigenberger P.: *The GGOS Bureau of Products and Standards*. EGU General Assembly, online, 2021
- Angermann D., Gruber T., Gerstl M., Heinkelmann R., Hugentobler U., Sánchez L., Steigenberger P.: *The role and activities of the GGOS Bureau of Products and Standards*. IAG Scientific Assembly, online, 2021
- Angermann D., Gruber T., Gerstl M., Heinkelmann R., Hugentobler U., Sánchez L., Steigenberger P.: *BPS – Bureau of Products and Standards*. GGOS Days 2021, online, 2021
- Benveniste J., Dinardo S., Buchhaupt C., Scagliola M., Passaro M., Fenoglio-Marc L., Sabatino G., Restano M., Abis B., Ambrozio A., Orru C.: *SAR, SARin, RDSAR and FF-SAR Altimetry Processing on Demand for Cryosat-2 and Sentinel-3 at ESA's Altimetry Virtual Lab*. AGU Fall Meeting, online, 2021
- Benveniste J., Dinardo S., Buchhaupt C., Scagliola M., Passaro M., Fenoglio-Marc L., Sabatino G., Restano M., Ambrozio A.: *SAR, SARin, RDSAR and FF-SAR Altimetry Processing on Demand for Cryosat-2 and Sentinel-3 at ESA G-POD*. CryoSat 10th Anniversary Science Conference, online, 2021
- Bloßfeld M.: *Die Vermessung der Erde als Grundlage für die Erdsystemforschung - Herausforderungen an geodätische Referenzsysteme und deren gesellschaftliche Relevanz*. Geodätisches Kolloquium, Universität Innsbruck, online, 2021
- Bloßfeld M.: *Status and plans for an SLR contribution to COST-G*. COST-G team meeting, Bern, Switzerland, online, 2021
- Bloßfeld M.: *Using SLR observations for the estimation of scaling factors of the upper (neutral) atmospheric density*. GGOS IAG JWG 2 meeting, online, 2021
- Bloßfeld M., Hart-Davis M.G., Glomsda M., Dettmering D. : *The impact of the EOT20 global ocean tide model on space geodetic measurements, satellite orbits and derived geodetic parameters*. IAG Scientific Assembly, online, 2021
- Cotton D., Garcia-Mondéjar A., Gommenginger C., Andersen O.B., Nielsen K., Fenoglio-Marc L., Uebbing B., Stolzenberger S., Fernandes J., Lazaro C., Vieira T., Bauer-Gottwein P., Vignudelli S., Tarpanelli A., de Biasio F., Passaro M., Dettmering D., Slobbe C., Shaw A., Thorne P., Zakharova E., Scagliola M., Fabry P.L., Gomez-Enri J., Bercher N., Cancet M., Fouchet E., Benveniste J., Restano M., Ambrozio A.: *Improving SAR Altimeter processing over the coastal zone - the ESA HYDROCOASTAL project*. AGU Fall Meeting, online, 2021
- Cotton D., Garcia-Mondéjar A., Gommenginger C., Andersen O.B., Nielsen K., Fenoglio-Marc L., Uebbing B., Stolzenberger S., Fernandes J., Lazaro C., Vieira T., Bauer-Gottwein P., Vignudelli S., Tarpanelli A., de Biasio F., Passaro M., Dettmering D., Slobbe C., Shaw A., Thorne P., Zakharova E., Scagliola M., Fabry P.L., Gomez-Enri J., Bercher N., Cancet M.,

- Fouchet E., Benveniste J., Restano M., Ambrozio A.: *Improving SAR Altimeter processing over Inland Water - the ESA HYDROCOASTAL project*. AGU Fall Meeting, online, 2021
- Cotton D., Garcia-Mondejar A., ..., Passaro M., Dettmering D., ..., Benveniste J.: *Improving SAR Altimeter processing over the coastal zone and inland waters - the ESA HYDROCOASTAL project*. EGU General Assembly, online, 2021
- Cotton D., Garcia-Mondejar A., ..., Passaro M., Dettmering D., ..., Benveniste J.: *Improving SAR Altimeter processing over the coastal zone and inland waters - the ESA HYDROCOASTAL project*. CryoSat 10th Anniversary Science Conference, online, 2021
- Dettmering D.: *Sentinel-3 orbit validation by means of altimetry crossover analysis*. Copernicus POD Quality Working Group Meeting 10, online, 2021
- Dodet G., Passaro M., Piolle J.F., Quilfen Y., Quartly G., Arduin F.: *Recent developments in multi-mission altimeter sea state products: the ESA CCI dataset v2*. Sea State Climate Change Initiative: 2nd User Consultation Meeting, online, 2021
- Elger K., Angermann D., Bock Y., Bonvalot S., Botha R., Bradke M., Bradshaw E., Bruyninx C., Carrion D., Coetzer G., Fridez P., Ince E.S., Lamothe P., Navarro V., Noll C., Reguzzoni M., Riley J., Roman D., Soudarin L., Thaller D., Yokota Y., Amponsah G., Blevins S., Craddock A., Craymer M., Michael P., Miyahara B., Pearlman M., Romero N., Schwatke C., Sehnal M., Tyahla L.: *News from the GGOS DOI Working Group*. EGU General Assembly, online, 2021
- Erdogan E., Goss A., Schmidt M., Dettmering D., Seitz F., Müller J., Lexen E., Görres B., Kersten W. F.: *Real-time regional VTEC modeling based on B-splines using real-time GPS and GLONASS observations*. EGU General Assembly, online, 2021
- Fernandez-Gomez I., Goss A., Schmidt M., Borries C.: *Hindcasting the Ionosphere via the assimilation of thermospheric mass density into physics-based models*. DFG SPP 1788 "Dynamic Earth" Colloquium, online, 2021
- Fernandez-Gomez I., Goss A., Schmidt M., Kosary M., Kodikara T., Forootan E., Borries C.: *The impact of severe storms on forecasting the Ionosphere-Thermosphere system through the assimilation of SWARM-derived neutral mass density into physics-based models*. EGU General Assembly, online, 2021
- Garcia-Rigo A., Soja B., Belehaki A., Berdermann J., Cid C., Dettmering D., Lee J., Mannucci A.J., Monte-Moreno E., Pi X., Qahwaji R., Zucca P.: *Overview on GGOS JWG3 -Improved understanding of space weather events and their monitoring*. EGU General Assembly, online, 2021
- Garcia-Rigo A., Soja B.S., Belehaki A., Berdermann J., Cid C., Dettmering D., Lee J., Mannucci A.J., Monte-Moreno E., Pi X., Qahwaji R., Zucca P.: *Towards a better understanding of space weather events and their impact on geodetic measurements*. IAG Scientific Assembly, online, 2021
- Glomsda M., Seitz M., Bloßfeld M., Angermann D., Rudenko S., Zeitlhöfler J.: *DTRF2020: the ITRS 2020 realization of DGFI-TUM*. Frontiers of Geodetic Science (FROGS), online, 2021
- Goss A., Hernández-Pajares M., Schmidt M., Erdogan E.: *Dissemination of High-Resolution Ionosphere Information from VTEC B-spline Expansions for Single-Frequency Positioning*. EGU General Assembly, online, 2021



- Goss A., Schmidt M., Erdogan E., Dettmering D., Florian Seitz F., Müller J., Lexen E., Barbara Görres B., Kersten W.F.: *Detection of ionospheric disturbances by modelling the electron density as three-dimensional B-spline expansions: a simulation study*. IAG Scientific Assembly, online, 2021
- Göttl F., Groh A., Kappelsberger M., Strößenreuther U., Schröder L., Helm V., Schmidt M., Seitz F.: *The influence of Antarctic and Greenland ice loss on polar motion: an assessment based on GRACE and multi-mission satellite altimetry*. EGU General Assembly, online, 2021
- Göttl F., Groh A., Kappelsberger M., Strößenreuther U., Schröder L., Helm V., Schmidt M., Seitz F.: *The influence of Antarctic and Greenland ice loss on polar motion: an assessment based on GRACE and multi-mission satellite altimetry*. IAG Inter-Commission Committee on Geodesy for Climate Research (ICCC) JWG C.1 meeting, online, 2021
- Göttl F., Nandagopalakrishnan D.J., Royston S., Seitz F., Schmidt M., Schwatke C.: *Oceanic mass-related excitation of polar motion: an assessment based on GRACE and multi-mission satellite altimetry*. IAG Scientific Assembly, online, 2021
- Gouzenes Y., Cazenave A., Birol F., Calafat F.M., Passaro M., Leger F., Nino F., Shaw A.G.P., Legeais J.F., Benveniste J., Oelmann J.: *New network of altimetry-based virtual stations in the world coastal zones*. AGU Fall Meeting, online, 2021
- Guimarães G., de Matos A.C.O.C., Pereira A., Antokoletz E.D., Carrión J.L., Sánchez L., et al.: *An overview of SIRGAS activities towards the IHRF*. IAG Scientific Assembly, online, 2021
- Hart-Davis M.G.: *The importance of ocean tides in sea level research using satellite altimetry*. NERSC Seminar Series, 2021
- Hart-Davis M.G., Dettmering D., Piccioni G., Schwatke C., Passaro M., Seitz F.: *EOT20: A new global empirical ocean tide model derived from multi-mission satellite altimetry*. EGU General Assembly, online, 2021
- Hellmers H., Modiri S., Bachmann S., Thaller D., Bloßfeld M., Seitz M., Gipson J.: *Combined IVS contribution to the ITRF2020*. 25th EVGA Working Meeting, 2021
- Jarmołowski W., Belehaki A., Hernández Pajares M., Schmidt M., Goss A., Wielgosz P., Yang H., Krypiak-Gregorczyk A., Monte-Moreno E., García-Rigo A., Tsagouri I., Paouris E., Milanowska B., Erdogan E., Graffigna V., Haagmans R.: *Seismic ionospheric disturbances related to various earthquakes and tsunamis observed by Swarm and other LEOs, GNSS and ionosondes: new approaches for potential warnings*. 2021 Virtual Swarm Science Workshop, 2021
- Krypiak-Gregorczyk A., Komjathy A., Milanowska B., Jarmołowski W., Wielgosz P., Qi L., Lyu H., Hernández-Pajares M., Goss A., Erdogan E., Schmidt M., Hoque M., Shengfeng G., Ghoddousi-Fard R., Orus-Perez R., Nava B., Bilitza D., Dao T., Jin S., Yuan Y., Nicholson H.: *Recent activities of the JWG 4.3.4 - Validation of VTEC models for high-precision and high resolution applications*. IAG Scientific Assembly, online, 2021
- Liu Q., Schmidt M.: *Regularization parameter determination in case of combining different types of gravity data for regional gravity field refinement*. IAG Scientific Assembly, online, 2021
- Liu Q., Schmidt M., Sánchez L.: *The combination and contribution of different gravity measurements in regional quasi-geoid determination based on spherical radial basis functions*. EGU General Assembly, online, 2021

- Liu Q., Schmidt M., Sánchez L.: *Regional gravity field modeling based on a spectral combination through the multi-resolution representation*. Frontiers of Geodetic Science (FROGS), online, 2021
- Mao X., Arnold D., Villiger A., Jäggi A., Dettmering D.: *Impact of satellite dynamics parameterization on precise orbit determination of Sentinel-3*. 43rd COSPAR Scientific Assembly 2021, hybrid, 2021
- Miyahara B., Sánchez L., Sehnal M., Craddock A.: *GGOS: The Global Geodetic Observing System*. AGU Fall Meeting, online, 2021
- Miyahara B., Sánchez L., Sehnal M., Craddock A.: *The Global Geodetic Observing System (GGOS) - fundamental infrastructure for science and society*. IAG Scientific Assembly, online, 2021
- Moreau T., Cadier E., Amarouche L., Amraoui S., Dinardo S., Guerou A., Mangilli A., Taburet N., Tran N., Vayre M., Ablain M., Jugier R., Passaro M., Dettmering D., Schlembach F., Scagliola M, Giudici D., da Silva J.C.B., Santos-Ferreira A.M., Gommenginger C., Timmermans B., Banks C., Donlon C.: *Sentinel-6 Michael Freilich and Jason-3 Tandem Phase Exploitation (S6-JTEX)*. Sentinel-6 Validation Team Meeting, online, 2021
- Natras R., Schmidt M.: *Ensemble Machine Learning for Geodetic Space Weather Forecasting*. IAG Scientific Assembly, online, 2021
- Natras R., Schmidt M.: *Ionospheric VTEC Forecasting using Machine Learning*. EGU General Assembly, online, 2021
- Natras R., Schmidt M.: *Machine Learning Model Development for Space Weather Forecast*. Workshop on Complex Data Challenges in Earth Observation (CDCEO) 2021 at the 30th ACM International Conference on Information and Knowledge Management (CIKM), online, 2021
- Natras R., Schmidt M.: *Time-series Forecasting of Ionospheric Space Weather using Ensemble Machine Learning*. Affinity Workshop Women in Machine Learning (WiML) at the 38th International Conference on Machine Learning (ICML), online, 2021
- Oelsmann J., Passaro M., Müller F.L., Dettmering D., Hart-Davis M.G., Abulaitijiang A., Andersen O.B., Chalençon E., Hoyer J.L., Johansson M., Rautiainen L., Ringgaard I.M., Rinne E., Särkkä J., Scarrott R., Schwatke C., Seitz F., Skovgaard Madsen K., Tuomi L., Ambrozio A., Restano M., Benveniste J.: *Absolute Baltic Sea Level Trends in the Satellite Altimetry Era: A Revisit*. EGU General Assembly, online, 2021
- Oelsmann J., Passaro M., Sánchez L., Dettmering D., Schwatke C., Seitz F.: *Bayesian modelling of discontinuities and piecewise trends (trend changes) improves coastal vertical land motion estimates*. IAG Scientific Assembly, online, 2021
- Passaro M.: *Reprocessing S6 LRM data to enhance the internal performances of S6 Low Resolution Mode in the coastal zone: preliminary results*. Sentinel-6 Validation Team Meeting, online, 2021
- Passaro M.: *Observing sea level and climate change at the coast and at the polar latitudes with reprocessed altimetry: a review*. 1st Workshop of Inter-Commission Committee on Geodesy for Climate Research (ICCC) of the International Association of Geodesy (IAG), online, 2021

- Passaro M.: *Recent advances in coastal altimetry and implications for sea level monitoring closer to the coast*. Ocean Decade Laboratories, Laboratory 2: "A Predicted Ocean" Satellite Activity, Designing observing systems for ocean boundaries, online, 2021
- Passaro M., Müller F.L., Abulaitijiang A., Andersen O.B., Chalençon E., Dettmering D., Hart-Davis M.G., Høyer J.L., Oelmann J., Rautiainen L., Ringgaard I.M., Särkkä J., Scarrott R., Schwatke C., Seitz F., Madsen K.S., Tuomi L., Restano M., Benveniste J.: *Baltic SEAL: new insights into the mean and variability of the sea level in the Satellite Altimetry era*. 1st Workshop of IAG Inter-Commission Committee on Geodesy for Climate Research (ICCC), online, 2021
- Passaro M., Müller F.L., Abulaitijiang A., Andersen O.B., Chalençon E., Dettmering D., Hart-Davis M.G., Høyer J.L., Oelmann J., Rautiainen L., Ringgaard I.M., Särkkä J., Scarrott R., Schwatke C., Seitz F., Madsen K.S., Tuomi L., Restano M., Benveniste J.: *Baltic SEAL: new insights into the mean and variability of the sea level in the Satellite Altimetry era*. 1st ESA Ocean Science Cluster Collocation Meeting, online, 2021
- Passaro M., Müller F.L., Abulaitijiang A., Andersen O. B., Dettmering D., Høyer J., Johansson M., Oelmann J., Rautiainen L., Ringgaard I., Rinne E., Särkkä J., Scarrott R., Schwatke C., Seitz F., Skovgaard Madsen K., Tuomi L., Ambrozio A., Restano M., Benveniste J.: *Baltic SEAL: New regional sea level product offers opportunities to clarify basin sea level budgets*. HYDROSPACE-GEOGloWS, online, 2021
- Passaro M., Rautiainen L., Müller F.L., Abulaitijiang A., Andersen O.B., Dettmering D., Høyer J.L., Madsen K.S., Oelmann J., Ringgaard I.M., Särkkä J., Scarrott R., Schwatke C., Seitz F., Tuomi L., Restano M., Benveniste J.: *Baltic SEAL: assessment and perspectives of Ku and Ka band sea level retrieval with and without sea ice coverage*. DUAL-CRYO ESA Workshop, online, 2021
- Rose S.K., Andersen O.B., Passaro M., Ludwigsen C., Benveniste J., Bouffard J. : *CryoSat-2's contribution to the complete sea level records from the Polar Oceans*. CryoSat 10th Anniversary Science Conference, online, 2021
- Rudenko S., Bloßfeld M., Zeitlhöfler J. : *Recent activities of the IDS Associate Analysis Center at DGFITUM*. IDS DORIS Analysis Working Group Meeting, online, 2021
- Rudenko S., Dettmering D., Bloßfeld M., Zeitlhöfler J., Alkahal R.: *On the current accuracy of altimetry satellite orbits*. EGU General Assembly, online, 2021
- Sánchez L.: *Reprocessing of the SIRGAS reference frame from January 2000 to December 2020*. Symposium SIRGAS, online, 2021
- Sánchez L.: *Advances in the implementation of the International Height Reference Frame*. Splinter meeting on Physical Height Systems, IAG Scientific Assembly, online, 2021
- Sánchez L.: *The International Association of Geodesy (IAG) and the Global Geodetic Observing System (GGOS): the science for the Global Geodetic Reference Frame (GGRF)*. Summer school: New geodetic techniques for Latin America and the Caribbean, Universidad Nacional de La Plata (UNLP), Argentinean German Geodetic Observatory (AGGO), La Plata, Argentina, 2021
- Sánchez L.: *Lecture on Vertical Datum Unification*. 13th International Geoid School, International Service for the Geoid (IGS), online, 2021
- Sánchez L.: *Status of the International Height Reference Frame (IHRF)*. Symposium SIRGAS, online, 2021

- Sánchez L.: *Towards a global unified height system*. 2021 Scientific Meeting of the Turkish National Geodesy Commission (TUJK), online, 2021
- Sánchez L.: *Towards an integrated global geodetic reference frame*. Forschungsbereich Höhere Geodäsie der TU Wien, Vienna, Austria, 2021
- Sánchez L.: *Report on the International Height Reference Frame (IHRF)*. Steering committee meeting of IAG Commission 2, online, 2021
- Sánchez L.: *Geodesy's contribution to the observation and modelling of the Earth System*. Geodetic Colloquium, Universidad de Jaén, Spain, 2021
- Sánchez L.: *GGOS Focus Area Unified Height System: On-going activities*. GGOS Coordinating Board Meeting, online, 2021
- Sánchez L., Barzaghi R.: *Report of the GGOS Focus Area Unified Height System*. GGOS Days 2021, online, 2021
- Sánchez L., Barzaghi R., Huang J., Vergos G.S., Ågren J., Mäkinen J., et al.: *Status of the International Height Reference Frame (IHRF)*. IAG Scientific Assembly, online, 2021
- Sánchez L., Huang J., Barzaghi R., Vergos G.S.: *Towards a Global Unified Physical Height System*. EGU General Assembly, online, 2021
- Sánchez L., Huang J., Barzaghi R., Vergos G.S.: *GGOS Focus Area Unified Height System: achievements and open challenges*. IAG Scientific Assembly, online, 2021
- Scagliola M., Altiparmaki O., Bercher N., Fenoglio-Marc L., Nielsen K., Passaro M., Restano M., Abis B., Fornari M., Sabatino G., Benveniste J.: *The Aresys FF-SAR Service for Cryosat-2 at ESA GPOD*. CryoSat 10th Anniversary Science Conference, online, 2021
- Scherer D., Schwatke C., Dettmering D.: *Contributions of Cryosat-2 to Hydrological Applications: How DAHITI benefits from 10 years of LRM and SAR data from a long-repeat orbit mission*. CryoSat 10th Anniversary Science Conference, online, 2021
- Schmidt M.: *Ionosphere modeling from space-geodetic satellite observations*. WHU Summer School International, online, 2021
- Schmidt M., Erdogan E., Goss A., Dettmering D., Seitz F., Müller J., Lexen E., Görres B., Kersten W.F.: *Vorhersage des vertikalen absoluten Elektronengehalts der Ionosphäre unter Verwendung eines neuronalen Netzwerkes und Berücksichtigung geomagnetischer Indizes*. 5. Nationaler Weltraumwetterworkshop, online, 2021
- Schmidt M., Goss A., Erdogan E.: *Monitoring and Modelling of ionospheric disturbances by means of GRACE, GOCE and Swarm in-situ observations*. EGU General Assembly, online, 2021
- Schmidt M., Goss A., Erdogan E., Jarmołowski W., Wielgosz P., Krypiak-Gregorczyk a., Milanowska B., Hernández Pajares M., García-Rigo A., Monte-Moreno E., Graffigna V., Yang H., Belehaki A., Tsagouri I., Paouris E., Haagmans R.: *Detection of earthquake and tsunami signatures in the ionosphere from the combination of different observation techniques*. IAG Scientific Assembly, online, 2021
- Schmidt M., Goss A., Lalgudi Gopalakrishnan G.: *Electron density modelling based on an inequality constrained optimization algorithm using a combination of radio occultation and GNSS STEC observations*. DFG SPP 1788 "Dynamic Earth" Colloquium, online, 2021

- Schwatke C.: *DAHITI - Monitoring water levels of Nile river and its reservoirs using satellite altimetry*. 6th Nile Basin Development Forum, online, 2021
- Schwatke C., Dettmering D., Scherer D.: *DAHITI – Satellite-derived Hydrological Products for Monitoring the Global Water Cycle*. 4th Hydrospace-GEOGloWS, online, 2021
- Schwatke C., Rinklefs R.: *Data Formats and Procedures Standing Committee - Status Report*. ILRS Virtual World Tour, online, 2021
- Sehna M., Angermann D., Sánchez L.: *New GGOS Website – An Extensive Information Platform about Geodetic Products, Observations and Services*. IAG Scientific Assembly, online, 2021
- Seitz F.: *Geodätische Erdbeobachtung aus dem Weltraum: Aktuelle Arbeiten am Deutschen Geodätischen Forschungsinstitut*. DGK Annual Meeting, Munich, 2021
- Seitz M., Bloßfeld M., Glomsda M., Angermann D., Rudenko S., Zeitlhöfler J.: *DTRF2020: the ITRS 2020 realization of DGFI-TUM*. AGU Fall Meeting, online, 2021
- Seitz M., Glomsda M., Bloßfeld M., Kehm A., Gerstl M., Angermann D.: *First VLBI-only TRF/CRF solution based on DGFI-TUM data for ITRF2020*. 25th EVGA Working Meeting, 2021
- Sulzbach R., Wziontek H., Hart-Davis M.G., Dobsław H., Thomas M.: *Signatures of degree-3 tidal loading effects in superconducting gravimeter records predicted by data-unconstrained ocean tide modeling*. Grace-FO Science Team Meeting (GSTM), online, 2021
- Tarrío J.A., Sánchez L., Costa S., Silva A., et al.: *Recent achievements and current challenges in the maintenance of the geodetic reference frame of the Americas*. IAG Scientific Assembly, online, 2021
- Wang N., Li Z., Yuan Y., Hernández-Pajares M., Blot A., Krankowski A., Hauschild A., Garcia-Rigo A., Goss A., Komjathy A., Wang C., Erdogan E., Olivares G., Nakayama K., Liu L., Bergeot N., Zhao Q., Orús R., Ghoddousi-Fard R., Lee W., Huo X., Xiaodong Ren X., Liu Z.: *IAG JWG 4.3.1 Real-time Ionosphere Monitoring and Modeling: Status during 2019-2021*. IAG Scientific Assembly, online, 2021
- Zeitler L., Corbin A., Vielberg K., Rudenko S., Löcher A., Bloßfeld M., Schmidt M., Kusche J.: *Scale factors of the thermospheric neutral density - a comparison of SLR and accelerometer solutions*. DFG SPP 1788 "Dynamic Earth" Colloquium, online, 2021
- Zeitler L., Corbin A., Vielberg K., Rudenko S., Löcher A., Bloßfeld M., Schmidt M., Kusche J., Forootan E.: *Scale factors of the thermospheric neutral density - a comparison of SLR and accelerometer solutions*. EGU General Assembly, online, 2021
- Zeitlhöfler J., Bloßfeld M., Rudenko S., Seitz F.: *Estimation of station-dependent LRA correction parameters for the TOPEX/Poseidon mission*. EGU General Assembly, online, 2021
- Zeitlhöfler J., Bloßfeld M., Rudenko S., Seitz F.: *Station-dependent laser retroreflector array correction function for TOPEX/Poseidon*. Frontiers of Geodetic Science (FROGS), online, 2021

## 4.4 Participation in Meetings, Symposia, Conferences

- 2021-01-12 : **COST-G meeting, online**  
*Bloßfeld M.*
- 2021-01-13/14 : **ESA DUAL-CRYO Workshop, online**  
*Passaro M., Müller F.L.*
- 2021-01-14 : **IAG Inter-Commission Committee on Geodesy for Climate Research (ICCC) Joint Working Group C.1 "Climate Signatures in Earth Orientation Parameters": 5th online meeting**  
*Bloßfeld M., Kehm A.*
- 2021-01-15 : **ESA Sea State Climate Change Initiative, Progress Meeting 8, online**  
*Passaro M., Schlembach F.*
- 2021-01-19 : **ESA Sea Level Climate Change Initiative, Progress Meeting, online**  
*Passaro M.*
- 2021-01-26 : **IDS Governing Board Meeting, online**  
*Dettmering D.*
- 2021-01-27 : **ESA BalticSEAL Final Review, online**  
*Dettmering D., Müller F.L., Passaro M., Seitz F., Oelsmann J.*
- 2021-01-28 : **SWOT Working Group "River Science", online**  
*Schwatke C.*
- 2021-01-28 : **ESA COSTO Final Review, online**  
*Schmidt M., Goss A., Erdogan E.*
- 2021-02-01/02 : **SWOT Working Group "Science for Lakes and Wetlands", online**  
*Schwatke C.*
- 2021-02-03 : **SWOT Working Group "Global Hydrology and Remote Sensing", online**  
*Schwatke C.*
- 2021-02-04 : **ESA HYDROCOASTAL Progress Meeting 2, online**  
*Passaro M., Dettmering D.*
- 2021-02-08/09 : **SWOT Science Team Meeting, online**  
*Schwatke C.*
- 2021-02-25 : **ILRS Networks and Engineering Standing Committee Meeting, online**  
*Kehm A.*
- 2021-03-02 : **Annual meeting of DGK Section Geodesy, online**  
*Seitz F.*
- 2021-03-03/05 : **NERO GRAV Status Meeting, online**  
*Dettmering D., Hart-Davis M.G.*
- 2021-03-09 : **EuroTech Space and Earth Observation, online**  
*Dettmering D., Seitz F.*

- 2021-03-15/18 : **25th EVGA Working Meeting, online**  
*Glomsda M., Seitz M.*
- 2021-03-18 : **IAG Inter-Commission Committee on Geodesy for Climate Research (ICCC) Joint Working Group C.1 "Climate Signatures in Earth Orientation Parameters": 6th online meeting**  
*Göttl F., Kehm A.*
- 2021-03-19 : **2nd ESA Fully Focused SAR Expert Users Progress Meeting, online**  
*Passaro M.*
- 2021-03-23 : **Copernicus POD Quality Working Group Meeting, online**  
*Dettmering D.*
- 2021-03-23/25 : **ESA Sea State Climate Change Initiative, 2nd User Consultation Meeting, online**  
*Passaro M., Schlembach F.*
- 2021-03-29/30 : **Sentinel-3 Next Generation Topography MAG, online**  
*Passaro M.*
- 2021-03-29/31 : **IAG Inter-Commission Committee on Geodesy for Climate Research (ICCC) Workshop, online**  
*Passaro M., Müller F.L.*
- 2021-03-30 : **INSIGHT-II Project Meeting, online**  
*Schmidt M., Goss A.*
- 2021-04-06/07 : **IDS Analysis WG Meeting, online**  
*Dettmering D., Rudenko S., Zeitlhöfler J.*
- 2021-04-13 : **ESA Sea State Climate Change Initiative, Progress Meeting 9, online**  
*Passaro M., Schlembach F.*
- 2021-04-15 : **ILRS Networks and Engineering Standing Committee Meeting, online**  
*Kehm A., Schwatke C., Zeitlhöfler J.*
- 2021-04-19/30 : **EGU General Assembly 2021, online**  
*Angermann D., Bloßfeld M., Erdogan E., Goss A., Göttl F., Hart-Davis M.G., Liu Q., Oelsmann J., Rudenko S., Sánchez L., Schmidt M., Seitz F., Seitz M., Zeitler L., Zeitlhöfler J.*
- 2021-05-05 : **ESA HYDROCOASTAL Progress Meeting 3, online**  
*Passaro M., Dettmering D.*
- 2021-05-07 : **GGOS Coordinating Meeting, online**  
*Angermann D., Sanchez L., Schmidt M.*
- 2021-05-11 : **OPTIMAP Project Meeting, MS22, online**  
*Schmidt M., Goss A., Erdogan E., Seitz F.*
- 2021-05-18 : **SWOT Working Group "Science for Lakes and Wetlands", online**  
*Schwatke C.*
- 2021-05-19/20 : **Sentinel-6 Validation Team (S6VT) Meeting 2, online**  
*Dettmering D., Passaro M.*

- 2021-05-20 : **3rd ESA Fully Focused SAR Expert Users Progress Meeting, online**  
*Passaro M.*
- 2021-05-27 : **SWOT Working Group "River Science", online**  
*Schwatke C.*
- 2021-05-31/06-02 : **SPP 1788 "Dynamic Earth" Colloquium, online**  
*Schmidt M., Goss A., Zeitler L., Rudenko S.*
- 2021-05-31/06-04 : **Crash Course on Data Assimilation - Theoretical Foundations and Advanced Applications, online**  
*Hart-Davis M.G.*
- 2021-06-01/03 : **Workshop on "Optical Clock Comparison using VLBI", online**  
*Glomsda M.*
- 2021-06-02 : **Tour de l'IGS 1st Stop: ITRF and the outcomes of the activities of the third IGS reprocessing (repro3), online**  
*Rudenko S., Seitz M.*
- 2021-06-07/11 : **ESA 4th Hydrospace-GEOGloWS 2021, online**  
*Dettmering D., Müller F., Scherer D., Schwatke C.*
- 2021-06-14/17 : **CryoSat 10th Anniversary Science Conference, online**  
*Dettmering D., Müller F., Scherer D., Schwatke C., Veng T.*
- 2021-06-15 : **IAG Inter-Commission Committee on Geodesy on Theory (ICCT) Joint Study Group T.29 "Machine Learning in Geodesy": 2nd meeting, online**  
*Natras, R.*
- 2021-06-17 : **IAG Inter-Commission Committee on Geodesy for Climate Research (ICCC) Joint Working Group C.1 "Climate Signatures in Earth Orientation Parameters": 7th online meeting**  
*Göttl F.*
- 2021-06-22 : **ESA HYDROCOASTAL Progress Meeting 4, online**  
*Passaro M., Dettmering D.*
- 2021-06-24 : **ILRS Networks and Engineering Standing Committee Meeting, online**  
*Schwatke C., Kehm A.*
- 2021-06-24 : **SWOT Working Group "River Science", online**  
*Scherer D., Schwatke C.*
- 2021-06-28/07-02 : **IAG Scientific Assembly 2021, online**  
*Angermann D., Erdogan E., Göttl F., Goss A., Liu Q., Schmidt M.*
- 2021-06-29 : **ESA Sea State Climate Change Initiative, Progress Meeting 10, online**  
*Passaro M.*
- 2021-06-29 : **IDS Governing Board Meeting, online**  
*Dettmering D.*
- 2021-07-06 : **ESA Sea Level Climate Change Initiative, Progress Meeting, online**  
*Passaro M., Oelsmann J.*



- 2021-07-16 : **TIPOD Project Meeting, online**  
*Schmidt M., Zeitler L., Bloßfeld M.*
- 2021-07-20/22 : **OPTIMAP Project Meeting, MS23, Munich**  
*Schmidt M., Goss A., Erdogan E., Seitz F.*
- 2021-08-23/26 : **IAU XXXI General Assembly Business Sessions, online**  
*Seitz F.*
- 2021-08-23/27 : **United Nations Committee of Experts on Global Geospatial Information Management (UN-GGIM), Eleventh Session, online**  
*Angermann D.*
- 2021-09-03 : **ESA S6-JTEX Kick-off meeting, online**  
*Dettmering D., Schlembach F.*
- 2021-09-13/15 : **SWOT Science Team Meeting 2021, online**  
*Schwatke C.*
- 2021-09-21/23 : **5. Nationaler Weltraumwetterworkshop, online**  
*Schmidt M., Goss A.*
- 2021-09-22/23 : **Frontiers of Geodetic Science (FROGS), online**  
*Angermann D., Bloßfeld M., Glomsda M., Göttl F., Liu Q., Rudenko S., Schmidt M., Seitz F., Zeitlhöfler J.*
- 2021-09-23 : **ESA Sea State Climate Change Initiative, Progress Meeting 10, online**  
*Passaro M., Schlembach F.*
- 2021-09-28/29 : **DGK/DLR Kolloquium "Geodätische Grundlagen der Erdbeobachtung - Aktuelle Fragen und Perspektiven", Munich**  
*Dettmering D., Seitz F.*
- 2021-10-07/08 : **GlobalCDA status meeting, online**  
*Dettmering D., Ellenbeck L., Scherer D., Schwatke C.*
- 2021-10-11/13 : **GGOS Days 2021, online**  
*Angermann D., Bloßfeld M., Rudenko S.*
- 2021-10-12 : **IDS Governing Board Meeting, online**  
*Dettmering D.*
- 2021-10-13/15 : **Towards a Copernicus Calibration and Validation Solution (CCVS) Workshop, online**  
*Dettmering D.*
- 2021-10-18 : **ESA Sea Level Climate Change Initiative, Progress Meeting, online**  
*Passaro M.*
- 2021-10-19/20 : **Sentinel-3 Next Generation Topography MAG, online**  
*Passaro M.*
- 2021-10-21 : **GNSS-IR Short Course, online**  
*Hart-Davis M.G., Schwatke C.*
- 2021-10-25/29 : **ILRS Virtual World Tour 2021, online**  
*Bloßfeld M., Kehm A., Rudenko S., Schwatke C., Zeitlhöfler J.*

- 2021-10-26/27 : **OPTIMAP Final Meeting, MS24, Munich**  
*Dettmering D., Erdogan E., Goss A., Seitz F.*
- 2021-10-26/28 : **Sentinel-6 Validation Team (S6VT) Meeting 3, online**  
*Dettmering D., Schlembach F.*
- 2021-10-27 : **ESA HYDROCOASTAL Progress Meeting 5, online**  
*Dettmering D., Passaro M.*
- 2021-10-28 : **SWOT Working Group "River Science", online**  
*Scherer D., Schwatke C.*
- 2021-11-09/10 : **GlobalCDA ECR Gender Equality Workshop on "Self-Presentation and Networking", Limburg an der Lahn**  
*Scherer D.*
- 2021-11-12 : **ESA S6-JTEX Down Selection Meeting, online**  
*Dettmering D.*
- 2021-11-16/18 : **DORIS Days 2021, online**  
*Bloßfeld M., Dettmering D., Rudenko S., Zeitlhöfler J.*
- 2021-11-24/26 : **DGK Annual meeting, online**  
*Seitz F.*
- 2021-11-29/12-02 : **1st ESA Ocean Science Cluster Collocation Meeting, online**  
*Passaro M., Müller F.L.*
- 2021-12-09 : **NERSC Seminar, Bergen, Norway, online**  
*Hart-Davis M.G.*
- 2021-12-10 : **ESA S6-JTEX Progress Meeting 1, online**  
*Dettmering D., Schlembach F.*
- 2021-12-13/17 : **AGU Fall Meeting, online**  
*Angermann D., Seitz M.*

## 4.5 Guests

- 2021-01-01/12-31 : Dr. Stephan Paul, AWI, Bremerhaven, Germany
- 2021-09-13/12-12 : Ana Aldarias, University of Cadiz, Spain

## 4.6 Internet Portals

For the exchange of scientific knowledge, results and data with national and international partners, interested parties and the public, DGFI-TUM maintains the following internet portals and public databases:

### Deutsches Geodätisches Forschungsinstitut der Technischen Universität München (DGFI-TUM)

The DGFI-TUM website at [www.dgfi.tum.de](http://www.dgfi.tum.de) highlights the latest research results and provides information on the structure and research of the institute. It presents the national and international projects as well as the institute's involvement in various international scientific organizations. The website contains complete lists of publications, reports and presentations since 1994 and provides the scientific data products of DGFI-TUM. It has a media section and presents information on teaching.

To reach out to the public and students, DGFI-TUM maintains its own Facebook page ([www.facebook.com/dgfitum](http://www.facebook.com/dgfitum)) where it publishes current results, job offers and opportunities for scientific work. The posts receive considerable feedback and reach several hundred followers.

## Open Altimeter Database (OpenADB): Ocean science data from space

OpenADB is the DGFI-TUM platform for the dissemination of multi-mission altimetry data and derived high-level science products of oceanic and atmospheric quantities. It serves scientists from various disciplines as well as users in research and practice. OpenADB data are widely used for the study of ocean and climate processes, for monitoring purposes, or for the creation and validation of new products, models, and algorithms.

Currently, OpenADB provides the following data:

- Sea Surface Heights (SSH)
- Sea Level Anomalies (SLA)
- Adaptive Leading Edge Subwaveform (ALES) Retracker heights
- Instantaneous Dynamic Ocean Topography Profiles (iDOT)
- Empirical Ocean Tide Model (EOT)
- Vertical Total Electron Content (VTEC)

All altimetry data is provided free of charge to registered users in standard data formats. The data in OpenADB are preprocessed and already corrected with the latest geophysical models. In addition, data from all missions have been carefully harmonized and cross-calibrated so that observation data from different missions can be combined and analyzed together. The database is available at [openadb.dgfi.tum.de](http://openadb.dgfi.tum.de).

Open Altimeter Database (OpenADB)  
Deutsches Geodätisches Forschungsinstitut  
Technische Universität München

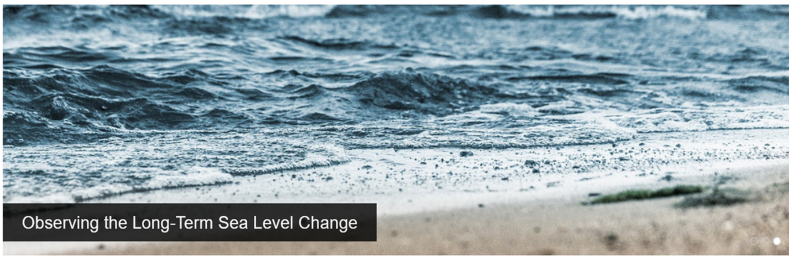


**OpenADB**

- Products +
- Mean Sea Level
- Missions +
- Pass Locator
- Documentation +
- Data Access**

OpenADB

### Open Altimeter Database (OpenADB)



Observing the Long-Term Sea Level Change

**WELCOME TO OPENADB ...**

OpenADB is a database for satellite altimetry data and derived high-level products. It shall serve users with little experience in satellite altimetry and scientific users evaluating data, generating new products, models and algorithms.

The following products are available via OpenADB:

- **Sea Surface Heights (SSH)**
- **Sea Level Anomalies (SLA)**
- **Instantaneous Dynamic Ocean Topography Profiles (iDOT)**
- **Empirical Ocean Tide Model (EOT)**
- **Vertical Total Electron Content (VTEC)**
- **Adaptive Leading Edge Subwaveform (ALES) Retracker**

All products are provided along-track in a sequential data structure following the usual hierarchy mission-cycle-pass with cycles identifying (in general) a repeat period after which the ground track pattern repeats itself and passes are decomposed into ascending and descending portions of the ground track.

**Contact**

**Christian Schwatke**  
christian.schwatke@tum.de

80333 München  
Arcisstr.21  
Tel. +49 89 23031-1109  
Fax +49 89 23031-1240

## Database for Hydrological Time Series of Inland Waters (DAHITI)

Database for Hydrological Time Series of Inland Waters (DAHITI)

Deutsches Geodätisches Forschungsinstitut  
Technische Universität München

DAHITI - Products

- Water Level Time Series from Satellite Altimetry**  
This product "Water Levels (Altimetry)" provides water level time series for lakes, reservoirs, rivers and wetlands derived from multi-mission satellite altimetry. [\[More\]](#)
- Surface Area Time Series from Optical Imagery**  
The product "Surface Areas" contains surface area time series for lakes and reservoirs derived from optical imagery such as Landsat and Sentinel-2. [\[More\]](#)
- Time Series of Volume Variations**  
The product "Volume Variations" provides time series of volume variations, estimated for lakes and reservoirs using water levels from satellite altimetry and surface areas from optical imagery. [\[More\]](#)
- Bathymetry**  
The product "Bathymetry" provides the bathymetry above the minimum observed surface area used for the estimation of volume variations. [\[More\]](#)
- Water Occurrence Masks**  
The product "Water Occurrence Mask" provides the water probability of lakes and reservoirs derived from optical imagery since 1984. [\[More\]](#)
- Land-Water Masks**  
The product "Land-Water Masks" contains binary land-water masks which are derived in the processing step of computing surface area time series. [\[More\]](#)
- Hypsometry**  
The product "Hypsometry" describes the relationship of water levels and surface areas of lakes and reservoirs called hypsometric curve. [\[More\]](#)
- Time Series of Water Levels from Hypsometry**  
The product "Water Levels (Hypsometry)" contains a water level time series derived from the hypsometric curve of a lake or reservoir in combination with surface areas from optical imagery. [\[More\]](#)
- Time Series of River Discharge**  
The product "River Discharge" provides the discharge of rivers derived from satellite altimetry and optical imagery. [\[More\]](#)

Contact  
Christian Schwabe [christian.schwabe@tum.de](mailto:christian.schwabe@tum.de)  
80333 München  
Arcisstr. 21  
Tel. +49 89 23031-1109  
Fax +49 89 23031-1240

DAHITI-Targets

Africa	1282
Asia	642
Australia	29
Europe	277
North America	584
South America	3227
Global	6146

Related Project(s):  
Global CDA

DAHITI-Flyer

In DAHITI ([dahiti.dgfi.tum.de](http://dahiti.dgfi.tum.de)), DGFI-TUM provides various satellite-based quantities for more than 5900 lakes, reservoirs, rivers and wetlands distributed worldwide. Water level time series based on multi-mission satellite altimetry are available for all targets in DAHITI. In addition, DAHITI provides surface water extent time series (based on Landsat and Sentinel-2 optical imagery), derived bathymetry, and water occurrence masks for a variety of lakes and reservoirs. Also available in DAHITI are lake and reservoir water storage changes (volume changes) from a combination of satellite altimetry and optical imagery. In 2021, DGFI-TUM expanded the availability of river discharge time series (Section 2.3).

## EUROLAS Data Centre (EDC)

EUROLAS Data Center (EDC)  
Deutsches Geodätisches Forschungsinstitut  
Technische Universität München

Welcome

Welcome to the EUROLAS Data Center (EDC)

Wettzell, Germany

Current implementation status of

- Consolidated Prediction Format (CPFv2)
- Consolidated Laser Ranging Data Format (CRDv2)

News

- 2022-02-12 The satellite **ELSA-d (Target)** (2182239) was added to the EDC satellite database.
- 2022-02-02 The satellites **Galileo-223 (211581)** and **Galileo-224 (211582)** were added to the EDC satellite database.
- 2021-11-29 The satellite **QZS-1R (2159602)** was added to the EDC satellite database.
- 2021-11-11 The station **Tenerife, Spain (7781)** was added to the EDC database and the station status was changed to quarantine.
- 2021-10-06 The satellite **TURIN (2156922)** was added to the EDC satellite database.

Contact  
Christian Schwabe [christian.schwabe@tum.de](mailto:christian.schwabe@tum.de)  
80333 München  
Arcisstr. 21  
Tel. +49 89 23031-1109  
Fax +49 89 23031-1240

The EUROLAS Data Center (EDC) is - along with NASA's CDDIS - one of two global Data Centers of the International Laser Ranging Service (ILRS). The EDC has been operated by DGFI-TUM since 1998. The website [edc.dgfi.tum.de](http://edc.dgfi.tum.de) and the corresponding FTP server (<ftp://edc.dgfi.tum.de>) provide the ILRS community with access to all SLR original observations and derived products. In addition, the EDC website provides information about real-time data management in the ILRS Operations Center (OC) at EDC and about the Data Center's data holding.

## GGOS Focus Area Unified Height System

DGFI-TUM has chaired the GGOS Focus Area *Unified Height System* since 2015. Its main objective is the implementation of a global vertical reference system in accordance with the International Association of Geodesy (IAG) Resolution No. 1, 2015 for the definition and realization of an International Height Reference System (IHRs). The Focus Area website ([ihrs.dgfi.tum.de](https://ihrs.dgfi.tum.de)), maintained by DGFI-TUM, summarizes the actions, plans, and recent achievements, and provides an inventory of work documents, relevant publications, and presentations.

## Geocentric Reference System for the Americas (SIRGAS)

DGFI-TUM has been involved in SIRGAS research activities since the establishment of SIRGAS in 1993. The institute coordinated the 1995 and 2000 SIRGAS GPS campaigns and acted as an analysis center for both campaigns, contributing to the final solutions SIRGAS95 and SIRGAS2000. In June 1996, DGFI-TUM, in agreement with the International GNSS Service (IGS), established the IGS Regional Network Associate Analysis Centre for SIRGAS (IGS RNAAC SIRGAS) and assumed responsibility for the weekly processing of the continuously operating SIRGAS network. This also includes the computation of cumulative (multi-year) solutions and surface velocity models (known as VEMOS) to monitor the kinematics of the SIRGAS reference frame. Since 2008, DGFI-TUM has focused on the computation of the SIRGAS core network and on the combination of this network with the solutions provided by the Latin American data centers for national SIRGAS densification. DGFI-TUM also plays a central role in the determination of SIRGAS reference frame multi-year solutions and surface deformation models.

The SIRGAS portal hosted by DGFI-TUM until July 2021 has moved to <https://sargas.ipgh.org/>. DGFI-TUM's SIRGAS website [www.sargas.org](http://www.sargas.org) will continue to present analysis strategies, research results and data products generated by DGFI-TUM as SIRGAS Processing and Combination Centre and as IGS RNAAC SIRGAS.

SIRGAS Analysis Centre at DGFI-TUM  
Deutsches Geodätisches Forschungsinstitut  
Technische Universität München



- Home
- About SIRGAS
- Realizations +
- Stations +
- Data processing
- Data combination +
- Weekly solutions
- Multi-year solutions
- VEMOS velocity model +
- Publications
- Presentations
- Updates

**Contact**

Dr.-Ing. Laura Sanchez [✉](mailto:lm.sanchez@tum.de)  
lm.sanchez@tum.de

80333 München  
Arcisstr.21  
Tel. +49 89 23031-1295  
Fax +49 89 23031-1240

---

**SIRGAS Analysis Centre at DGFI-TUM**

**SIRGAS** as geocentric reference system is defined identical to the **International Terrestrial Reference System (ITRS)** [✉](#). Its realization is a regional densification of the global **International Terrestrial Reference Frame (ITRF)** [✉](#). The reference station positions are associated to a specific (reference) epoch and their variation with time is taken into account by discrete station velocities or by a continuous velocity model, which comprises tectonic plate movements and crustal deformations. Realizations or densifications of SIRGAS associated to different reference epochs and referring to different ITRF solutions materialize the same reference system and, after reducing their coordinates to the same frame (ITRF) and reference epoch, they are compatible at the cm-level. The extension of the SIRGAS frame is carried out by national densifications of the continental network, which serve as local reference frames.

## 5 Projects

*A large part of DGFI-TUM's research activities is financed through third-party funds from various sources. Funding of the following projects is gratefully acknowledged (in alphabetic order):*

**AROCCIE** Arctic Ocean Surface Circulation in a Changing Climate and its Possible Impact on Europe (IGSSE)

**Baltic+ SEAL** BALTIC+ Sea Level (ESA)

**Baltic+ SAR-HSU** BALTIC+ Geodetic SAR for Baltic height system unification (ESA)

**CIEROT** Combination of space geodetic observations for the determination of mass transports in the cryosphere and their impact on Earth rotation (DFG)

**CIRCOS** Circulation from In-situ and Remote Sensing Data in Coastal and Shelf Ocean (DFG)

**COSTO** Contribution of SWARM data to the prompt detection of Tsunamis and other natural hazards (ESA)

**CPOD** Copernicus Sentinels Precise Orbit Determination (ESA)

**FOR 2630, ARISAS** Advances in Remote Sensing of Inland Waters by Satellite Altimetry with Special Focus on SWOT (DFG)

**FOR 2630, WALESA** Refined estimates of absolute water levels for inland waters from multi-mission satellite altimetry (DFG)

**FOR 2736, TIDUS** Improved tidal dynamics and uncertainty estimation for satellite gravimetry (DFG)

**Geo-H** Enhanced Geopotential Field Modelling as Basis for the Establishment of Precise Height Systems (DFG)

**Hydrocoastal** Sentinel-3 and Cryosat SAR/SARIn radar altimetry for coastal zone and inland water (ESA)

**ML-IonoCast** Machine learning for forecasting the ionospheric total electron content (DAAD)

**MEPODAS** Mitigation of the current errors in precise orbit determination of altimetry satellites (DFG)

**OPTIMAP** Operational Tool for Ionospheric Mapping And Prediction (ZGeoBw)

**ORG4Heights** Optimally combined regional geoid models for the realization of height systems in developing countries (DFG)

**S6-JTEX** Sentinel-6 Michael Freilich and Jason-3 Tandem Flight Exploitation (ESA)

**SPP 1788, INSIGHT-2** Interactions of low-orbiting satellites with the surrounding ionosphere and thermosphere (DFG)

**SPP 1788, MuSE** Multi-satellite reconstruction of the electron density in ionosphere and plasmasphere (DFG)

**SPP 1788, TIPOD** Development of high-precision thermosphere models for improving precise orbit determination of Low-Earth-Orbiting satellites (DFG)

**SL-CCI Plus** Sea Level Climate Change Initiative Plus (ESA)

**SS-CCI Plus** Sea State Climate Change Initiative Plus (ESA)

**Nile Monitoring** Nile Basin Strategic Water Resources Analysis (GIZ/Sydro GmbH)

**VLAD** Vertical land motion by satellite altimetry and tide gauge difference (DFG)



## 6 Personnel

### 6.1 Lectures and Courses at Universities

- Angermann D. :** Lecture 'Satellite Geodesy: Global Geodata for Society and Politics',  
TUM, SS 2021
- Bloßfeld M. :** Lecture 'Realization and Application of Global Geodetic Reference Systems',  
TUM, SS 2021
- Bloßfeld M. :** Lecture 'Geokinematics',  
TUM, WS 2020/21 and WS 2021/22
- Dettmering D. :** Lecture 'Hydrogeodesy: Monitoring Surface Waters from Space',  
TUM, WS 2020/21 and WS 2021/22
- Passaro M. :** Lecture 'Oceanography and Satellite Altimetry',  
TUM, WS 2020/21 and WS 2021/22
- Passaro M. :** Lecture 'Numerical Modeling',  
TUM, WS 2021/22
- Sánchez L. :** Lecture 'Advanced Aspects of Height Systems',  
TUM, WS 2020/21 and WS 2021/22
- Schmidt M. :** Lecture 'Numerical Modeling',  
TUM, WS 2020/21
- Schmidt M. :** Lecture 'Numerical Methods in Satellite Geodesy',  
TUM, SS 2021
- Schmidt M. :** Lecture 'Ionosphere Monitoring and Modeling',  
TUM, WS 2020/21 and WS 2021/22
- Schmidt M., Seitz F., Müller F.L., Glomsda M. :** Lecture 'Numerical Methods',  
TUM, WS 2020/21 and WS 2021/22
- Seitz F. :** Lecture 'Seminar ESPACE',  
TUM, SS 2021
- Seitz F. :** Seminar for Doctoral Candidates at the DGFI-TUM,  
TUM, WS 2020/21, SS 2021 and WS 2021/22
- Seitz F. :** Lecture 'Earth Rotation',  
TUM, WS 2020/21 and WS 2021/22

## 6.2 Lectures at Seminars, Schools, and Public Relations

- Sánchez L.:** 'Geodesy's contribution to the observation and modeling of the Earth System'. Geodetic Colloquium, Master Program "Geodetic Engineering and Applied Geophysics", Universidad de Jaén, Spain, 2021-03-03
- Sánchez L.:** 'The International Association of Geodesy (IAG) and the Global Geodetic Observing System (GGOS): the science for the Global Geodetic Reference Frame (GGRF)'. Summer school: New geodetic techniques for Latin America and the Caribbean, Universidad Nacional de La Plata (UNLP), Argentinean German Geodetic Observatory (AGGO), La Plata, Argentina, 2021-04-05
- Bloßfeld M.:** 'Die Vermessung der Erde als Grundlage für die Erdsystemforschung - Herausforderungen an geodätische Referenzsysteme und deren gesellschaftliche Relevanz'. Geodetic Colloquium, University Innsbruck, online, 2021-04-07
- Sánchez L.:** 'Towards an integrated global geodetic reference frame'. Research Unit Higher Geodesy, TU Wien, Vienna, Austria, 2021-06-16
- Schmidt M.:** 'Ionosphere modeling from space-geodetic satellite observations'. Wuhan University Summer School International, Wuhan, China, online, 2021-07-19
- Passaro M.:** 'Recent advances in coastal altimetry and implications for sea level monitoring closer to the coast'. Ocean Decade Laboratories, Laboratory 2: "A Predicted Ocean", Satellite Activity, Designing observing systems for ocean boundaries, online, 2021-09-16
- Sánchez L.:** 'Vertical Datum Unification'. 13th International Geoid School, International Service for the Geoid (IGS), online, 2021-10-14

## 6.3 Thesis Supervision

### Master theses

- Bloßfeld M., Seitz F.:** Master Thesis Geißendörfer O., TUM: Computation of a global terrestrial reference frame based on SLR solutions. 2021-03-31
- Dettmering D., Seitz F.:** Master Thesis Koch J., TUM: Analysis of coastal sea level trends. 2021-03-31
- Hart-Davis M.G.:** Master Thesis Heye S., University of Cape Town: The Natal Bight Coastal Counter-Current: a modeling study. 2021-12-01
- Hart-Davis M.G.:** Honours Thesis Birkett G., University of Cape Town: Nurdle Spill Scenarios: Using a Numerical Model to Identify High Risk Coastal Regions. 2021-12-01

## Doctoral theses

**Seitz F.** (supervisor): Doctoral Thesis Müller F.L., TUM: Improved polar geostrophic surface currents from satellite altimetry. 2021-01-22

**Seitz F.** (supervisor): Doctoral Thesis Piccioni G., TUM: Exploit satellite altimetry to improve coastal tide estimation 2021-02-03

**Schmidt M.** (supervisor): Doctoral Thesis Goss A., TUM: Generation of high-resolution global and regional multi-scale B-spline models of the vertical total electron content based on low-latency GNSS data. 2021-09-13

## 6.4 Conferral of Doctorates

**Müller F.L. :** *Title:* Improved polar geostrophic surface currents from satellite altimetry. *Supervisors:* Prof. Dr.-Ing. F. Seitz (TUM), Prof. Dr.-Ing. M. Horwath (Technical University of Dresden), Prof. Dr. P. Knudsen (Technical University of Denmark). *Day of defense:* 2021-01-22. *Institution:* TUM

**Piccioni G. :** *Title:* Exploit satellite altimetry to improve coastal tide estimation. *Supervisors:* Prof. Dr.-Ing. F. Seitz (TUM), Prof. Dr. O. Andersen (Technical University of Denmark). *Day of defense:* 2021-02-03. *Institution:* TUM

**Goss A. :** *Title:* Generation of high-resolution global and regional multi-scale B-spline models of the vertical total electron content based on low-latency GNSS data. *Supervisors:* Prof. Dr.-Ing. M. Schmidt (TUM), Prof. Dr. U. Hugentobler (TUM), Prof. Dr. M. Hernandez-Pajares (Universitat Politecnica de Catalunya). *Day of defense:* 2021-09-13. *Institution:* TUM

## 6.5 International Research Stays

### TUM Graduate School

**Oelsmann J. :** Academic Institution: Mediterranean Institute for Advanced Studies (IMEDEA), Spain  
Duration: 2021-10-04 until 2021-12-10  
Supervisor: Dr. Marta Marcos

**Schlembach F. :** Delft University of Technology: Geoscience and Remote Sensing  
Duration: from 2021-05-04 (ongoing, telework)  
Supervisor: Dr.ir. D.C. Cornelis Slobbe